EXPERIMENTAL AND NUMERICAL STUDY OF OSCILLATORY FLUID FLOW AND
HEAT TRANSFER IN HEAT EXCHANGERS

By

Saad Mohammed Jalil

A DISSERTATION

Submitted to
Michigan State University
in partial fulfillment of the requirements
for the degree of

Mechanical Engineering – Doctor of Philosophy

2020

ABSTRACT

EXPERIMENTAL AND NUMERICAL STUDY OF OSCILLATORY FLUID FLOW AND
HEAT TRANSFER IN HEAT EXCHANGERS

By

Saad Mohammed Jalil

The enhancement of heat transfer in fluids is an important factor in the design of many practical engineering devices. One particular technique for increasing heat transport is to impose oscillatory flow on a duct connecting two reservoirs. In the current study, axial heat transfer enhancements by incompressible laminar oscillatory flow between cold and hot reservoirs connected by a bundle of tubes are examined experimentally and numerically. The dimensionless frequency parameter or Womersley number Wo was varied from 0.1 to 100 at different fluid tidal displacements. The oscillatory thermal conductivity was found to scale quadratically on the tidal displacement and pressure-gradient amplitude, and on the square root of the frequency of oscillation, and could exceed its molecular counterpart by up to five orders of magnitude.

Correlations were determined for the oscillatory thermal conductivity enhancement as a function of Wo and tidal displacement. The correlations showed that the axial heat transfer rate scaled in proportion to $Wo^{1.62}$ for $Wo > 3$ and behaved exponentially for low Wo with different scalings depending on pressure gradient amplitude. The study suggested a classification for the oscillatory heat transfer which partitioned the flow into four different regions varying from low tidal displacement to bulk convective exchange. It was shown that for unsteady flow the unsteady axial conduction is usually small for $Wo > 3$, but becomes significant below $Wo = 3$. This criterion is in contradiction to results of previous studies for $Wo < 3$, which underestimated effective conductivity because unsteady differential axial conduction was neglected. Finally, enhancement by a further factor of ten was observed in the axial heat transfer rate in tubes when walls were conductive and of sufficient thickness.

The effect of viscous heat dissipation in raising the field temperature of incompressible oscillatory air flow was also studied. A threshold was established for when the viscous heat dissipation term in the thermal energy equation changes or does not change significantly the temperature

field for the case of oscillatory air flow in a tube connecting two reservoirs. According to this threshold, the effect of dissipative bulk heating can be described by a correlation in terms of Womersley number Wo and axial tidal displacement ΔZ of the oscillatory flow. These results were determined using numerical simulations of oscillatory air flow $(Pr = 0.7)$ for different adiabatic non-conductive tube-reservoirs' systems configurations over a wide range of oscillatory frequencies and tidal displacements. The effect of viscous heat dissipation in oscillatory air flow can be ignored only below a specific limit of unsteadiness depending on Womersley number and axial tidal displacement. Otherwise, it becomes more significant with increasing Wo and ΔZ.

To My Mother

ACKNOWLEDGMENTS

TABLE OF CONTENTS

LIST OF TABLES

LIST OF FIGURES

KEY TO SYMBOLS AND ABBREVIATIONS

Roman Symbols

A	diaphragm's axial amplitude, m
A_t	tube cross-sectional area, m^2
C	constant
c_p	specific heat(constant pressure), $J/kg.K$
c_v	specific heat(constant volume), $J/kg.K$
d_i	inner tube diameter, m
d_o	outer tube diameter, m
f	frequency, $1/s$
g	gravitational constant r, m^2/s
h	tube wall thickness, m
k	thermal conductivity, $W/m.K$
k_{eff}	effective thermal conductivity, $W/m.K$
k_{osc}	oscillatory thermal conductivity, $W/m.K$
L	tube length, m
L_r	reservoir length, m
m	mass, kg
n	number of points in radial direction of the tube
n_p	number of exported file data per cycle
n_{ph}	Number of phase angles per cycle
n_t	Number of tubes
p	pressure, N/m^2
P	pressure gradient amplitude, Pa/m
$\overline{P}$	normalized pressure gradient amplitude
Q_{cond}	conduction heat transfer, W

Q_{conv}	convection heat transfer, W
Q_{in}	heat input, W
Q_{out}	heat output, W
R	tube radius, m
R_r	reservoir radius, m
t	time, s
T	temperature, K
$\overline{T}$	normalized temperature
T_C	cold temperature, K
T_H	hot temperature, K
U	field velocity, m/s
$\overline{U}$	normalized velocity, m/s
u	velocity, m/s
$|u_{avg}|$	averaged cross-sectional-area velocity amplitude, m/s
u_r	radial velocity, m/s
u_z	axial velocity, m/s
V_H	hot reservoir volume, m^3
W	work done, J
Δr	cell height, m
Δt	time step size, s
ΔZ	tidal displacement, m

Acronyms

CFD	Computational Fluid Dynamics
VHD	Viscous Heat Dissipation
UDF	User Defined Function

Dimensionless Numbers

Br Brinkman number

CFL Courant–Friedrichs–Lewy number

Ec Eckert number

Pe Peclet number

Pr Prandtl number

Re Reynolds number

Re_s Oscillatory Reynolds number

Wo Womersley number

Greek Symbols

α thermal diffusivity, m^2/s

δ_{st} Stokes layer thickness, m

μ dynamic viscosity, $kg/m.s$

ν kinematic viscosity, m^2/s

ρ density, kg/m^3

τ_w wall shear stress, N/m^2

ϕ phase angle, degree

Φ viscous heat dissipation, W

ω angular frequency, $1/s$

CHAPTER 1

INTRODUCTION

1.1 Background

In the past few decades, the processes of heat transfer in oscillatory flow have received interest from many researchers. The enhancement in heat transfer as a result of oscillatory flow can be helpful in various practical applications. Therefore, many experimental, numerical, and analytical studies have been carried out. In many applications, gases are used as the working fluid for energy transfer in devices such as thermo-acoustic systems, Stirling engines or coolers, and pulse tube coolers. Also, it is encountered in the flow inside many technical applications such as pulsed heat exchangers, nuclear reactors, discharge of piston pumps, the flow in pneumatic lines etc. Therefore, it is necessary to understand the heat transfer and fluid mechanics in oscillatory flow in order to design components like heat exchangers, regenerators, and thermal buffer tubes and to join technologies such as heat staking or thermoplastic staking, which are used in pulse heat process to bond two components.

The oscillatory flow analysis is more complex than the steady or unidirectional flow, due to the existence of time and space dependent effects within the oscillatory cycle, which leads to a cyclic variation of the flow conditions. The oscillatory flow can be classified into two flow types

1. Pulsating flow

2. Oscillating flow

The first type is a unidirectional oscillation about a mean, which consists of two components: the steady and the unsteady component as shown in Figure 1.1a. A well-known example of this kind of flow is the flow of blood in the arteries. The second type is a reciprocating flow, which is fully reversing as the flow changes its direction cyclically with zero mean velocity, as shown in Figure 1.1b. Several heat exchangers utilize reciprocating flow. Using this type of flow in enclosed

spaces has the advantage of a limited amount of mass inside the system. Therefore, this allows the mass to be kept minimal due to zero net flow and one need only fill the heat exchanger with fluid once. These types of systems can use different fluids like air, water, and oil. Another advantage of the oscillatory system is that it is clean and safe and does not use chemical substances to achieve its purpose. In some practical industrial applications, there is an excess of heat generated, which must be removed from the system to maintain it as specified. Also, the ability of the oscillatory flow to remove heat quickly and efficiently makes it useful for many applications.
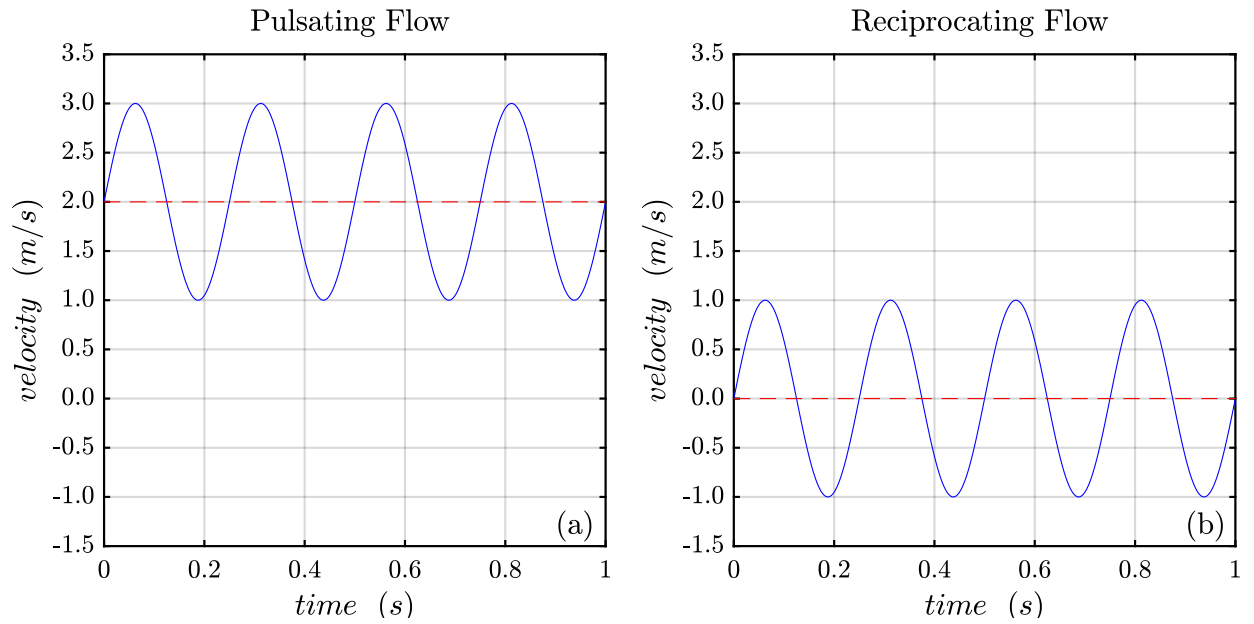
Figure 1.1: Oscillatory flow types

1.2   Motivation of the Work

Viscous heat dissipation, compressibility, diffusivity, and axial conduction are important factors in heat transfer in fluid flow in enclosed systems; therefore, it is important to understand their roles in oscillatory flow. The need to develop and improve the thermal performance in many applications, which depend on gases as the working fluid, has recently increased [1]. The design of many oscillatory flow heat transfer devices is often based on steady-flow correlations and some assumptions. These assumptions include considering the flow as an incompressible flow, with constant

properties, no entrance region in ducts, no viscous heat dissipation, and a linear axial temperature gradient along the duct. Therefore, theoretical designs may not be applicable to real reciprocating flow devices. Moreover, many unsteady-flow problems are modeled as linear problems under the above assumptions. Assumptions of low tidal displacement and close to quasi-steady conditions are also used to exploit the simplicity of linearity in solutions.

In the present study, common boundary conditions and the design of the heat exchanger are chosen to match a practical application. However, slight differences in real and assumed conditions may still lead to discrepancies between analytic and numerical or experimental results. In the current study, experimental and numerical investigations into the heat transfer between two reservoirs at different temperature connected by a bundle of tubes are carried out. Heat transfer measurements have been made under these conditions to provide reference data for comparison with numerical predictions. The main goal of this field of study is to observe the effect of oscillatory flow on thermal performance under different working conditions. Also, the study is interested in identifying the limitations imposed by the real constraints that exist in many practical devices. Therefore, the principal variables will be identified as dimensionless quantities and we study the heat transfer enhancement between two reservoirs connected by laminar flow oscillation in circular tubes with insulated and conductive tube walls.

1.3   Convection Heat Transfer in Oscillatory Flow

The high heat transport rate were achieved by the oscillatory flow heat exchangers with its efficient capability in removing and spreading the heat is the main reason for employing it as a replacement for heat pipes. The rapid change in fluids' instantaneous velocity enhances the heat diffusion during the axial mixing along the tube. The presence of an axial temperature gradient in oscillatory flow also causes an axial heat transport. This back and forth motion provides a periodic transverse change in temperature gradient along the tube, which provides continuous heat transfer axially [1, 2].

The oscillatory motion of the fluid over a solid surface with the no-slip condition penetrates
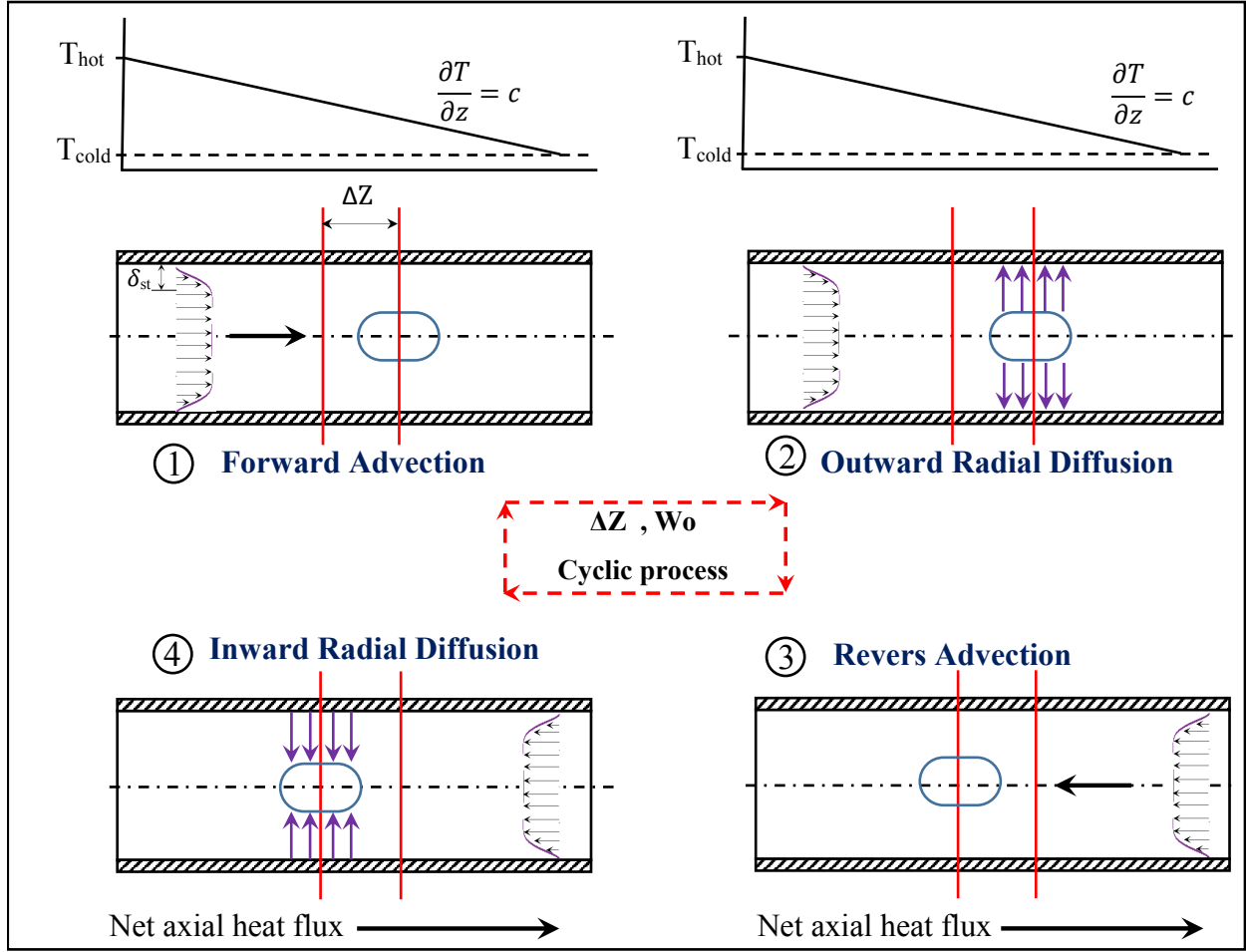
Figure 1.2: Oscillatory heat transport sequential mechanism

into the fluid with a distance $\sqrt{2\nu/\omega}$, called the Stokes layer δ_s, where ν and ω represent fluid kinematic viscosity and angular frequency respectively. Different levels of fluid enthalpy between the two halves of the cycle period and the radial heat diffusion exchange through the Stokes layer and beyond it will result in a net axial heat transfer. Further, using a finite tube wall thickness provides heat storage-release processes which enhance the heat transfer rate. The enhancement in diffusion by oscillatory motion depends on a specific physical mechanism. The working fluid fills pipes that connect the hot and cold reservoirs. The fluid will be forced to oscillate back and forth through a cycle of oscillation as shown in Figure 1.2. In the first half of the cycle, the fluid will go forward downstream from the hot to the cold region following the criteria of natural convection as there is an axial temperature gradient along the tube. In this phase of oscillation, the warmer fluid

4

will be moved by advection to the cooler fluid close to the wall. In the last phase of oscillation, the process will be reversed and the fluid near the tube wall will transfer heat from itself to the fluid in the center of the tube. These processes will drive the heat transfer at a higher rate when compared with molecular diffusive processes. Therefore, there are two main parameters that control this type of flow represented by tidal displacement and normalized frequency. The tidal displacement, ΔZ, represents the axial displacement in which the fluid moves every half period of the oscillatory cycle. It is calculated from the cross-sectional area averaged velocity over a cycle of oscillation as calculated in section 2.4.1 for numerical data and section 3.3.3.1 for experimental data. The relation of the oscillatory flow frequency to the viscous effect is represented by Womersley number Wo, which is the dimensionless frequency [3].

$$Wo = R\sqrt{\frac{\omega}{\nu}} \tag{1.1}$$

where R is the tube radius. Figure 1.2 shows the cyclic sequence of the diffusion and advection processes by moving axially, conduct radially, move back axially, and conduct back radially. This cyclic motion of the flow can be effective in enhancing the heat transfer rate by orders of magnitude compared with only axial conduction along a temperature gradient.

1.4 Previous Works

Previous research is classified into three categories; experimental, numerical, and theoretical studies.

1.4.1 Experimental Studies

This section presents summaries of experimental studies in the oscillating flow. It focuses on studies that are most relevant to the current study in dealing with oscillation in circular tubes connecting two reservoirs at different temperatures. Joshi et al. [4] conducted experiments to study the effect of oscillatory flow in enhancing the axial diffusional transfer of the concentration (rather than temperature) of methane in air. This study focused on laminar flow and showed a good

agreement with previous theoretical works, especially at high Womersley numbers. It showed that there is an enhancement in the axial diffusion of the concentration up to one thousand times when compared to molecular diffusion. There are also several studies related to engineering applications carried out by Kurzweg and co-authors, some of which are experimental works. Kurzweg and Zhao [5] used a bundle of capillary tubes to connect a hot reservoir at 350K and a cold reservoir at 295K to study the heat transfer between them when oscillating the fluid axially inside the tubes. Their experimental results showed that the rates of heat conduction in the axial direction were large, exceeding in magnitude the heat pipe enhancement by several orders when using water as the fluid. In another experimental work, Kurzweg et al. [6] studied the enhancement in the mass dispersion of gas oscillated axially in tubes, which expanded on the previous work of Kurzweg and Jaeger [7]. They showed that when an axial gradient in concentration was accompanied by flow oscillation, the separation of a gas mixture could be achieved much more rapidly by using oscillation to enhance the natural diffusion.

In a related experimental study, Kaviany and Reckker [8] presented a study of a heat exchanger consisting of a bundle of capillary tubes, which connects two reservoirs at different temperatures. They studied its performance for the case of fluid oscillation enhancing heat diffusion. Their experimental findings showed a good agreement with idealized predictions. They also showed that the enhancement in its performance is mainly dependent on the heat removed or supplied to the tube ends. Zhao and Cheng [9] carried out an experimental and numerical study of laminar flow in a uniform heat flux heated tube subjected to oscillation flow of air. Their predictions also showed a good agreement with experimental results. They obtained, based on the experimental results, a correlation equation for average Nusselt number using dimensionless parameters related to laminar oscillated air flow in tubes, which is useful in the design of Stirling engines.

Habib et al. [10] investigated the heat transfer enhancement in laminar pulsatile flow in tubes at different Reynolds numbers and frequencies of pulsation. Their results showed that the frequency has a strong effect on the Nusselt number while there is a slight effect of Reynolds number on it. Therefore, the mean Nusselt number increases as the Reynolds number or the pulsation frequency

decreases. They developed empirical equations for relative mean Nusselt numbers in the form of Reynolds number and pulsation frequency in later experiments on oscillatory flow. Akdog et al. [11] studied the heat removal in a vertical annular channel subjected to oscillating flow at four different frequencies under constant amplitude, and showed that the heat flux depended on the cyclic-averaged values in their experimental calculation. According to their results, at a constant Prandtl number, fluid tidal displacement, and geometric parameters, the rate of the heat removal over a cycle was proportional to the frequency of oscillation.

Pendyala et al. [12] studied experimentally the effect of oscillations in vertical tubes on heat transfer. They examined the effect of oscillatory motion on the heat transfer coefficient, and they found that in laminar flow the heat transfer coefficient increased with oscillation. From their results, they developed a correlation for local Nusselt number enhancement in terms of Reynolds number and acceleration. In addition, they used their proposed expression to find the mean Nusselt number in terms of tube length. Akadog and Ozgue [13] investigated experimentally the heat transfer from a vertical tube subjected oscillatory flow at constant wall heat flux. Their experiments were carried out for four different frequencies applied to the water column with three different heat fluxes and three different amplitudes. As in most other related studies, they also considered the cycle-averaged values using an approximation for a control volume. An empirical correlation was obtained for the cycle averaged Nusselt number in terms of the dimensionless amplitude and kinetic Reynolds number. They showed that the enhancement in heat transfer increased with frequency and amplitude of oscillation. They concluded that the heat transfer by oscillating flow depends mainly on the frequency of oscillation and its amplitude.

Recent experimental study was carried out by Patil and Gawali [1] on heat transfer by oscillatory flow in a heat exchanger under different frequencies, flow displacement, and heat fluxes. They used correlations of previous studies to investigate the influence of different parameters on experimental effective thermal conductivity and convective heat transfer coefficient in the cooling region. They derived a correlation for effective thermal conductivity based on experimental data in terms of the oscillation tidal displacement and the angular frequency of the oscillation. Their

correlation showed that there is an over prediction in Kurzweg's correlation [14] for effective thermal conductivities for all cases. Both over predictions and under predictions have been found compared to Nishio's correlation [15], according to the specific tidal displacement and frequencies ranges. Mehta and Khandekar [16] studied a pulsating flow through a square mini-channel under constant velocity amplitude and Reynolds number. The frequency was the only variable that was changed. They showed that the time-averaged heat transfer worsened at low Womersley because of insignificant convection at low frequencies.

Kamsanam et al. [17, 18] studied the oscillatory flow in a heat exchanger to calculate the heat transfer coefficient for the water side. They developed measurement techniques and experimental apparatus to analyze the behavior of the oscillatory flow heat transfer in thermoacoustic heat exchangers with finned and un-finned tubes. They developed correlations in term of primary studied parameters for each case. They suggested using these correlations to get the heat transfer effectiveness. Wantha [19] studied the enhancement in heat transfer in finned tube heat exchanger by pulsating flow experimentally. They presented their results in terms of the unsteady velocity amplitude and the frequency as an empirical correlation with the enhancement in heat transfer due to pulsating flow. For the purpose of characterizing the heat transfer enhancement in pulse tube refrigerator heat exchangers, Tang et al. [20] carried out experiments to study the heat transfer enhancement of a finned heat exchanger by the oscillatory flow. They suggested a correlation as a function of Nusselt, Reynolds, and Valensi numbers.

1.4.2 Numerical Predictions

Computational predictions have been used for problems that cannot easily be investigated analytically. Many numerical studies in axial heat transfer use laminar oscillatory flow with a time-dependent motion for a single tube as an analogy. Zhang and Kurzweg [21] studied numerically the enhanced axial heat transfer in oscillated flow inside a pipe. They obtained for different Womersley numbers the temperature profile, time-averaged velocity profile, tidal displacement, and Lagrangian displacement. They calculated the enhancement in axial heat flux for different tidal

displacement; also, they studied the effect of wall thickness on axial heat flux during oscillation. They found that the optimum thickness was about 20% of the tube radius in their cases. The study showed that the enhanced axial heat transfer could be very effective in removing a large amount of heat without mixing, at large tidal displacements.

Zhao and Cheng [22] carried out another laminar forced convection study for a circular tube subjected to a periodically reversing flow at constant wall temperature conditions. They showed that there are four principle parameters in their case study: the above three parameters in addition to the Prandtl number, which is specified by the working fluid. Moreover, they found there is an annular effect that exists near the entrance and exit regions in temperature profiles. Their results showed that the increase in kinetic Reynolds number and the amplitude of oscillatory flow led to enhanced rates of heat transfer, which were inversely proportional to the ratio of the tube length to diameter. Therefore, they suggested a correlation for the space-time averaged Nusselt number for air as a function of the first three parameters. Another study in reciprocating flow for finite tube length was carried out by Zhao and Cheng [23] for laminar incompressible flow. They showed that there is excellent agreement with analytical results in the fully developed region. From numerical results, they obtained an equation for the space-cycle averaged friction coefficient in terms of three similarity parameters for laminar reciprocating flow: kinetic Reynolds number, dimensionless oscillation displacement, and length to tube diameter.

Li and Yang [24] studied the heat transfer and fluid mechanics in two-dimensional channels at low frequencies and high amplitudes for zero-mean oscillatory flow. Their results showed that there is an intracycle oscillation, which is not normally observed in long ducts. They found that the intracycle oscillation is responsible for the enhancement in heat transfer because of the sudden changes in pressure as a result of the reversal of flow. In a later study of oscillatory flow, Sert and Beskok [25] presented a numerical simulation for a two-dimensional channel subjected to laminar forced convection heat transfer reciprocating flow. They presented their results in terms of penetration length, Womersley number, and Prandtl number. The study considered constant wall temperature and uniform heat flux as boundary conditions for a specific area on the upper

surface, while the lower surface was insulated. They showed that at high Womersley number there is a significant effect of Richardson number on the temperature field. They also indicated that an increase in penetration length leads to an increase in forced convection.

Aktas and Ozgumus [26] studied a nonzero mean oscillatory flow to examine the symmetric heating effect on it for shallow enclosures filled with air. They noticed that the velocities and acoustic streaming structures are strongly affected by the symmetric temperature gradient. They showed that, with an increase in the wall temperature, the field behavior of the steady flow became less erratic. Recent 2D and 3D numerical predictions were presented by Yu et al. [27] and Dai et al. [28]. Yu et al. [27] focused on understanding the effect of pulsatile flow on heat transfer and flow from a heated two-dimensional square cylinder inside a channel, with laminar flow and frequencies less than 20Hz. They found a good agreement with previous studies, especially when compared at the same Strouhal number. They observed the kinematics of the flow and various macroscopic flow parameters. Also, they found that there is an enhancement in heat transfer as the tidal displacement of pulsatile flow increases.

Dai et al. [28] carried out a three-dimensional model for oscillating flow and heat transfer in a pulse tube and a pulse tube refrigerator heat exchanger. They found that the variation of transient temperature behaved like a sinusoid in the center region of the tube and was non-sinusoidal within 10mm from the ends of the tube (length 60mm). They studied factors that play roles in the performance of pulse tubes like phase angle, heat transfer coefficient, the gravity, and the mass flow rate. In addition, their study revealed mechanisms of losses in such a pulsatile tube flow. Liu et al. [29] carried out a numerical investigation of unsteady laminar flow past two cylinders. They found that the imposed oscillatory motion enhanced the heat transfer compared with the effect of natural vortex streets. In addition, they showed that with increasing velocity amplitude ratio the Nusselt numbers were increased in both cylinders.

1.4.3 Analytical Research

In this section, analytical works are described, which usually require assumptions to simplify the problem. Typical shortcomings of analytical solutions are:

1. The flow is usually fully developed and so cannot account for entrance effects.

2. The solutions typically ignore differential axial conduction and so are invalid for low Peclet number phases of oscillation.

3. The fully developed flow restriction and the length of the tube places limitations on the tidal displacement of flows oscillation for which analytical results are trustworthy.

4. Most analytical solutions are for constant property flows (incompressible) without temperature dependence and so are strictly valid only for heat transfer over small temperature differences.

5. Most analytic solutions neglect the viscous dissipation heating and effects of fluid mixing in reservoirs.

Some analytical solutions relevant to this study are given in the appendix .

In earlier work, Taylor [30] studied the axial gradient in concentration in pipe flow and how diffusion can be enhanced by the oscillation of flow by several orders of magnitude. Watson [2] and Chatwin [31] analyzed fully developed oscillatory laminar flow with axial dispersion of contaminants. They found a significant enhancement in dispersion compared to a stationary fluid. Kurzweg and his co-workers conducted a wide range of analytical studies for tubes with oscillatory flow. In one such study, with low tidal displacement, no viscous heating, and fully developed flow, examined by Kurzweg [32], they observed an enhancement in conduction heat transfer in tubes connecting cold and hot reservoirs via oscillatory flow. They found that improvement in heat transfer by oscillation is proportional to the square of tidal displacement and is a function of tube radius, frequency of oscillation, and Prandtl number. In a later work, Kurzweg [33] showed that it is

possible to use oscillatory motion in liquid mixtures in capillary tubes to accomplish the separation of liquids. The product of the parameters, molecular diffusion coefficient of species, Womersley number, and the ratio of tidal displacement to the tube radius, was shown to be a coefficient of effective axial diffusion.

Other important parameters in oscillatory-flow heat transfer have been analyzed by Kaviany [34]. His work also depended on the assumptions of fully developed flow, constant properties, and negligible differential axial molecular heat diffusion. The study was for a tube radius nearly equal to the Stokes boundary layer thickness subjected to oscillatory flow. He analyzed the fluid flow and heat transfer between two reservoirs maintained at two different constant temperatures. The study investigated tube wall thickness, oscillatory flow motion in the reservoirs, viscous heat dissipation, and the effect of different fluid and tube parameters. The results showed that the enhancement in performance of the heat exchanger becomes less favorable when the tube radius becomes larger than the thermal boundary layer. When water was the working fluid, the viscous heat dissipation was found to be negligible.

Nishio et al. [15]discussed ways of enhancing the heat transfer coefficient in oscillation-controlled heat transport in tubes. They proposed increasing the ratio of heat flow enhancement to the power input with a novel kind of oscillatory flow with phase shift in the tube. They found a relation between the frequency, cross-sectional area, and amplitude of oscillation in term of Womersley and Prandtl numbers, which described an optimum operating condition. Zhang et al. [35] examined the effect of sinusoidal oscillation for fluid in tubes connecting two reservoirs filled with contaminated groundwater with different concentrations of species, in enhancing axial dispersion of contaminants. They observed that there is a large enhancement in the axial transfer of contaminant through the tube as a result of fluid oscillation. A parallel study was carried out by Moschandreou and Zamir [36] to evaluate the effect of Prandtl number and pulsation frequency on the heat transfer rate at constant heat flux from a circular tube. They found that over a moderate range of pulsatile oscillations there is an optimum enhancement in Nusselt number, but this improvement is lost if the frequency is outside the preferred range.

Later Walther et al. [37] performed a study of the influence of developing flow on heat transfer in laminar oscillating pipe flow and its effect on the mean Nusselt number. They suggested an appropriate heat transfer correlations for laminar oscillatory flow conditions in a tube for one-dimensional simulation models of oscillatory flow. As oscillatory flow is useful for many applications, Lambert et al. [38] examined enhancing heat transfer from solar collectors using oscillatory laminar flows. They showed that the transfer of the heat, which was collected from a solar device to a storage tank, was enhanced as the thermal diffusivity of the fluid increased by several orders relative to stationary molecular diffusivity. Therefore, the axial heat transport along the tube was enhanced. Another analysis by Chattopadhyay [39] has been carried out to find the effect of laminar pulsating flow on flow and heat transfer in pipes. The results showed, for a range of frequencies less than 20Hz and low amplitudes, that there is no effect of pulsation on time averaged heat transfer.

Yin and Ma [40] studied the influence of oscillatory flow on heat transfer coefficient in capillary tubes with uniform heat flux boundary conditions. They observed that the principle parameters that affect directly the heat transfer from the tube are the dimensionless oscillating frequency, Prandtl number, and the amplitude of oscillated flow, which can be used to find the maximum heat transfer coefficient. Yuan et al. [41] analyzed the heat transfer of the pulsatile flow inside a circular tube by including the thermal wall inertia. They observed that the heat transfer was enhanced by increasing the velocity amplitude and the frequency, but decreased for some ranges especially at large pulsing amplitude and low frequencies. Yin and Ma [42] studied analytically the oscillatory flow in a round tube at uniform heat flux. In addition, they analyzed the oscillatory motion of the fluid to determine the effect of a triangular velocity waveform on the heat transfer coefficient. They observed that the oscillating flow can improve the rate of heat transfer inside the tube and the triangular waveform of oscillating motion can result in a higher heat transfer coefficient than sinusoidal waveform of oscillating motion.

Recently, Brereton and Jalil [43] focused on the enhancement in axial heat transfer along the circular tube by laminar flow oscillation. Their results showed that there are several orders of

13

magnitude of enhancement in axial diffusivity comparing with molecular diffusivity, and are proportional to the square pressure-gradient amplitude and the Prandtl number. Also, the study indicated a further increase in axial diffusivity by about ten times through conduction in tube walls of sufficient thickness.

Most previous studies are of flow in tubes, but there are also many studies of oscillatory flow through channels [44–53]. Different channels geometries were considered in these studies to study the enhancement of heat transfer by oscillatory flow. Some researchers have studied the effect of the entrance length [54–58]. Some oscillatory flows are turbulent so many studies have focused on turbulent unsteady flow, using quasi-steady turbulent models, direct numerical simulations, or experimental studies [59–77].

1.5 Objectives and Proposed Contributions

In the current study, an experimental and numerical investigation into the performance of a specific design of heat exchanger, which consists of two reservoirs at different temperatures connected by cylindrical tubes, is examined [78]. The experiment was designed as a variation on an earlier design of Kurzweg and Zhao [5] in which the flow between hot and cold reservoirs oscillated axially but with a different oscillating mechanism. The oscillation mechanism was designed to simultaneously force the fluid in both reservoirs with same axial displacement as shown in Figure 1.3. Experimental results will be used to validate a numerical model for a device with the same dimensions and over a range of experimentally applied frequencies and tidal displacements. An initial objective is to validate a numerical prediction tool (ANSYS 17.2) using the analytical results for ideal flow by Brereton and Jalil [43] and experimental data. The objective of the numerical model is to establish a database and find trends in behavior to improve understanding of oscillatory heat transfer devices under a range of operating conditions. The limitations in analytic and experimental models make it challenging to address the more complex effects in this type of flow.

In most of the previous studies, the reservoirs were ignored and only the tubes were considered.

In cases that involved the reservoirs, the flow was oscillated from one side and an absorber was installed on the other side [5]. This method of oscillating the flow from one side will lead to an asymmetry in flows during the oscillation, which affects the measured parameters. Also, using the tube without a piston-cylinder system will not allow the researcher to specify a fixed tidal displacement for different frequencies. In practical applications like a Stirling engine or other oscillatory flow heat exchangers, the system supplies fluid from both sides by a specific displacement various frequencies. Therefore, specifying these quantities is more helpful than applying unsteady velocity or pressure at one end of the system. These applied unsteady quantities (velocity and pressure) will provide the system with different axial displacements for each frequency which is not desirable. Hence, the method used and proposed in the current study is the oscillation from both sides with a specified axial displacement and frequency. The oscillatory flow deals with two main parameters, which are the normalized frequency *Wo* and the axial flow displacement. Therefore, it is important for researchers to benefit from these studies by presenting the findings in normalized form. These two parameters are useful for any geometry. It is also necessary to involve another parameter to generalize the obtained results. This parameter is the pressure gradient amplitude that depends on the frequency, axial displacement, and the size of the system represented by the length of the tube. Therefore, in the current study, the results defined in normalized quantities to be useful in validation, design, and comparison are for various Womersley numbers, tidal displacements, and pressure gradients.

The heat transfer enhancement between two identical reservoirs through laminar oscillatory flow with insulated and conductive walls is studied. In addition to the experimental setup, 2D and 3D numerical models were studied in the current study. The goal of the study is to define the axial heat transfer enhancement in terms of oscillatory thermal conductivity as a function of Womersley numbers for different tidal displacements. Another important objective of the study is to specify the limitations of the axial heat conduction and the viscous heat dissipation, which were neglected in previous unsteady flow studies. Moreover, correlations for the axial heat transfer enhancement for different Womersley numbers and tidal displacements will be proposed. The correlations will be

for the actual working conditions of practical applications as they will be obtained by considering most terms in governing equations. The correlations will be helpful for applications dependent on fixed tidal displacements with various oscillatory speeds. In addition, the study is interested in partitioning the oscillatory flow into different regions depending on axial flow displacement. Also, the effect of conductive tube wall thickness will be a part of the current study objectives. The study will address several shortcomings that have been observed but neglected in previous unsteady flow studies.
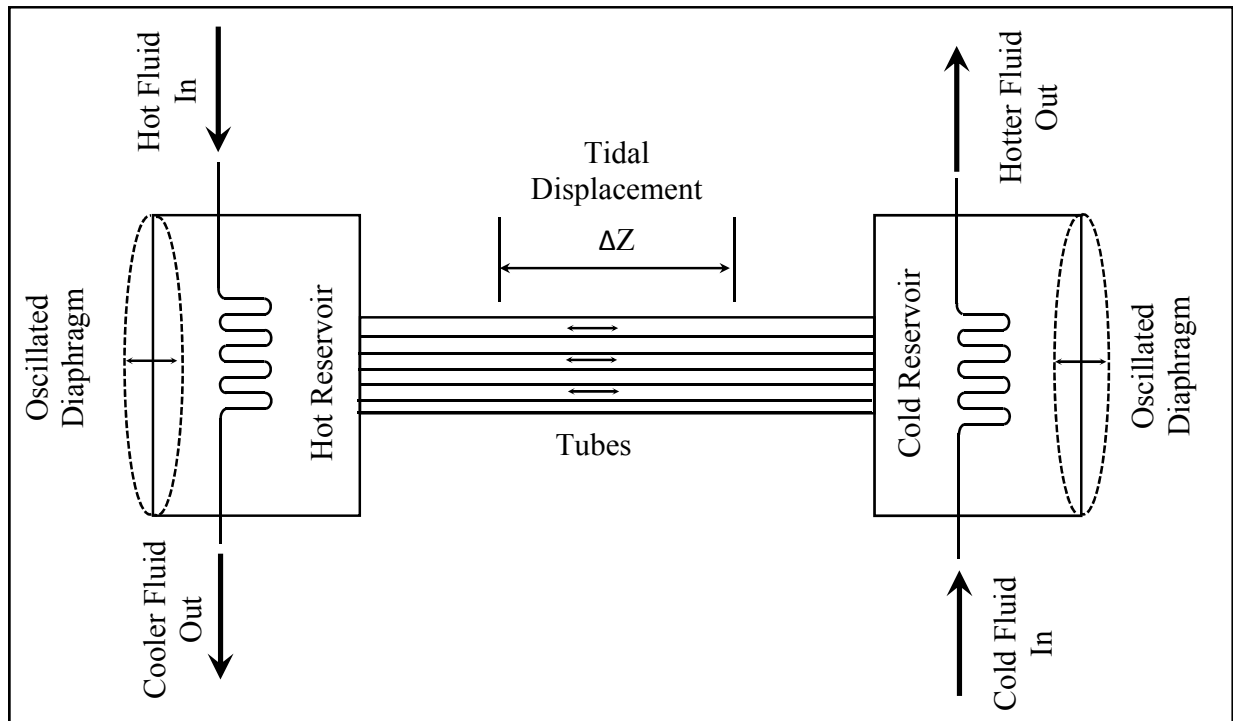
Figure 1.3: Schema of the oscillatory heat exchanger

The diagram in Figure 1.4 summaries the objectives and goals of the current study. Each factor indicated in the diagram will be analyzed separately for its effect on the rate of heat transfer. There-fore, the study will focus on clarifying the actual behavior of oscillatory flow with the following objectives;

1. To make accurate numerical predictions of the oscillatory flow under realistic working con-ditions.

2. To identify when and why the effect of viscous heat dissipation of air is important.

3. To establish the effect of reservoir fluid mechanics near the tube entrance and its effect on velocity and temperature profiles.

4. To understand how and why high axial heat fluxes can be best achieved.

5. To classify the oscillatory flow into different regions depending on relevant flow parameters.
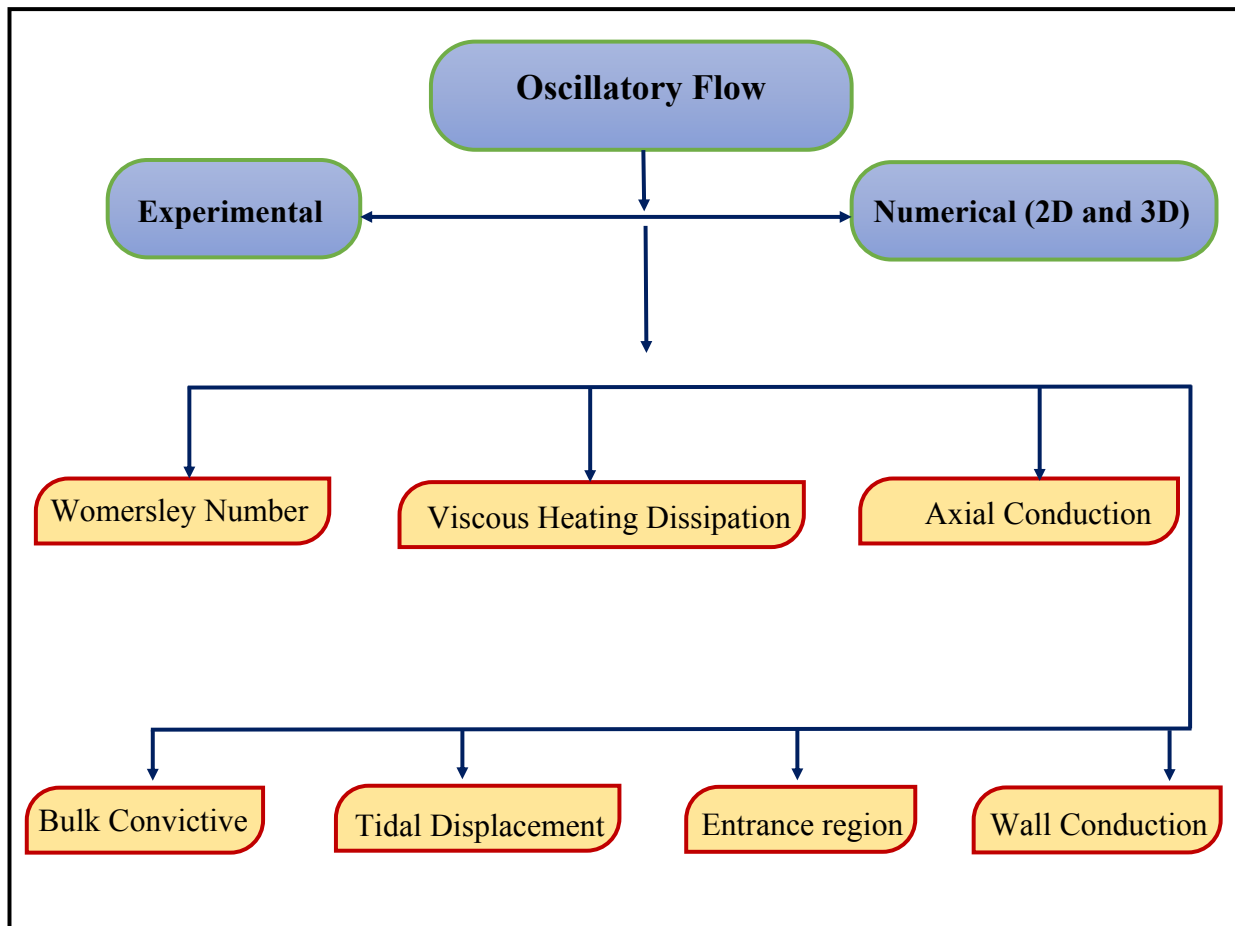
Figure 1.4: Research objectives

In order to meet these objectives, which will explain the thermal performance of oscillatory heat transfer systems; we plan to carry out the following tasks, as new contributions to understanding of these devices;

1. Study the rate of heat transfer enhancement for various tidal displacements ΔZ and Womersley numbers Wo.

2. Study at low oscillation frequencies $(Wo < 3)$ or low Peclet number $(Pe = PrRe < 100)$ the effect of differential axial conduction on total heat transport.

3. Study the importance of viscous heat dissipation in oscillatory flow especially at high frequencies, which does not appear to have been studied previously.

4. Study the velocity and temperature profile development in the tube entrance/exit regions.

5. Study the effect of the reservoirs on the rate of viscous heat dissipation.

CHAPTER 2

GOVERNING EQUATIONS AND NUMERICAL SIMULATIONS

2.1 Introduction

In this chapter, the governing equations, numerical methods, and previous analytical solutions are considered. The study investigates numerical simulations for different cases of oscillatory flow. The numerical prediction consists of laminar 2D axisymmetric and 3D models. The 2D axisymmetric model was used to reduce the simulation cost over a wide range of parameters. While this model is similar to those used in previous numerical and analytical studies, it is different in that it includes reservoirs in the domain and uses a new form of oscillation by bounding the cold and hot reservoirs with diaphragms. The 3D model replicates precisely all components of the experimental apparatus. The fully-developed analytical solutions of oscillatory flow through a tube are used to validate the predicted results at low tidal displacement. In addition, the predicted results are validated with the experimental results in chapter three.

2.2 Governing Equations

Computational Fluid Dynamics (CFD) solves the fundamental governing equations of fluid mechanics; the continuity, momentum, and energy equations with some level of numerical and approximation error. These equations are mathematical expressions of the physical principles represented by three fundamental laws on which fluid dynamics depends:

- Conservation of Mass

- Conservation of Momentum

- Conservation of Energy

2.2.1 Conservation of Mass

Conservation of mass equation or the continuity equation has the form [79, 80]

$$\frac{\partial \rho}{\partial t} + \nabla . (\rho \vec{u}) = S_m \tag{2.1}$$

where $(\vec{u})$ represents the velocity vector components, which can be obtained as follows

$$\vec{u} = u_r \vec{i_r} + u_\theta \vec{i_\theta} + u_z \vec{i_z} \tag{2.2}$$

Equation 2.1is a general equation that is valid for compressible and incompressible flows. S_m represents a source for added mass to the continuous phase from a second phase, and it will be zero in the current study as there is no mass added from a dispersed second phase to the continuous phase or any external source. For incompressible flow, the continuity equation will be simplified to:

2.2.1.1 2D Axisymmetric

$$\nabla . \vec{u} = 0$$
$$\frac{\partial u_z}{\partial z} + \frac{\partial u_r}{\partial r} + \frac{u_r}{r} = 0 \tag{2.3}$$

2.2.1.2 3D Cylindrical Coordinates Flow

$$\nabla . \vec{u} = 0$$
$$\frac{1}{r}\frac{\partial (r u_r)}{\partial r} + \frac{1}{r}\frac{\partial u_\theta}{\partial \theta} + \frac{\partial u_z}{\partial z} = 0 \tag{2.4}$$

2.2.2 Conservation of Momentum

The linear momentum equation can be written as [79, 80]:

$$\frac{\partial}{\partial t}(\rho \vec{u}) + \nabla . (\rho \vec{u}\vec{u}) = -\nabla p + \nabla . (\overline{\overline{\tau}}) + \rho \vec{g} + \vec{F} \tag{2.5}$$

20

This form involves a force balance according to Newton's second law, which says that the net force on a fluid element equals its mass times the acceleration of the element. In the equation, p is the static pressure, $\bar{\bar{\tau}}$ is the stress tensor, and $\rho\vec{g}$ and $\vec{F}$ represent the gravitational body force and external body force respectively. The stress tensor is defined as:

$$\bar{\bar{\tau}} = \mu\left[\left(\nabla\vec{u} + \nabla\vec{u}^T\right) - \frac{2}{3}\nabla.\vec{u}I\right] \tag{2.6}$$

where (I) is the unit tensor [79, 80].

2.2.2.1 2D Axisymmetric Unsteady Flow

The gravitational body forces and the external forces are ignored in all 2D simulations and a Newtonian fluid is assumed. The momentum equations are then

$$\frac{\partial}{\partial t}(u_z) + \frac{1}{r}\frac{\partial}{\partial z}(ru_zu_z) + \frac{1}{r}\frac{\partial}{\partial r}(ru_ru_z) =$$
$$-\frac{1}{\rho}\frac{\partial p}{\partial z} + \frac{1}{r}\frac{\partial}{\partial z}\left[rv\left(2\frac{\partial u_z}{\partial z}\right)\right] \tag{2.7}$$
$$+ \frac{1}{r}\frac{\partial}{\partial r}\left[rv\left(\frac{\partial u_z}{\partial r} + \frac{\partial u_r}{\partial z}\right)\right]$$

$$\frac{\partial}{\partial t}(\rho u_r) + \frac{1}{r}\frac{\partial}{\partial z}(ru_zu_r) + \frac{1}{r}\frac{\partial}{\partial r}(ru_ru_r) =$$
$$-\frac{1}{\rho}\frac{\partial p}{\partial r} + \frac{1}{r}\frac{\partial}{\partial r}\left[rv\left(2\frac{\partial u_r}{\partial r}\right)\right] \tag{2.8}$$
$$+ \frac{1}{r}\frac{\partial}{\partial z}\left[rv\left(\frac{\partial u_r}{\partial z} + \frac{\partial u_z}{\partial r}\right)\right] - 2\mu\frac{u_r}{r^2}$$

2.2.2.2 3D Unsteady Flow

To match the experimental calculations, the gravitational body forces are included in 3D simulations and only the external forces are ignored. Therefore

$$\frac{\partial}{\partial t}(\vec{u}) + \nabla.(.\vec{u}\vec{u}) = -\frac{1}{\rho}\nabla p + \frac{1}{\rho}\nabla\left(\bar{\bar{\tau}}\right) + \vec{g} \tag{2.9}$$

2.2.3 Conservation of Energy

The energy equation in its most general form can be written as

$$
\underbrace{\frac{\partial}{\partial t}(\rho E)}_{\text{\color{red}Changes with time}} + \underbrace{\nabla(\vec{u}(\rho E + p))}_{\text{\color{red}Convection}} = \underbrace{(\nabla.k\nabla T)}_{\text{\color{red}Conduction}} + \underbrace{\nabla.\left(\bar{\bar{\tau}}_{eff}\vec{u}\right)}_{\text{\color{red}Viscous Dissipation}} + S_h \tag{2.10}
$$

This equation represents the first Law of Thermodynamics applied to a fluid element moving with the flow. Therefore, the rate of the change inside a fluid element equals to the net flux of heat into the element plus the rate of work done on it due to the body and surface forces. The energy E per unit mass is defined as

$$
E = h - \frac{p}{\rho} + \frac{U^2}{2} \tag{2.11}
$$

The heat source S_h is ignored, as there is no chemical reaction or any external heat source. The viscous heat dissipation term will be included in the solver setup in chapter five to study its effect. Previous analytic studies [2, 27, 32, 43] did not include the differential axial conduction in their exact solutions, which can have a significant effect at low Peclet numbers. Kays et al. [81] discussed this effect of axial conduction at $(Pe < 100)$ for steady-state cases. Therefore, with the absence of dissipation, the energy equation is

$$
\frac{\partial}{\partial t}(\rho E) + \nabla(U(\rho E + p)) = \nabla.(k\nabla T) \tag{2.12}
$$

In the case of conjugate heat transfer when there is a coupling wall between the fluid and a solid wall, Equation 2.12 will be used for the fluid region, and for the solid region the equation will be

$$
\frac{\partial}{\partial t}(\rho E) = \nabla.(k\nabla T) \tag{2.13}
$$

where

$$\nabla.(k\nabla T) = \frac{1}{r}\frac{\partial}{\partial r}\left(kr\frac{\partial T}{\partial r}\right) + \frac{1}{r}\frac{\partial}{\partial \theta}\left(\frac{k}{r}\frac{\partial T}{\partial \theta}\right) + \overbrace{\frac{\partial}{\partial z}\left(k\frac{\partial T}{\partial z}\right)}^{\text{Differential Axial Conduction}} \tag{2.14}$$

Numerical solutions can be obtained for all terms of the governing equations or for simplified equations under specific assumptions. These assumptions depend on the flow type, physical properties, and external sources.

2.3   Method of Numerical Simulation

Fluid flow and heat transfer in circular glass tubes, which connect hot and cold reservoirs filled with air, are simulated. This section describes the numerical methods used in the simulation of the unsteady heat transfer and fluid flow for the 2D-axisymmetric and 3D models for the tubes and the reservoirs. In addition, the software, discretization method, mesh size in the Stokes layer, initial and boundary conditions, grid independent test, and the validation are explained.

2.3.1   Software

All CFD simulations works have been carried out with ANSYS 17.2 software. The heat exchanger geometry was produced by using ANSYS Design Modeler (DM), where ANSYS meshing was used for meshing the geometries. All CFD cases were solved using ANSYS FLUENT. MATLAB was the main software used for post-processing data, though some was carried out using FLUENT. MATLAB was also used to do all integral calculations for the equations of tidal displacement and effective thermal conductivity as functions of the computed velocities, temperatures, and pressures profiles at different time steps.

2.3.2   Geometry

In the present study, two geometries were considered for numerical simulations. The first geometry was modeled as a 2D axisymmetric geometry, which represents one seventh of the 3D model size

that consists of seven tubes and connects the cold and hot reservoirs as in the experimental setup. Each model has layers of conductive walls of the tubes, reservoirs, and insulations.
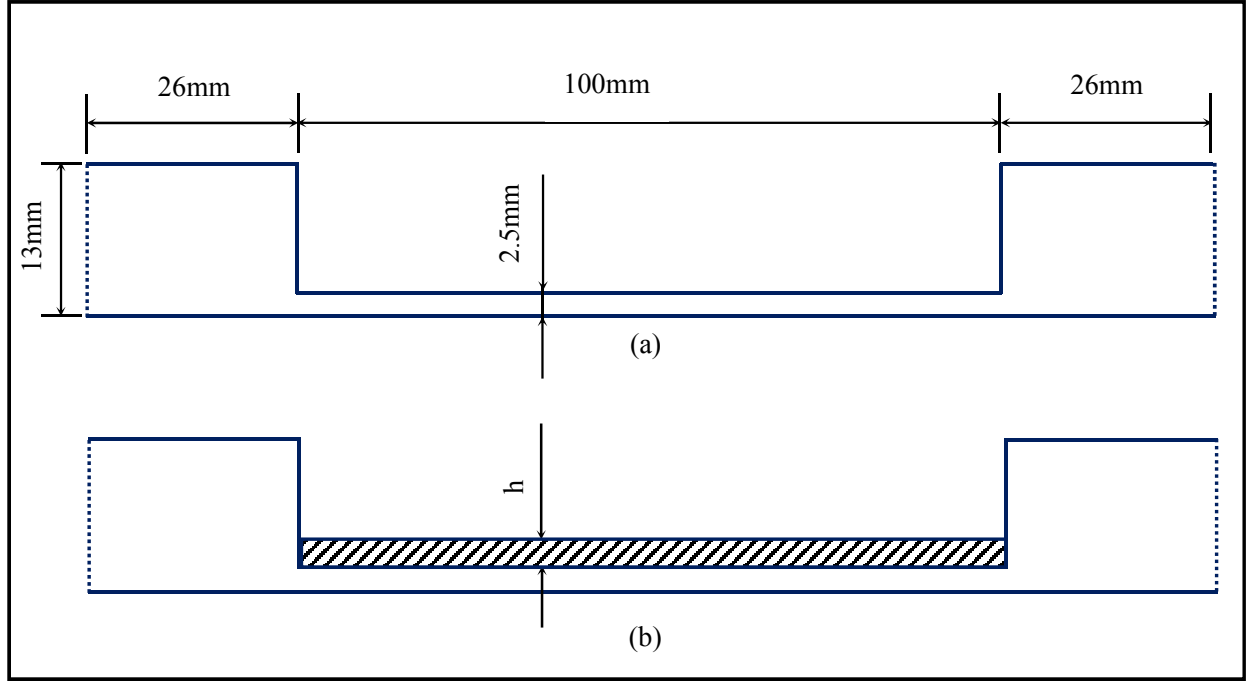
Figure 2.1: 2D-axisymmetric model dimensions and components

2.3.2.1 2D Axisymmetric Model

2.3.2.1.1 Insulated Tube Wall

As shown in Figure 2.1a, the model consists of three main parts: the hot reservoir, cold reservoir, and the tube that connects them. The reservoir radius is 13mm with length 26mm, and the tube radius is 2.5mm with length 100*mm*. This design was used in previous studies, but the current study included the reservoirs in the simulation to make it consistent with the practical applications.

2.3.2.1.2 Conductive Tube Walls

Conductive tube walls have the same dimension as insulated tube walls. The model includes the effect of conduction through the glass tube thickness by adding conductive glass layers to the tube to represent the heat conduction through the glass tube wall as shown in Figure 2.1b. The

heat transfers from the fluid to the solid region through the fluid/solid interface. Both ends of the reservoirs are oscillated back and forth to force the fluid to oscillate axially.

2.3.2.2 3D Model

Figure 2.2 shows the 3D model that was designed to be identical to the design used in experiments. It consists of PVC reservoirs, seven glass tubes, and fiberglass insulation covers the whole heat exchanger.
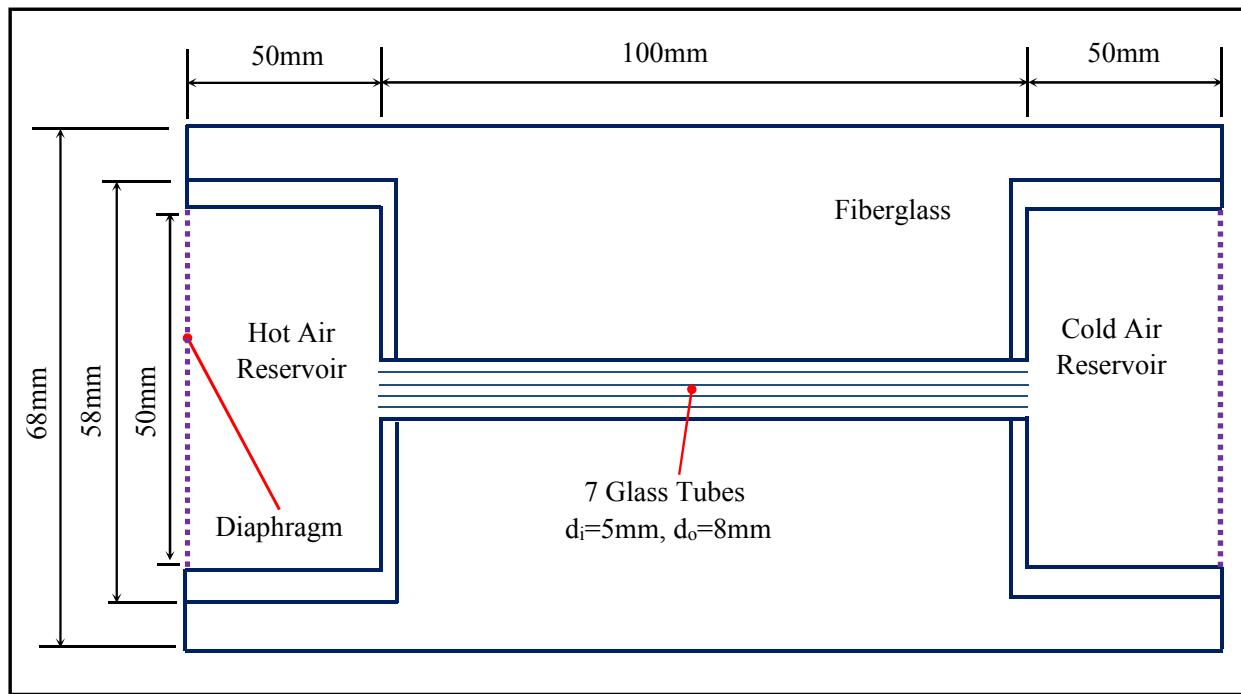
Figure 2.2: 3D model dimensions and components

2.3.3 Mesh

One of the most important features, which has a significant effect on the accuracy of the computational simulation, is the mesh. Therefore, it is necessary to make sure the simulation runs with an appropriate mesh. In the current study, it is important to resolve the Stokes layer thickness near the wall. This requires having a sufficient number of grid points to resolve the Stokes layer at different frequencies, as it becomes thinner with increasing frequency of oscillation.

Mesh1 (10680) cells

Mesh2 (22366) cells

Mesh3 (50481) cells

Mesh4 (93280) cells

Mesh5 (183276) cells

(a) 2D-axisymmetric

Insulation, PVC, Glass regions

PVC and Glass regions

Fluid region

(b) 3D
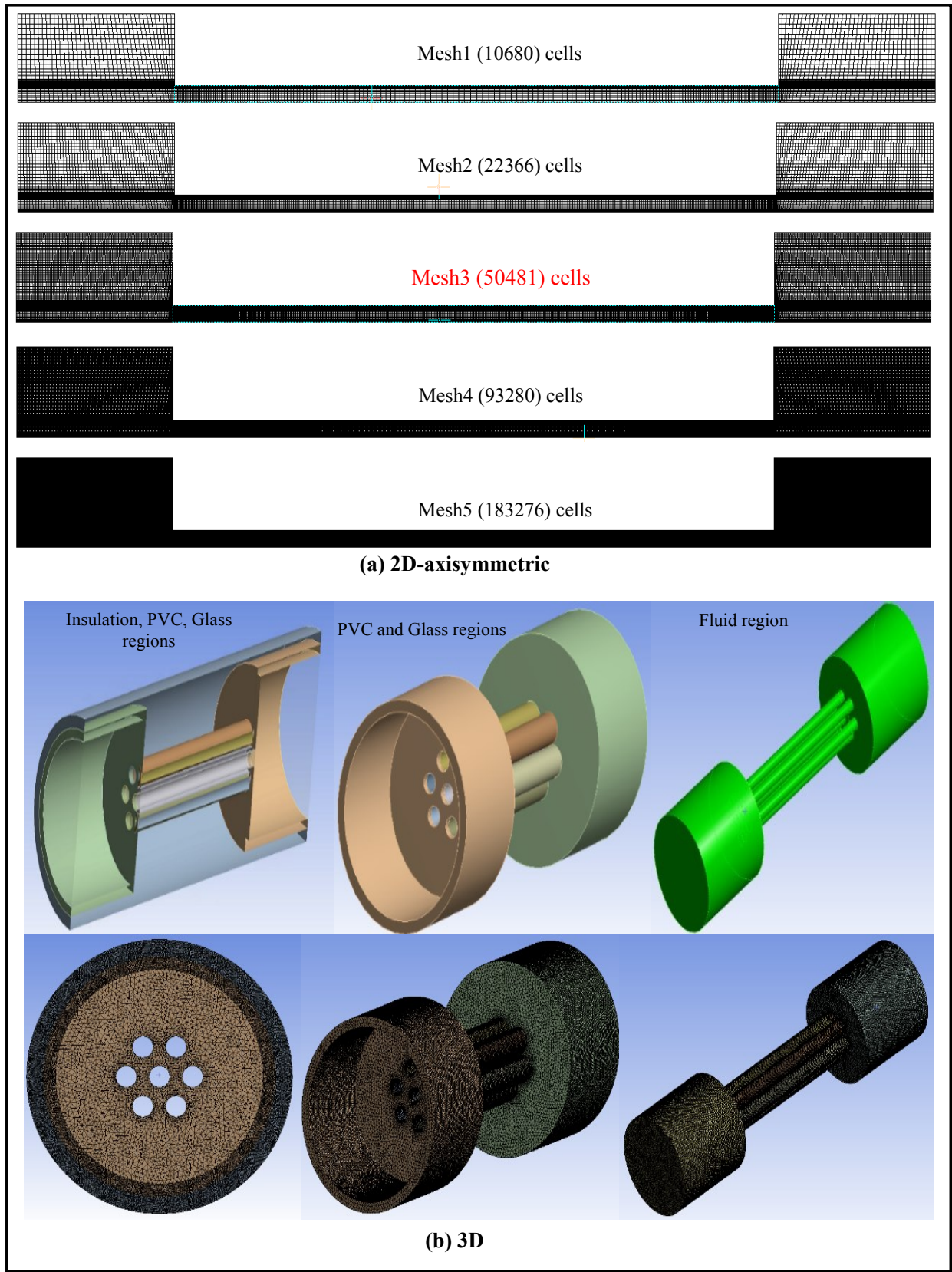
Figure 2.3: 2D and 3D models meshes and geometries

2.3.3.1 Mesh Generation

Figure 2.3 shows the mesh developed for the 2D and 3D models. The 2D model mesh is generated entirely from quadrilateral elements (structured mesh) and its geometry is divided into zones to get a fine mesh near the wall of the tube and in the tube inlet and outlet. For the 3D model the tetrahedron and hexahedron mesh were used, with the geometry meshed as a multi-zone, also with fine mesh close to the wall.

2.3.3.2 Mesh Independent Tests

To get grid-independent converged solutions and valid results, certain meshing requirements should be achieved. It is important to remember that the solution is a numerical solution to a problem, which has been posed by defining the model mesh and the initial and boundary conditions. Therefore, more refined meshing and running conditions may lead to a more or less accurate converged solution. Convergence is one indicator of accurate CFD simulations. Generally, we describe the convergence by observing the residual values while monitoring other parameters of quantities of interested in the study. These parameters are pressure drop, temperatures, wall shear stress, and velocity. Otherwise, the simulations may give different results if the simulations run for more iterations. Therefore, we have to identify values of interest, to be monitored in the calculation. In our study, all calculations depend strongly on the oscillatory pressure amplitude and the temperature gradient. According to above requirements, we need in our unsteady simulation to ensure that the solution will satisfy the following criteria:

1. The solution will not be affected by specific residual error value. Therefore, we run the solution for different residual values.

2. It will not be affected by refining the specific mesh size. Hence, we test the models with different mesh refinements.

3. Make sure there are enough grid points near the wall to resolve the Stokes layer. Thus, we started meshing with at least five cells in Stokes layer depending on the highest frequency to

be used in the simulation.

4. There are enough iterations to make sure that the solution has converged.

5. Monitor the pressure, temperature, and the velocity and observe that each parameter has converged to an almost constant value and there is no change with more iterations.

To achieve satisfactory simulations, the meshing process was started by considering the thickness of the Stokes boundary layer, equal to $\delta_{st} = \sqrt{2\nu/\omega}$ [21]. The thickness of this oscillating boundary layer δ_{st}, which penetrates into the fluid near the wall, decreases with an increase in the frequency of the oscillation and increases with an increase in the kinematic viscosity of the fluid. The first mesh developed for the 2D model has at least six grid points inside the Stokes layer at $Wo = 100$, which represents the highest Womersley number in the current study. For this starting mesh size the average ratio of the cell height in radial direction normally to the wall Δr to the Stokes layer thickness δ_{st} for the 2D model is about $\Delta r/\delta_{st} = 0.14$ and for 3D model at $Wo = 10$ is about $\Delta r/\delta_{st} = 0.17$ with five cells inside the Stokes layer.

Tables 2.1 and 2.2 indicate the distance from each grid point to the wall. Table 2.1 relates to the 2D model and indicates the number of grid points inside the Stokes layer at $Wo = 100$ for different meshes. The number of meshes inside the Stokes layer increased from 6 to 14 grid points. These various meshes have been studied to find a model that is grid independent. We have considered five different meshes for the 2D model and four different meshes for the 3D model as shown in Figure 2.3. In Table 2.2, the values represent the mesh of the 3D model and refers to the number of grid points inside the Stokes layer at $Wo = 10$, which represents the highest Womersley number at which accurate tidal displacements in the experiments were measured by flow visualization. The table shows the size of elements in the radial direction for different meshes and how the number of meshes increased from 6 to 12 grid points inside the Stokes layer. Figure 2.3b illustrates the 3D model design with its components, which is almost identical to the experimental heat exchanger.

Table 2.3 shows the principal aspects of the mesh test for the 2D model at $Wo = 1$ and $Wo = 100$ with a residual value 1×10^{-18} at 500 iterations. In the beginning, we started with 5000 iterations,

28

Table 2.1: Grid distance from the wall for the 2D model

Grid No.	Grid Distance from the wall (m)				
	Mesh1	Mesh2	Mesh3	Mesh4	Mesh5
1	5.8×10^{-6}	3.0×10^{-6}	3.0×10^{-6}	3.0×10^{-6}	2.5×10^{-6}
2	1.2×10^{-5}	6.0×10^{-6}	5.9×10^{-6}	6.0×10^{-6}	5.1×10^{-6}
3	1.7×10^{-5}	9.0×10^{-6}	8.9×10^{-6}	8.9×10^{-6}	7.6×10^{-6}
4	2.3×10^{-5}	1.2×10^{-5}	1.2×10^{-5}	1.2×10^{-5}	1.0×10^{-5}
5	2.9×10^{-5}	1.5×10^{-5}	1.5×10^{-5}	1.5×10^{-5}	1.3×10^{-5}
6	3.5×10^{-5}	1.8×10^{-5}	1.8×10^{-5}	1.8×10^{-5}	1.5×10^{-5}
7	4.1×10^{-5}	2.1×10^{-5}	2.1×10^{-5}	2.1×10^{-5}	1.8×10^{-5}
8	4.9×10^{-5}	2.4×10^{-5}	2.4×10^{-5}	2.4×10^{-5}	2.0×10^{-5}
9	5.8×10^{-5}	2.7×10^{-5}	2.7×10^{-5}	2.7×10^{-5}	2.3×10^{-5}
10	7.0×10^{-5}	3.0×10^{-5}	3.0×10^{-5}	3.0×10^{-5}	2.5×10^{-5}
11	8.4×10^{-5}	3.3×10^{-5}	3.3×10^{-5}	3.3×10^{-5}	2.8×10^{-5}
12	1.0×10^{-4}	3.5×10^{-5}	3.5×10^{-5}	3.5×10^{-5}	3.0×10^{-5}
13	1.2×10^{-4}	4.0×10^{-5}	4.0×10^{-5}	4.0×10^{-5}	3.3×10^{-5}
14	1.5×10^{-4}	4.5×10^{-5}	4.4×10^{-5}	4.5×10^{-5}	3.5×10^{-5}
15	1.8×10^{-4}	5.1×10^{-5}	5.0×10^{-5}	5.0×10^{-5}	3.9×10^{-5}
16	2.2×10^{-4}	5.7×10^{-5}	5.7×10^{-5}	5.7×10^{-5}	4.4×10^{-5}
17	2.6×10^{-4}	6.6×10^{-5}	6.5×10^{-5}	6.6×10^{-5}	4.8×10^{-5}
18	3.2×10^{-4}	7.7×10^{-5}	7.6×10^{-5}	7.6×10^{-5}	5.4×10^{-5}
19	3.8×10^{-4}	8.9×10^{-5}	8.8×10^{-5}	8.9×10^{-5}	6.2×10^{-5}
20	4.7×10^{-4}	1.0×10^{-4}	1.0×10^{-4}	1.0×10^{-4}	7.2×10^{-5}
21	5.8×10^{-4}	1.2×10^{-4}	1.2×10^{-4}	1.2×10^{-4}	8.3×10^{-5}
22	7.0×10^{-4}	1.5×10^{-4}	1.4×10^{-4}	1.4×10^{-4}	9.6×10^{-5}
23	8.6×10^{-4}	1.7×10^{-4}	1.7×10^{-4}	1.7×10^{-4}	1.1×10^{-4}
24	1.0×10^{-4}	2.1×10^{-4}	2.1×10^{-4}	2.1×10^{-4}	1.3×10^{-4}
25	1.3×10^{-4}	2.5×10^{-4}	2.5×10^{-4}	2.5×10^{-4}	1.6×10^{-4}
26	1.5×10^{-4}	3.0×10^{-4}	3.0×10^{-4}	3.0×10^{-4}	1.9×10^{-4}
27	1.8×10^{-4}	3.6×10^{-4}	3.6×10^{-4}	3.6×10^{-4}	2.3×10^{-4}
28	2.1×10^{-4}	4.4×10^{-4}	4.4×10^{-4}	4.3×10^{-4}	2.7×10^{-4}
29	2.3×10^{-4}	5.4×10^{-4}	5.3×10^{-4}	5.2×10^{-4}	3.3×10^{-4}
30	2.5×10^{-4}	6.6×10^{-4}	6.5×10^{-4}	6.2×10^{-4}	3.9×10^{-4}
31		8.0×10^{-4}	7.9×10^{-4}	7.5×10^{-4}	4.7×10^{-4}
32		9.7×10^{-4}	9.5×10^{-4}	8.9×10^{-4}	5.5×10^{-4}
33		1.2×10^{-3}	1.2×10^{-3}	1.0×10^{-3}	6.4×10^{-4}
34		1.4×10^{-3}	1.4×10^{-3}	1.2×10^{-3}	7.3×10^{-4}
35		1.6×10^{-3}	1.6×10^{-3}	1.3×10^{-3}	8.2×10^{-4}
36		1.9×10^{-3}	1.8×10^{-3}	1.5×10^{-3}	9.1×10^{-4}
37		2.1×10^{-3}	2.0×10^{-3}	1.6×10^{-3}	1.0×10^{-3}
38		2.3×10^{-3}	2.1×10^{-3}	1.8×10^{-3}	1.1×10^{-3}
39		2.4×10^{-3}	2.2×10^{-3}	1.9×10^{-3}	1.2×10^{-3}
40		2.5×10^{-3}	2.3×10^{-3}	2.1×10^{-3}	1.3×10^{-3}
41			2.4×10^{-3}	2.2×10^{-3}	1.4×10^{-3}
42			2.4×10^{-3}	2.3×10^{-3}	1.4×10^{-3}
43			2.5×10^{-3}	2.3×10^{-3}	1.5×10^{-3}
44				2.4×10^{-3}	1.6×10^{-3}
45				2.4×10^{-3}	1.7×10^{-3}
46				2.5×10^{-3}	1.8×10^{-3}
47					1.9×10^{-3}
48					2.0×10^{-3}
49					2.1×10^{-3}
50					2.2×10^{-3}
51					2.2×10^{-3}
52					2.3×10^{-3}
53					2.4×10^{-3}
54					2.4×10^{-3}
55					2.4×10^{-3}
56					2.5×10^{-3}
57					2.5×10^{-3}

Stokes Layer $W_o = 100$

Tube radius (2.5mm)

Table 2.2: Grid distance from the wall for the 3D model

Grid No	Grid Distance from the wall (m)			
	Mesh1	Mesh2	Mesh3	Mesh4
1	6.09×10^{-5}	1.72×10^{-5}	1.20×10^{-5}	1.02×10^{-5}
2	9.40×10^{-5}	3.98×10^{-5}	3.50×10^{-5}	1.78×10^{-5}
3	2.61×10^{-4}	6.06×10^{-5}	6.97×10^{-5}	2.47×10^{-5}
4	2.80×10^{-4}	8.45×10^{-5}	8.03×10^{-5}	4.76×10^{-5}
5	3.10×10^{-4}	1.10×10^{-4}	9.69×10^{-5}	5.12×10^{-5}
6	6.82×10^{-4}	1.76×10^{-4}	1.01×10^{-4}	5.97×10^{-5}
7	8.12×10^{-4}	2.94×10^{-4}	1.30×10^{-4}	7.53×10^{-5}
8	9.52×10^{-4}	3.21×10^{-4}	2.06×10^{-4}	9.98×10^{-5}
9	1.32×10^{-3}	8.73×10^{-4}	2.99×10^{-4}	1.16×10^{-4}
10	1.51×10^{-3}	1.05×10^{-3}	3.32×10^{-4}	2.04×10^{-4}
11	1.85×10^{-3}	1.18×10^{-3}	7.69×10^{-4}	2.82×10^{-4}
12	2.05×10^{-3}	1.31×10^{-3}	8.31×10^{-4}	3.10×10^{-4}
13	2.32×10^{-3}	1.42×10^{-3}	9.42×10^{-4}	7.85×10^{-4}
14	2.50×10^{-3}	1.53×10^{-3}	1.06×10^{-3}	1.11×10^{-3}
15		1.84×10^{-3}	1.12×10^{-3}	1.16×10^{-3}
16		2.14×10^{-3}	1.28×10^{-3}	1.22×10^{-3}
17		2.16×10^{-3}	1.29×10^{-3}	1.29×10^{-3}
18		2.18×10^{-3}	1.32×10^{-3}	1.37×10^{-3}
19		2.20×10^{-3}	1.46×10^{-3}	1.44×10^{-3}
20		2.21×10^{-3}	1.51×10^{-3}	1.51×10^{-3}
21		2.26×10^{-3}	1.64×10^{-3}	1.57×10^{-3}
22		2.32×10^{-3}	1.74×10^{-3}	1.63×10^{-3}
23		2.50×10^{-3}	1.82×10^{-3}	1.70×10^{-3}
24			1.96×10^{-3}	1.76×10^{-3}
25			1.99×10^{-3}	1.83×10^{-3}
26			2.09×10^{-3}	1.89×10^{-3}
27			2.17×10^{-3}	1.95×10^{-3}
28			2.19×10^{-3}	2.01×10^{-3}
29			2.35×10^{-3}	2.08×10^{-3}
30			2.42×10^{-3}	2.15×10^{-3}
31			2.50×10^{-3}	2.22×10^{-3}
32				2.30×10^{-3}
33				2.35×10^{-3}
34				2.40×10^{-3}
35				2.45×10^{-3}
36				2.50×10^{-3}

Tube radius (2.5mm); Stokes Layer; $W_0=10$

but we reduced it to 500, as it was found that there is no effect of extra iteration beyond 150. In this test, the peak value (maximum value) to peak value (minimum value) for four computed variables was monitored. Pressure, temperature, wall shear stress, and velocity are the four properties that have been chosen to check the mesh quality. For the five different 2D-axisymmetric meshes, the variation in the above four variables is calculated. The comparisons were related to the maximum peak-to-peak value of each variable for all meshes, where $\Delta Peak_{max}$ represents maximum peak-to-peak difference value for each quantity in all meshes and $\Delta Peak$ refers to the difference at each mesh size. The percentage of change in $(\Delta Peak_{max} - \Delta Peak)/\Delta Peak$ for mesh1 is equal to zero

Table 2.3: 2D-Axisymmetric model mesh independent tests

Variables		2D-Axisymmetric (residual 1×10^{-18}, iterations 500)					
		$\Delta Z/L$=0.12, Wo=1, $\delta_{st.}$=3.2×10^{-3} m			$\Delta Z/L$=0.12, Wo=100, δ_{st} =3.2×10^{-5} m		
		No. Cells	% (ΔPeak$_{max}$-ΔPeak)/ΔPeak	No. of Grids inside Stokes Layer	No. Cells	% (ΔPeak$_{max}$-ΔPeak)/ΔPeak	No. of Grids inside Stokes Layer
Pressure		10680	0	30	10680	0	6
		22366	0.3577	40	22366	0.2717	12
		50481	0.6917	43	50481	0.9500	12
		93280	0.3789	46	93280	0.7993	12
		183276	0.2517	57	183276	0.8908	14
Temperature		10680	0.0469	30	10680	0.0513	6
		22366	0.0275	40	22366	0.0255	12
		50481	0.0130	43	50481	0.0070	12
		93280	0.0031	46	93280	0.0028	12
		183276	0	57	183276	0	14
Velocity		10680	0.0510	30	10680	0.0495	6
		22366	0.0239	40	22366	0.0238	12
		50481	0.0059	43	50481	0.0058	12
		93280	0.0016	46	93280	0.0015	12
		183276	0	57	183276	0	14
Wall shear stress		10680	0.4728	30	10680	0.4421	6
		22366	0.3301	40	22366	0.0061	12
		50481	0.2669	43	50481	0.085	12
		93280	0.1128	46	93280	0	12
		183276	0	57	183276	0.824	14

as this mesh size at the maximum pressure difference, but this difference reduces with increasing number of cells. The temperature and velocity variation have maximum differences in their peaks at the highest mesh number. It is clear from Table 2.3 that the variation in peak difference percentage did not exceed 1% by doubling the number of cells for the 2D and 3D models.

From Figure 2.4, it is clear that the curves for the three properties at different mesh sizes match each other for both Womersley numbers. The negligible effect of the mesh size is related to the preprocessing design steps by requiring the mesh generator to provide a specific number of grids close to the wall, which is specified by the Stokes layer thickness. In all 2D-axisymmetric simulation, mesh number three (50481 cells) was used as it provides at least 12 grid points inside the Stokes layer so $\Delta r/\delta_{st} = 0.085$. The same mesh testing procedures have been followed for

the 3D model but with four different mesh sizes as shown in Table 2.4. As this model represents the design of the experimental heat exchanger, the temperature procedure test was different. The volume-averaged temperature gradients for the cold and hot reservoirs were monitored for all four mesh sizes.
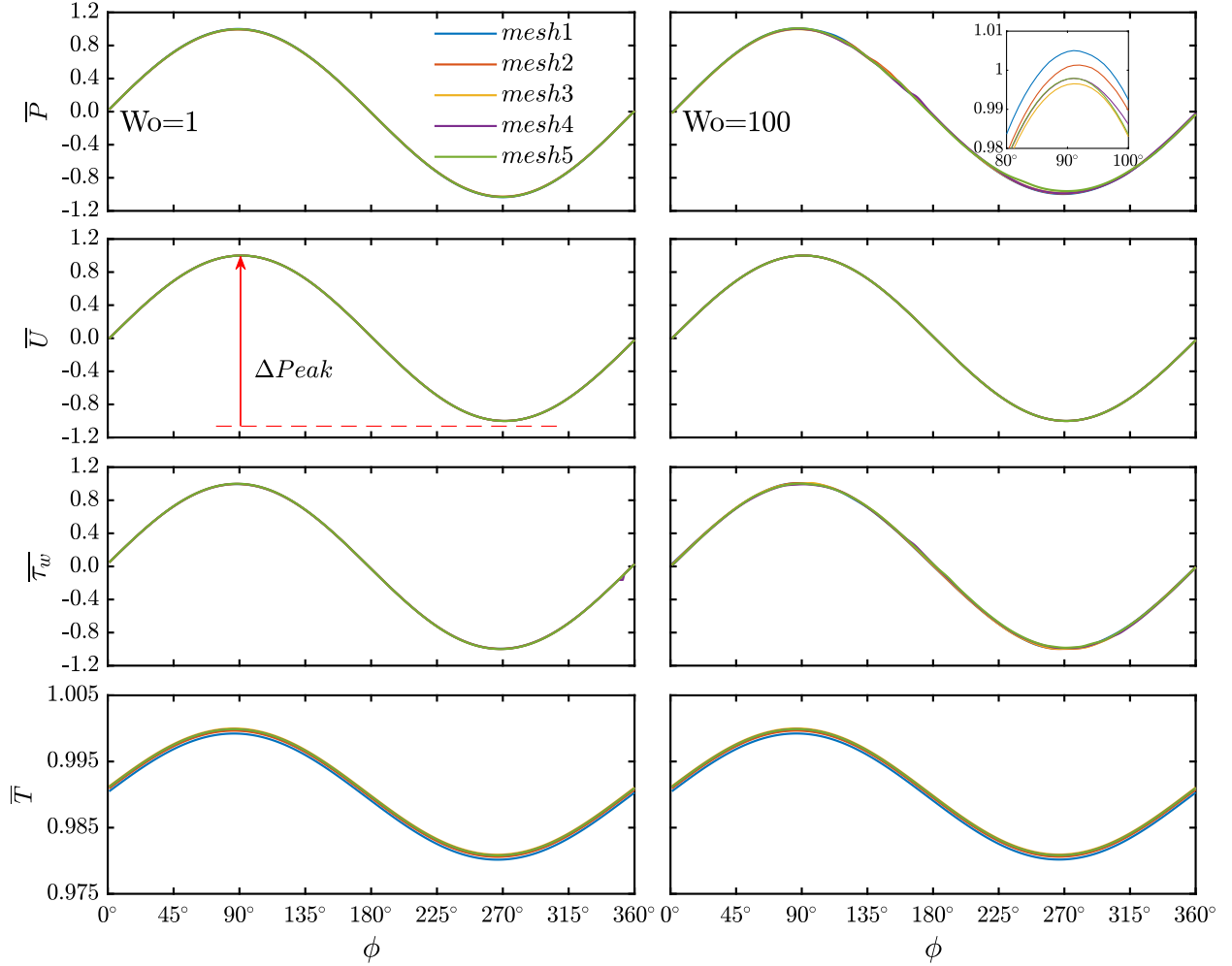
Figure 2.4: Effect of 2D model mesh size on normalized peak-to-peak values for the variables at $Wo = 1$ (left) and $Wo = 100$ (right)

Mesh2 was used in all modeling simulations for the 3D computations with (1106826) cells. Figure 2.5 shows the normalized temperature and pressure in the hot and cold reservoirs for the last cycle after five seconds, which represents the maximum time in the current study for the 3D model. According to Table 2.4, the difference did not exceed 1%, but we chose mesh2 nonetheless as it provides eight grid points inside the Stokes layer ($\Delta r/\delta_{st} = 0.125$). One of the costs of

Table 2.4: 3D model mesh independent tests

3D (residual 1×10^{-6}), Wo=10, Incompressible, $\delta_{st.}$=3.2×10⁻⁴ m								
		No. Cells	% $(T_{mesh\_min}-T_{min})$ / T_{min}	No. of Grids in Stokes Layer			No. Cells	% $(\Delta Peak_{max}-\Delta Peak)$ /$\Delta Peak$	No. of Grids in Stokes Layer
Temperature	Hot reservoir	455804	3.8×10^{-2}	5	Pressure	Hot reservoir	455804	0.796	5
		1106826	7.8×10^{-4}	8			1106826	0.726	8
		2221275	0.0×10^{0}	10			2221275	0.339	10
		4095276	4.5×10^{-3}	12			4095276	0.0	12
	Cold reservoir	455804	3.9×10^{-10}	5		Cold reservoir	455804	0.507	5
		1106826	1.7×10^{-11}	8			1106826	0.120	8
		2221275	9.6×10^{-12}	10			2221275	0.056	10
		4095276	0.0×10^{0}	12			4095276	0.0	12

the computational fluid dynamics is the simulation time. Hence, it is important to pay attention to optimum model and solver settings. After choosing an appropriate mesh, we need to decide which residual value will yield a converged solution. The residual represents the imbalance in a conservation equation summed over all cells of the computational simulation.

In current simulations, the scaled residual has been used. It defines the imbalance for any general variable summed over all domain cells and scales it by using a scale factor to indicate the flow rate of a variable through the whole domain. This scaled residual is considered an indicator of convergence in the current study, the pressure-based solver was used for these simulations. Different residual limits were tested to study their effect on the results of the primary properties. The left part of Table 2.5 lists the test of different residual value limits which are below 1×10^{-6} as an acceptable error. There is a very small effect of reducing the residual from 1×10^{-6} to 1×10^{-18}. Depending on these values, the imbalance of 1×10^{-6} has been considered for the 2D and 3D models as a criterion for convergence. Figure 2.6 shows the convergence for all governing equations at different residuals limits. The figure indicates that the continuity equation did not converge below around 1×10^{-13}, where the others did not below 1×10^{-16}. One more important
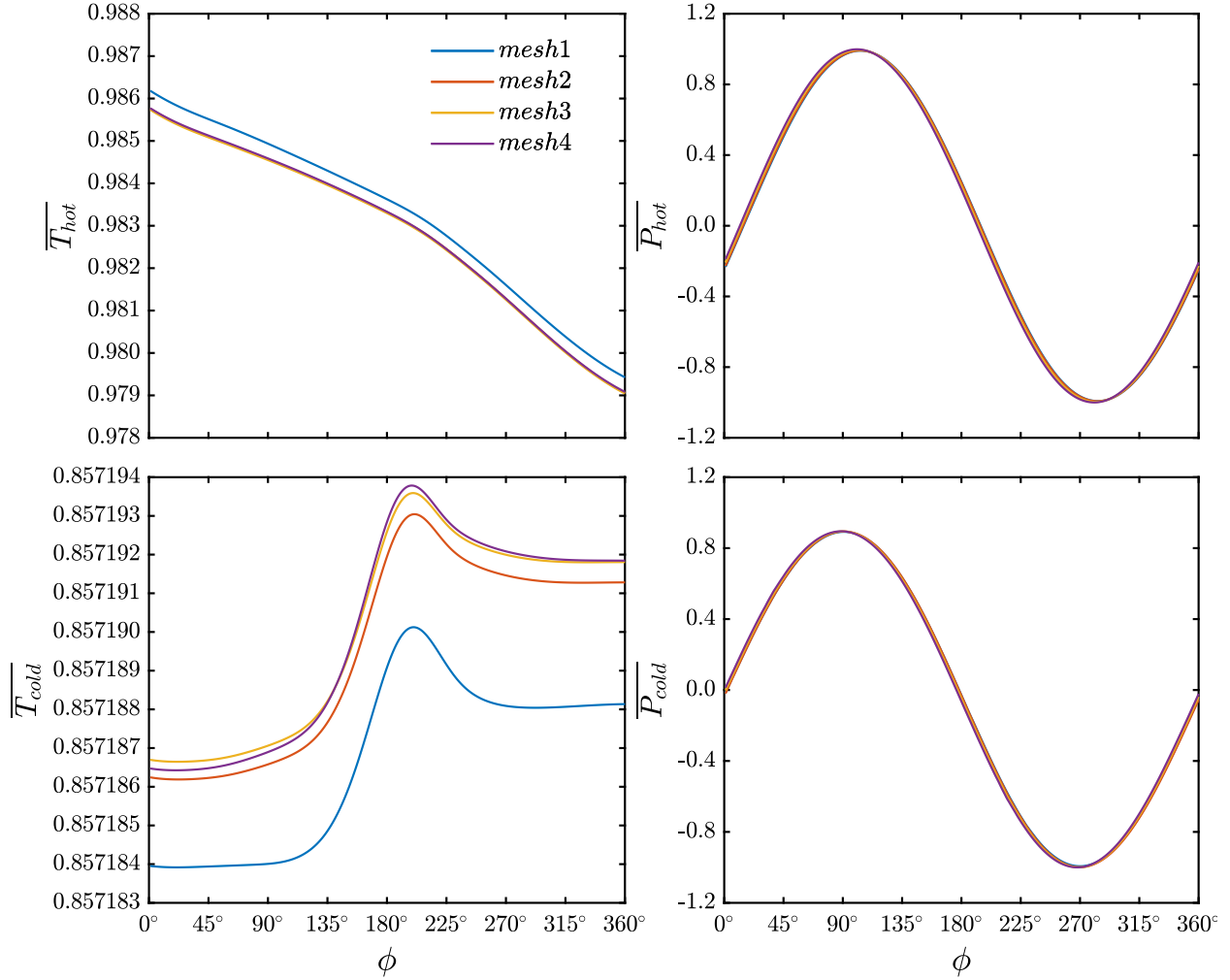
Figure 2.5: Effect of 3D model mesh size on normalized variables

parameter that should be involved in the study is the time step size. The influence of the residual limit on normalized pressure, velocity, temperature, and wall shear stress at $Wo = 100$ is presented in the left side of Figure 2.7.

2.3.3.3 Time Independent Tests

In addition to the mesh independent test or the spatial convergence test, to reduce the cost of simulations, it is necessary to resolve the fluid motion in an oscillatory flow. Therefore, it is required to quantify the temporal accuracy by studying the time step independence to check the effect of time steps on the simulation accuracy. To achieve time-step independent simulations,
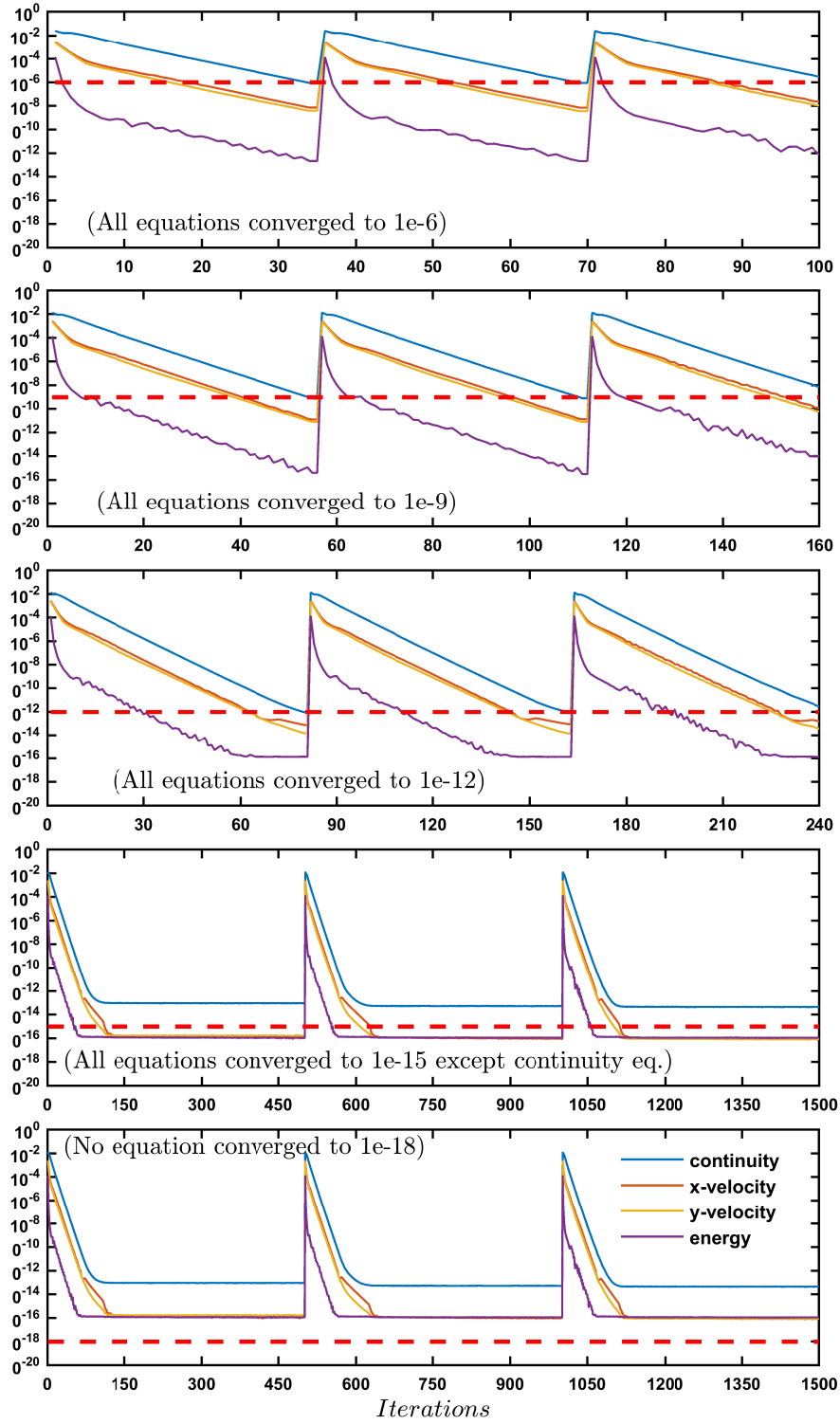
Figure 2.6: Convergence of continuity, momentum, and energy equations at different residual value limits and $Wo = 100$

Table 2.5: Residuals and time step effect

Parameters		2D-Axisymmetric, mesh3, ΔZ/L=0.12, Wo=100		
	Residual values	% ($\Delta Peak_{max}$-$\Delta Peak$)/$\Delta Peak$	Points/Cycle (residual 1×10^{-6})	% ($\Delta Peak_{max}$-$\Delta Peak$)/$\Delta Peak$
Pressure	1×10^{-6}	0	45	0
	1×10^{-9}	1.42×10^{-5}	90	0.756
	1×10^{-12}	1.42×10^{-5}	180	1.015
	1×10^{-15}	1.42×10^{-5}	360	1.271
	1×10^{-18}	1.42×10^{-5}	720	1.292
Temperature	1×10^{-6}	9.33×10^{-5}	45	0.049
	1×10^{-9}	6.52×10^{-7}	90	0.037
	1×10^{-12}	2.86×10^{-10}	180	0.00017
	1×10^{-15}	3.63×10^{-12}	360	0
	1×10^{-18}	0	720	8.17×10^{-5}
Velocity	1×10^{-6}	0	45	0
	1×10^{-9}	4.71×10^{-5}	90	0.388
	1×10^{-12}	4.73×10^{-5}	180	0.510
	1×10^{-15}	4.73×10^{-5}	360	0.541
	1×10^{-18}	4.73×10^{-5}	720	0.542
Wall shear stress	1×10^{-6}	0	45	0
	1×10^{-9}	8.19×10^{-5}	90	0.373
	1×10^{-12}	8.21×10^{-5}	180	0.753
	1×10^{-15}	8.21×10^{-5}	360	0.806
	1×10^{-18}	8.21×10^{-5}	720	0.757

there are two parameters which need to be tested for unsteady flow to choose an appropriate time-step-sizeΔt. These two parameters are

1. Number of phase angles per cycle (n_{ph}).

2. Courant–Friedrichs–Lewy number or condition (CFL) [79].

The first parameter (n_{ph}) is required to resolve the oscillatory cycle. The numerical simulations are run at different frequencies, so it is required to have an adequate number of phase angles through each oscillatory flow cycles. The maximum size of the time step may also be limited

by the stability of the equations being solved and the numerical method used. Depending on the oscillation frequency for each case study, the time step size Δt and CFL number are defined as

$$\Delta t = \frac{1}{f \cdot n_{ph}} \tag{2.15}$$

$$CFL = \frac{|u(r)_{max}| \cdot \Delta t}{\Delta r_{min}} < 1 \tag{2.16}$$

where f is the frequency of oscillation.

Since the time-step-size Δt, maximum velocity amplitude $|u(r)_{max}|$ over an oscillatory cycle, and minimum cell-size Δr_{min} are connected via the Courant–Friedrichs–Lewy number as defined in Equation 2.16 [79], it is necessary to specify a physical time step Δt that provides stable solutions with $CFL < 1$. Achieving this condition or stability criterion will ensure that information from a specific cell will pass only to its immediate next cell. In the current study, the Courant number is kept below one for all cases.

The right side of Figure 2.7 shows the effect of the time step size in terms of the number of phase angle per cycle n_{ph} on normalized pressure, velocity, temperature, and wall shear stress at $Wo = 100$. Also, the tests of the time step size or the number of phases per cycle were listed in the right part of Table 2.5. The results showed that the difference is very small, which is around 1%. For the current purposes of computing results at each phase angle, a time step with 360 phase angles was chosen $(n_{ph} = 360)$. For this number of phase angles, the specified time step sizes are decreased from 7.519×10^{-1} at $Wo = 0.1$ to 7.519×10^{-7} at $Wo = 100$. Therefore, this number of phase angles provide data for the oscillatory flow at each phase angle. This is important in calculating the temperature gradients of the hot and cold reservoirs with time as it will provide a smooth time dependence for computed results.

2.3.3.4 Dynamic Mesh

The current simulations have a geometry that deforms with time. This change in geometry requires a dynamic mesh for the deformed zones when cells may disappear, merge, or change shape
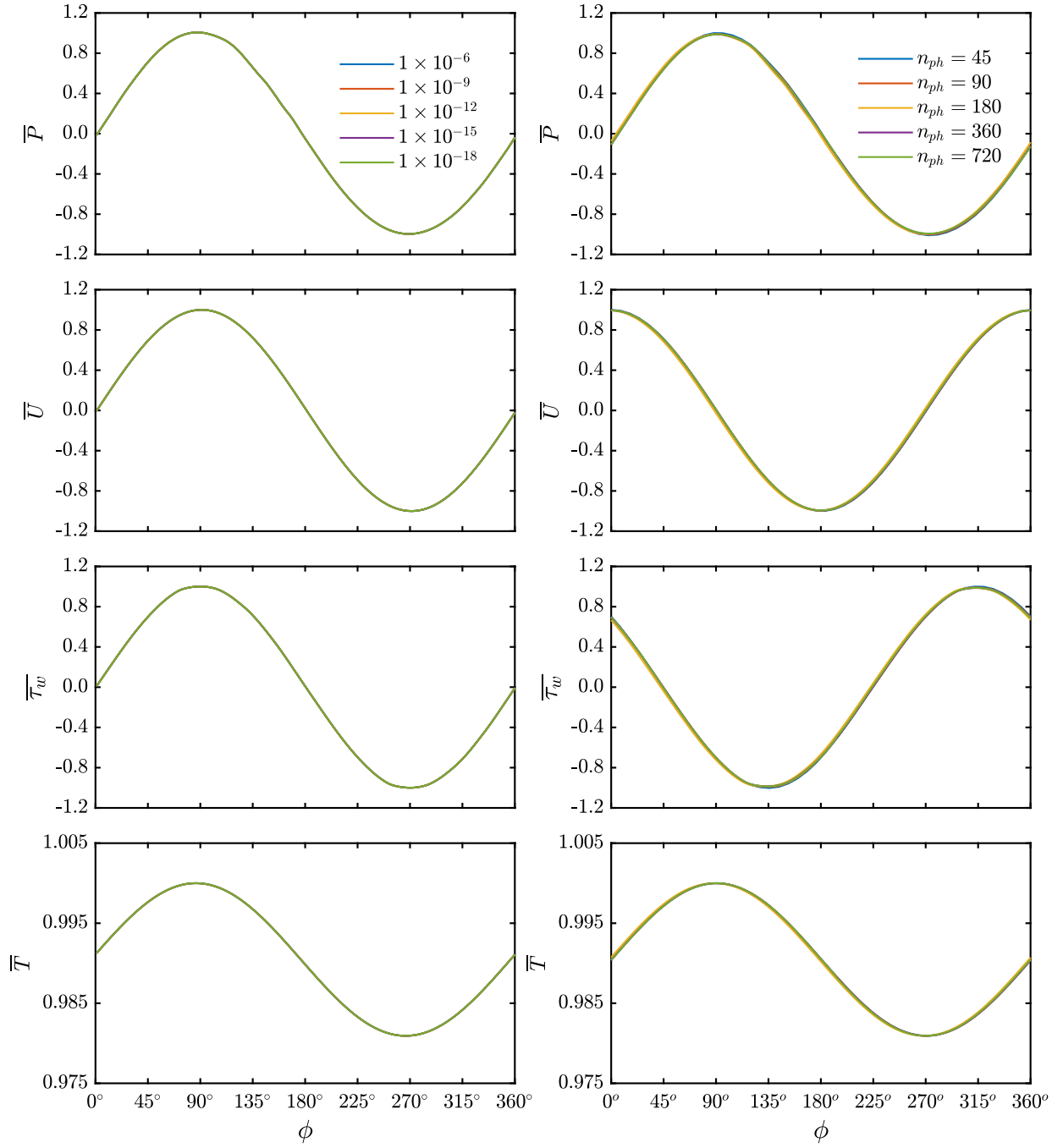
Figure 2.7: Effect of residuals limits (left) and time step size (right) on normalized variables at $Wo = 100$

38

during the unsteady simulation. The hot and cold reservoir diaphragms are represented by a moving domain for the simulation. In FLUENT there are three options for a dynamic mesh solver; smoothing, layering, and re-meshing. Smoothing and re-meshing the dynamic mesh motion were used together to define the deformation in each diaphragm. This deformation was used to model oscillatory flow inside the heat exchanger. The deformation of each diaphragm is controlled by appropriate axial displacements and frequencies. These two parameters which specify the required oscillatory flow are provided by the User Define Function (UDF).

2.3.3.4.1 UDF for Modeling Diaphragms Motion

The simulation run by ANSYS FLUENT has no built-in function to meet the needs of the current simulation to oscillate the diaphragms. However some control of the CFD model is provided by User Defined Functions. They are a text files written in the C program language. For the current study, UDF codes were written for FLUENT. Two UDFs codes were written, one for the 2D axisymmetric model and another for the 3D mode. Both codes depend on the FLUENT macro DEFIN-GRID-MOTION with a sine function to specify the axial displacements and the frequencies of the motion of the diaphragm. The diaphragm motion changes every time step to achieve one cycle of oscillation after 360-time steps. The edges of each diaphragm will be hinged to the boundaries of the reservoirs, and the diaphragm body will move from a maximum at the center to the zero at the edges. The motion was prescibed by defining the displacement of each grid point on the diaphragm as a function of its location and the time as below:

- **For 2D model**

$$z(y,t) = \left(A.\cos\left(\sqrt{\frac{y^2}{R_r^2}} . \frac{\pi}{2} \right) \right) . \sin(2\pi f t) \qquad (2.17)$$

- **For 3D model**

$$z(x,y,t) = \left(A.\cos\left(\frac{x^2 + y^2}{R_r^2} . \frac{\pi}{2} \right) \right) . \sin(2\pi f t) \qquad (2.18)$$

where x, y, z are the coordinates of each grid points on the diaphragm surfaces, A is the axial ampli-
tude applied to the center of each diaphragm, f is the frequency of oscillation, and R_r. is the radius
of the reservoir. These two equations were used to control the frequency and displacement of the
diaphragms to provide the appropriate tidal displacements and Womersley number for each case.
Microsoft Visual Studio 2012 was used to launch FLUENT which is necessary for compiling and
loading UDFs.

2.3.4   Solver Settings

FLUENT 17.2 has a wide variety of models readily available, with an array of settings and cor-
rection factors. For this study, both 2D axisymmetric and 3D simulations have identical settings
except for the gravitational force, which is included in the 3D model to match the experiments. All
simulations use a pressure-based laminar viscous model with specific initial and boundary con-
ditions. The pressure$-$velocity coupling uses the **SIMPLE** (**S**emi-**I**mplicit **M**ethod for **P**ressure
Linked **E**quations) scheme with the finite volume method FVM. The gradient calculation is least
squares cell based, the pressure calculation is second order in spatial discretization. The momen-
tum and energy equations are second order upwind to reduce the numerical errors. The transient
formulation is a second order implicit solver and the time step depends on equation 2.15. All
under-relaxation factors are set to the default FLUENT values which are 0.3, 1, 1, 0.7, and 1 for
pressure, density, body forces, momentum, and energy respectively. The assumptions of the sim-
ulations are those in governing equations for the 2D and 3D models. As mentioned before, the
simulation will continue until the scaled residuals being less than 1×10^{-6} with a sufficient num-
ber of iterations to achieve this limit. The simulation considers constant thermodynamics property
(incompressible) fluid problems. Table 2.6 lists the physical properties of all used materials.

Table 2.6: Physical properties of materials used

Material	Density (kg/m^3)	Specific heat (J/kg.K)	Thermal Conductivity (W/m.K)	Dynamic Viscosity (kg/m.s)
Air (Working Fluid)	1.225	1006	0.024	1.789×10^{-5}
Glass (Tubes walls)	2200	690	1.380	
PVC (Reservoirs Walls)	1350	1000	0.140	
Fiberglass (Insulation)	20	670	0.035	

2.3.4.1 Initial Conditions

2.3.4.1.1 Reservoirs

In all 2D axisymmetric and 3D model simulations, the working fluid (air) in the cold and hot reservoirs was initialized at 300 K and 350 K, and then left to change gradually with time under the effect of oscillation. The reservoirs temperatures were allowed to drop to match the experimental results. Many other studies did not include the effect of the reservoirs, which exists in practical applications. The solid walls, which are participating in conjugate heat transfer, were initialized at 300K.

2.3.4.1.2 Tubes

To make the models more consistent with previous studies, a linear gradient of temperature from hot to cold ends was used in initializing the fluid inside the tubes. This linear gradient will change depending on the tidal displacement and the frequency of oscillation. The linear gradient limits are 300K and 350K which represent the cold and hot reservoirs temperatures, respectively. In the case of a conducting tube wall, the temperature of the glass tube was initialized at 300K, which represents the environment temperature.

2.3.4.2 Boundary Conditions

All other boundaries are imposed as adiabatic boundaries with zero heat flux; therefore, there is no external source of heat and no slip conditions for all the stationary walls and deformed diaphragms. The cold and hot diaphragms have been defined as insulated walls with dynamic motion to oscillate the flow inside the reservoirs back and forth. The boundary conditions are same for the two-dimensional and three-dimensional models with insulated walls. In the 2D-axisymmetric model, the center line was defined in fluent dynamic mesh types as a deformed zone as it will be affected by the motion of the diaphragm. The boundary conditions on both diaphragms will change depending on the imposed axial displacement and the frequency of oscillation. For the conductive glass tube wall, the velocity at the coupling wall between the fluid and solid regions is zero and the heat flux is conserved across this coupling boundary.

2.4 Theoretical Calculations

As mentioned in previous studies, many numerical and analytical studies have been carried out, which depend on fully developed flow, ignoring viscous heat dissipation, and ignoring differential axial conduction [2, 34, 43]. In oscillatory axial pressure gradients, the linearity of the governing equations leads to exact solutions. Results such as the displacement of the fluid along the axis of the tube and the oscillatory thermal conductivity can be calculated using theoretical formulas and compared with numerical data. These results are presented in the appendix .

2.4.1 Tidal Displacement

According to equation A.6 in the appendix, that is derived in previous studies [21, 34, 43] , the tidal displacements in the current study were defined as:

$$\Delta Z = \frac{2}{R^2} \int_0^R \left[\int_0^{2\pi/\omega} u(r,t)\, dt \right] r\, dr \tag{2.19}$$

The numerical data used to calculate the tidal displacements were acquired radially at an axial position equal to half of tube length. These data provide the axial velocity at each radial grid
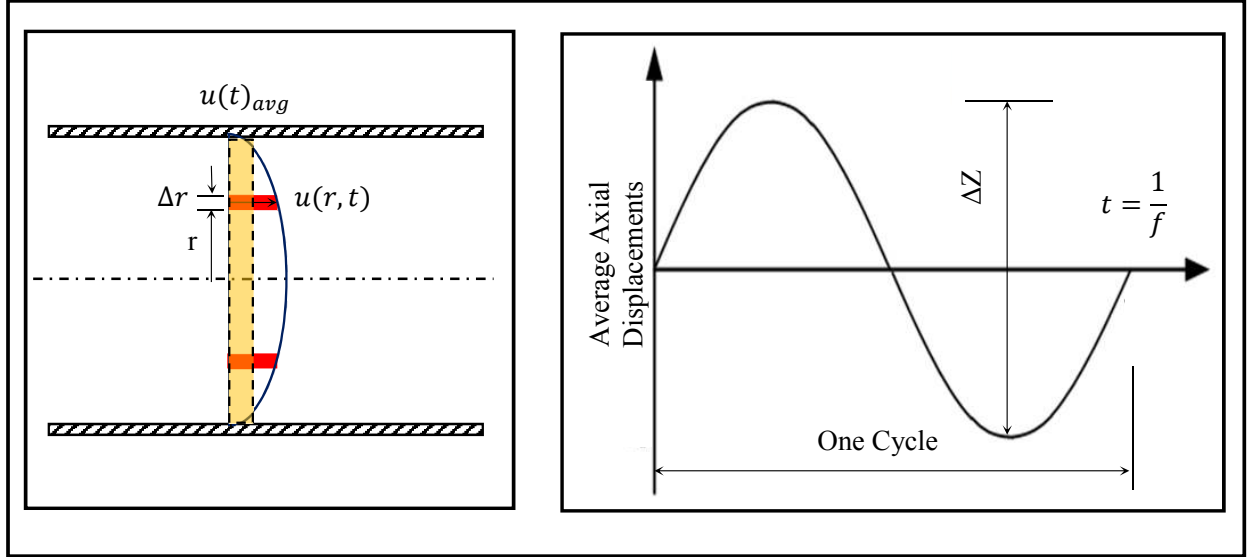
Figure 2.8: Tidal displacement components

point across the tube cross-section. In the current study, data was exported at ten equally spaced positions along the tube every fifteen time steps as an ASCII file. Therefore, we have data every fifteen degrees, which was analyzed by MATLAB to get the area averaged values of required quantities. For each cycle there are twenty-four phase angles of data, which were used to calculate the tidal displacements during one oscillation cycle. The tidal displacement was evaluated at each of fifteen time steps by area averaged velocity calculations as follows:

$$
\begin{aligned}
\Delta Z &= u(t)_{avg}.\Delta t \\
&= \frac{1}{2} \sum_{1}^{n_p} \left[\left(\frac{\sum_{1}^{n} u(r,t).2\pi r.\Delta r}{\pi R^2} \right).15\Delta t \right]
\end{aligned}
\tag{2.20}
$$

where ΔZ represents the maximum axial excursion of the fluid during one cycle of oscillation, $u(t)_{avg}$ is a cross-sectional area averaged velocity at different instants of oscillation, and $u(r,t)$ is the axial velocity at different radial positions, which is available from numerical data that results every fifteen time steps. n and n_{ph} are the number of radial grid points and the number of collected phase angles $(n_p = n_{ph}/15 = 360/15 = 24)$, data were exported at each of 15 time steps. Δt is the size of the time step at each different frequency of oscillations as defined in equation 2.15. Figure 2.8 shows these quantities.

43

2.4.2 Effective Thermal Conductivity in Oscillatory Flow

The effective thermal conductivity, or diffusivity, is an important parameters in the axial heat transfer enhancement for oscillatory flow. Therefore, it is important to calculate the time-averaged thermal conductivity under the effect of oscillatory motion, which is called the oscillatory thermal conductivity (k_{osc}). To determine how effective the overall heat transfer is, we introduce an effective thermal conductivity for both conductive and convective heat transfer inside the tubes as [5]:

$$\dot{Q}_{cond} + \dot{Q}_{conv} = -k_{eff}.A_t \left[\frac{T_H(t) - T_C(t)}{L} \right] \tag{2.21}$$

where k_{eff} is the effective thermal conductivity, which represents the sum of the molecular and oscillatory convective contributions. The definition in Equation 2.21 is useful in comparing the oscillatory thermal conductivity with a molecular counterpart to see how much greater it is. The equation also represents the rate of heat transfer from the hot reservoir to the tubes Q_{out}. By neglecting the work done inside the reservoirs and assuming the reservoirs are perfectly insulated so there is no heat added from the external source $(Q_{in} = 0)$, the heat balance according to the First Law of Thermodynamics was applied to the hot reservoir to obtain the effective thermal conductivity k_{eff}. Figure 2.9 shows the control volume for the heat balance for the hot reservoir.
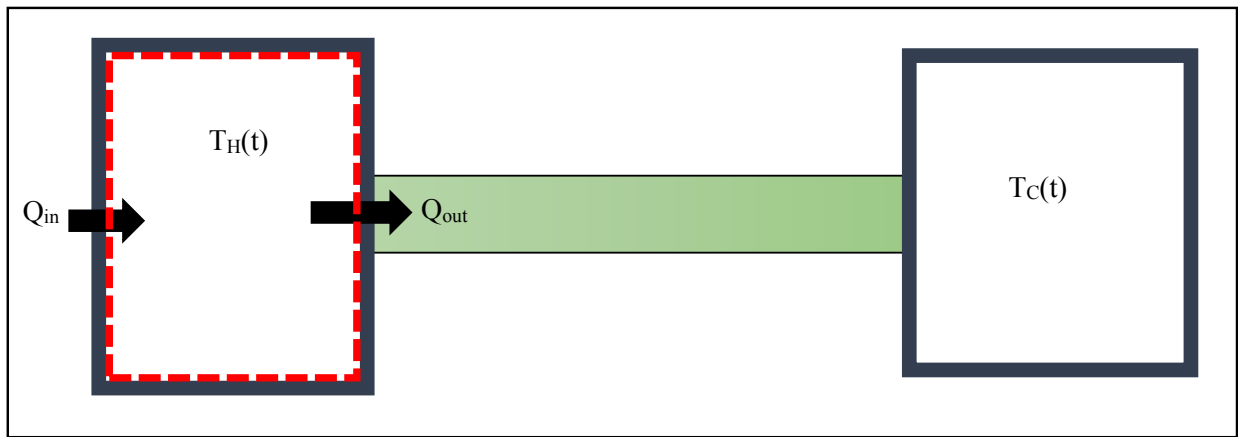
Figure 2.9: Hot reservoir heat balance

$$\sum \dot{Q} + \sum \dot{W} = \frac{dE}{dt} \tag{2.22}$$

and by neglecting the work done inside the reservoir:

$$\dot{Q}_{in} - \dot{Q}_{out} = mC_v \frac{dT_H}{dt} \tag{2.23}$$

As the reservoirs are insulated, there is no heat added to the hot reservoir from external sources:

$$-\dot{Q}_{out} = mC_v \frac{dT_H}{dt} \tag{2.24}$$

where $\dot{Q}_{out}$ equals to the net heat flux through all tubes:

$$\dot{Q}_{out} = -k_{eff}.A_t \frac{\Delta T(t)}{L} n_t \tag{2.25}$$

$$\left(-k_{eff}.A_t \frac{\Delta T(t)}{L} \right) n_t = \rho.V_H.C_v \frac{dT_H}{dt} \tag{2.26}$$

$$k_{eff} = \frac{\rho.V_H.C_v \frac{dT_H}{dt}}{A_t \frac{T_H(t) - T_C(t)}{L} n_t} \tag{2.27}$$

$$= k_{osc} + k$$

$$k_{osc} = k_{eff} - k \tag{2.28}$$

where $\frac{dT_H}{dt}$ represents the drop in hot reservoir temperature with time and $T_C(t)$ and $T_H(t)$ are the cold and hot reservoir temperatures as functions of time. V_H, ρ, A_t and n_t represent the hot reservoirs volume, fluid density, tube cross-section area, and number of tubes respectively. Figure 2.10 shows the temperature gradient of the cold and hot reservoirs over time, in an experiment in which they are initially at different temperatures, but then allowed to transfer heat axially with flow oscillation.

The oscillatory thermal conductivity varies with Womersley number and tidal displacement. To compare experimental results with numerical and analytical results, it is necessary to normalize
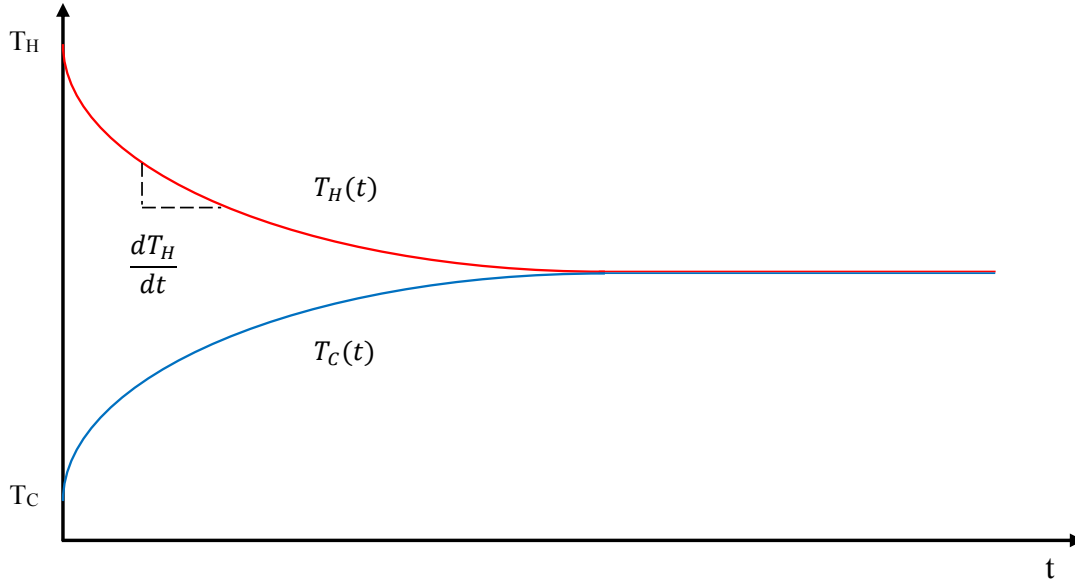
Figure 2.10: Hot and cold reservoirs temperature gradient

data. Hence, k_{osc}/k will be normalized by the pressure gradient amplitude (P), tube radius, and the fluid properties by following the normalization in equation A.14 that is given in the appendix . From experiments, the hot and cold temperatures and pressures were recorded for comparison with numerical results under the same initial and boundary conditions. Therefore, the temperature gradient of the reservoirs is available at different time steps. Also, the pressure gradient amplitudes P were measured to normalize the experimental data, allowing a comparison with numerical prediction data. The pressure gradient was calculated by dividing the instantaneous pressure difference between the hot and cold reservoir by the tubes length. Table 2.7 summarizes all numerical cases that were considered in the current study for the 2D and 3D simulations.

2.5 CFD Validation

Numerical prediction needs verification steps to achieve trustworthy results. In this section, the reliability and the accuracy of the CFD approach were tested. The validation has been carried out by comparing the numerical results with previous studies for fully developed flow, viscous fluid, and incompressible flow with no temperature dependency for the properties. As mentioned before,

46

Table 2.7: Numerical tests without viscous heat dissipation

2D-Axisymmetric								3D
Wo	**ΔZ/L**							**ΔZ/L**
0.1	0.12	0.24	0.36	0.48	0.72	0.96	1.2	
1	0.12	0.24	0.36	0.48	0.72	0.96	1.2	0.12
3	0.12	0.24	0.36	0.48	0.72	0.96	1.2	0.12
5	0.12	0.24	0.36	0.48	0.72	0.96	1.2	0.12
7	0.12	0.24	0.36	0.48	0.72	0.96	1.2	
10	0.12	0.24	0.36	0.48	0.72	0.96	1.2	0.12
20	0.12	0.24	0.36	0.48	0.72	0.96	1.2	
50	0.12	0.24	0.36	0.48	0.72	0.96	1.2	
100	0.12	0.24	0.36	0.48	0.72	0.96	1.2	

the previous studies used the above conditions in their calculation. In the current study, all results have been displayed in a normalized form. The validation consists of two main parts: a fluid flow validation and a heat transfer validation. For the first part, there are several results from previous studies to validate it. For the heat transfer validation, there are few normalized data with which we can compare, as many previous studies presented their results without normalization. Therefore, the analytical results that have been presented by Brereton and Jalil [43] were used in both validations as they provide normalized data for fluid mechanics and heat transfer enhancement. They are given in the appendix .

2.5.1   Fluid Mechanics Validation

An important parameter in the current problem, which is derived from the momentum and continuity equations, is the tidal displacement. According to analytical solutions (see equation A.7) $\Delta Z/(P/\rho\omega^2)$ depends only on the dimensionless frequency *Wo*. All calculations and comparison depend on the fluid motion and the axial displacements of the fluid inside the tubes. Therefore, it is an important parameter in the validation. To validate the numerical results, the dimensionless tidal displacements were plotted as a function of the flow Womersley number as shown in Figure 2.11. The tidal displacement was calculated from the area-averaged axial velocity as defined in Equation 2.20. The present numerical results for the 2D and 3D models have been compared with
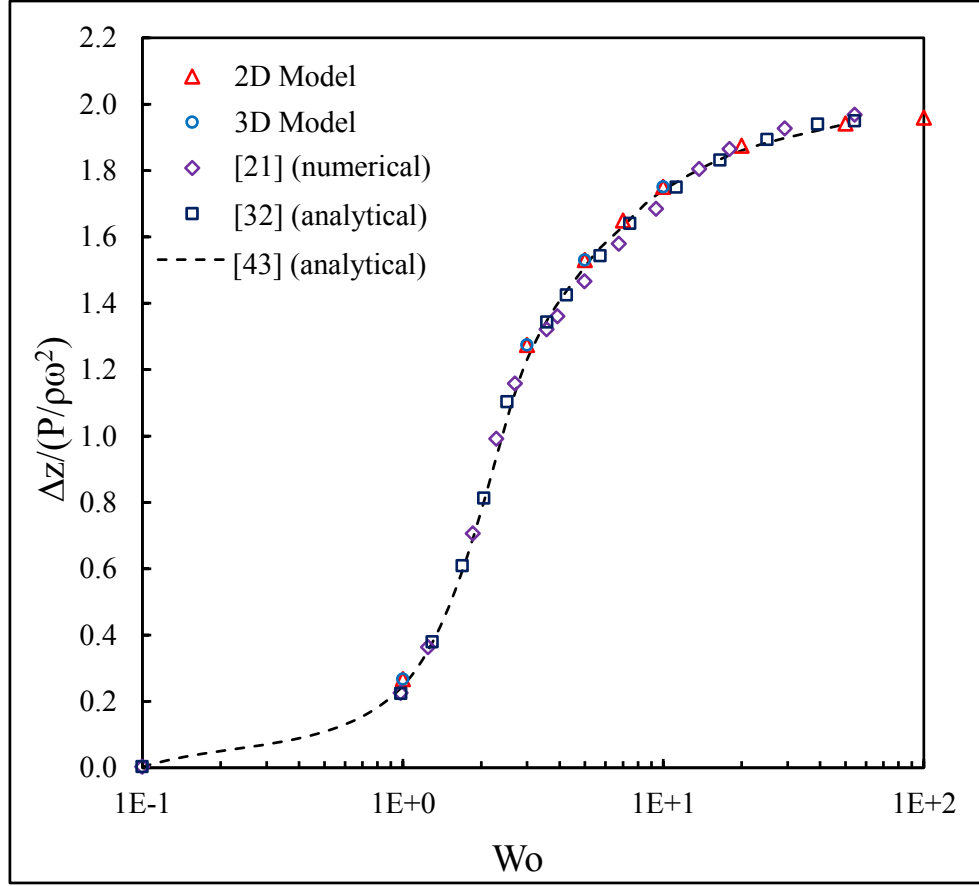
Figure 2.11: Dimensionless tidal displacement as a function of flow Womersley number

studies of fully developed incompressible flow [21,32,43] at low tidal displacement $(\Delta Z/L = 0.12)$ to be consistent with previous studies. Because of the simulation cost, the 3D model has only four data points which are at $Wo = 1, 3, 5$, and 10 for small tidal displacements. These four Womersley numbers are chosen to be identical to the frequencies of the experiments.

All results presented are for models without conductive walls, to match the available analytic results. The amplitude of the axial displacement ΔZ of the fluid during the oscillatory motion was normalized by the amplitude of the pressure gradient between the hot and cold reservoirs divided by the density times the square of the circular frequency [43]. The tidal displacement was measured at the middle of the tube $(z = 0.5L)$. The results showed that the axial displacement of the fluid inside the tube is proportional to $P/\rho\omega^2$ with a constant of proportionality varying from 0 to 2 depending on Womersley number. This comparison indicates that the present study has a

high accuracy related to the 2D and 3D models fluid mechanics predictions and that the dynamic mesh is used correctly. Therefore, under approximately the same boundary conditions and for this range of Womersley number the numerical prediction appears to be trustworthy.

2.5.2   Heat Transfer Validation

The thermal energy equation (Eqs 2.10 and 2.14) validation is more difficult as some terms were neglected in exact solutions. One such term is the differential axial conduction term $(\partial^2 T/\partial z^2)$, which can have a significant effect at low Peclet numbers (Pe). The axial conduction can effect the energy equation for steady flow if $Pe < 100$ [81] or at low frequencies for unsteady flow. This effect is significant especially with gases at low Reynolds numbers, whereas for most liquid the axial conduction is seldom of significance. Figure 2.12 shows the variation of normalized axial heat transfer enhancement and Peclet numbers as a function of Womersley number for the 2D models with insulated tube walls. It is clear from the figure that the agreement between the current numerical prediction and the exact solution is good at Womersley numbers larger than about three.

In the current study, for Womersley number equal to 3, the Peclet number is about 40. The discrepancy between the exact and numerical data starts at a region close to about $Pe < 50$ which is for $Wo < 3$ for incompressible flow and $\Delta Z/L = 0.12$. In addition to the differential axial conduction term $(\partial^2 T/\partial z^2)$ being ignored in the exact solution, fully developed flow and the absence of the reservoir entrance/exit effects are assumed. These effects can play an important role in explaining discrepancies between the analytic and numerical solutions, as the numerical solution considers all terms in the energy equation. As Womersley number increases, the numerical results become closer and match the analytic solution. Low Womersley numbers are for frequencies less than one cycle per second ($Wo < 1$), which provides the fluid with enough time for radial diffusion over the entire radius. This axial molecular diffusion was ignored in the exact solution. This comparison suggests that the numerical predictions are reliable and accurate, as they matched the exact solution when analytic assumptions held. Therefore, the contribution of the differential axial conduction is significant at low Womersley numbers and varies depending on the tidal displace-

ment. At low Womersley numbers, the oscillation will be close to quasi-steady. Joshi et al. [4] in their experiments showed that their experimental data starts to differ from the exact solution data at a Womersley number of around 3. A description of the unsteady axial conduction process is provided in chapter four.
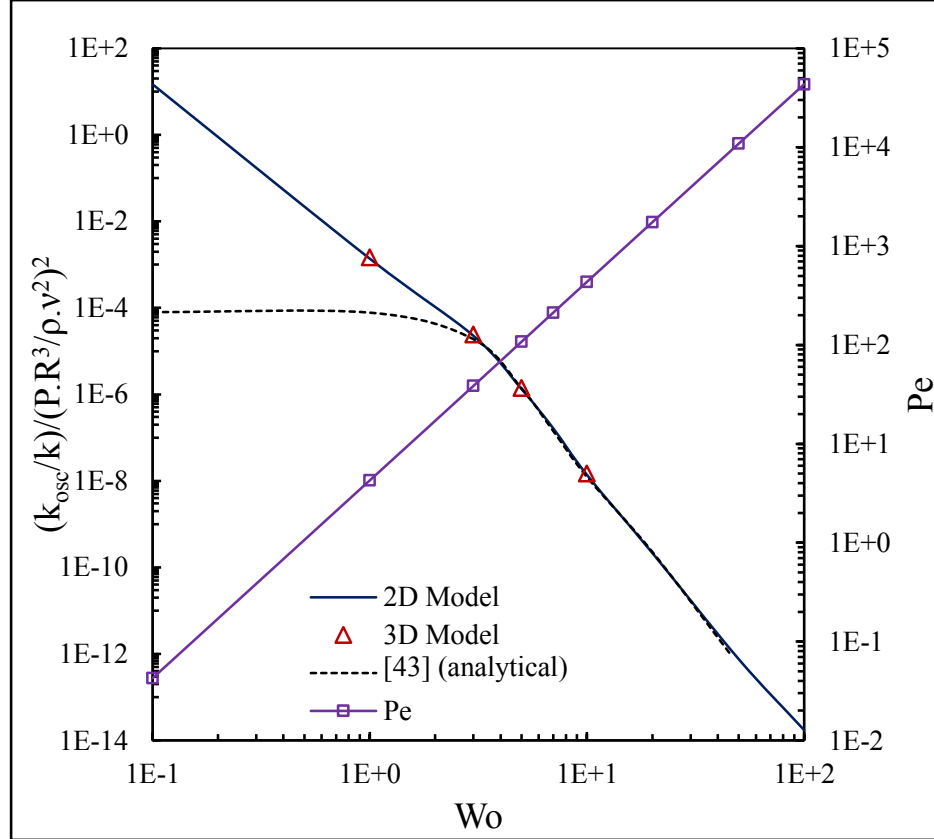
Figure 2.12: Normalized axial heat-transfer enhancement and Peclet numbers as a function of flow Womersley number

2.5.3 Instability Criteria

Akhavan et al. [82] and Hino et al. [83] proposed criteria for oscillatory flow instability and turbulent motion initiation. They stated that if the oscillatory Reynolds number, which is calculated based on the averaged cross-sectional-area velocity amplitude $|u_{avg}|$ and the characteristic length represented by Stokes layer thickness δ_{st} as defined in equation 2.29, exceeded 500, instability and turbulent motion appear. David and Grotberg [84], Van der A et al. [85], and Yuan and
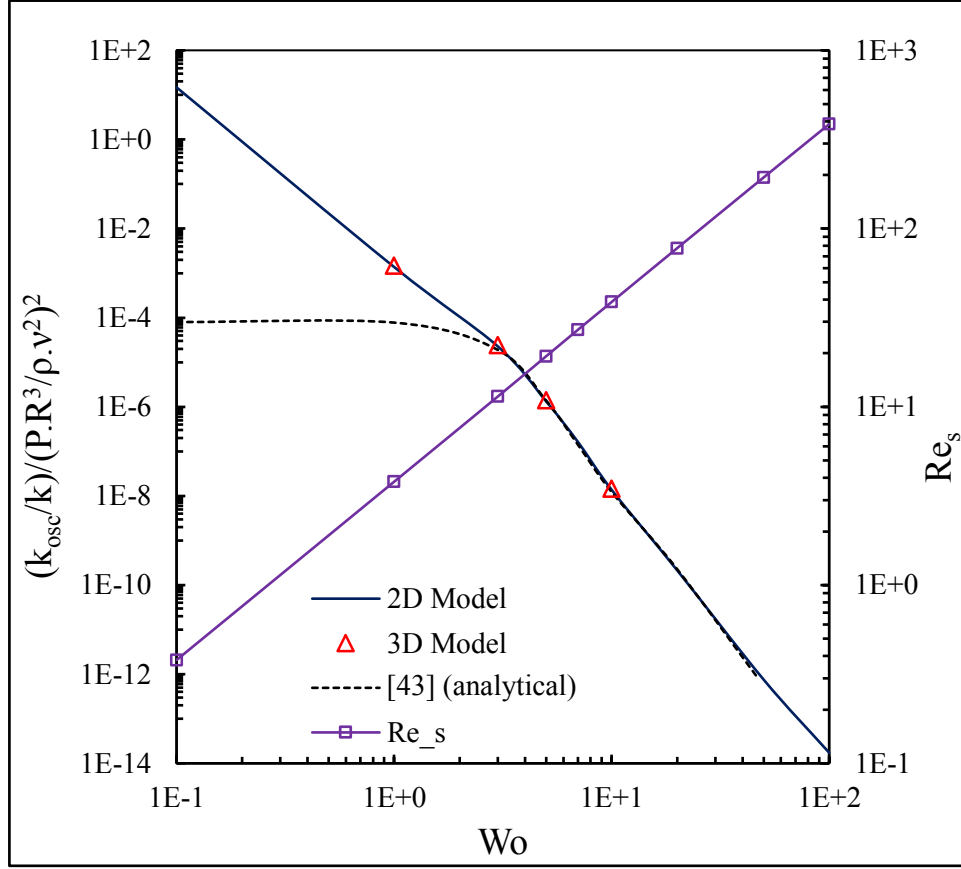
Figure 2.13: Normalized axial heat-transfer enhancement and oscillatory Reynolds numbers as a function of flow Womersley number

Madsen [86] in their experimental results observed that during the deceleration phase of the oscillatory motion, transition to turbulence arises for $500 < Re_s < 854$ or for Reynolds number of order $O(10^6)$, where $Re = |u_{avg}|.R/\nu$. These validations are only for laminar flow, which is for oscillatory Reynolds number less than 500. Figure 2.13 shows the variation of normalized axial heat transfer enhancement and oscillatory Reynolds number as a function of Womersley number at low tidal displacement $(\Delta Z/L = 0.12)$. The figure shows that the maximum value of Re_s is less than 500, the limit proposed for the transition to turbulent flow. All results of $Re_s > 850$ were ignored and excluded from any proposed correlations.

$$Re_s = \frac{|u_{avg}|.\delta_{st}}{\nu} \qquad (2.29)$$

2.6 Summary of Validation Studies

From the results of section 2.5, it appears that the fluid mechanics computations agree with analytical solutions at all frequencies of oscillations studied. However, the companion heat transfer computations agree with analytical solutions only for oscillation at Womersley number greater than three. Therefore, the computational technique is validated for $Wo > 3$ and is believed to be accurate at lower Womersley numbers, when discrepancies arise with analytical solutions because the assumptions on which the analytical solutions are based may not apply.

CHAPTER 3

EXPERIMENTAL DESIGN AND RESULTS

3.1 Introduction

In the present study, both numerical predictions and an experimental investigation were carried out to explore the effect of oscillatory flow conditions on axial heat transfer performance. To validate the numerical models, an experimental apparatus was designed. In this chapter, the experimental setup and the procedure are described in detail. A description of the heat exchanger parts, their assembly, instrumentation devices, experimental measurement procedures, and the objectives of experiments are given in this section. The setups for the oscillatory flow control and the methods that were used to collect the data are also described.

3.2 Objectives and Design Criteria

The objectives of the experimental setup are represented by two main goals:

1. To validate the 2D and 3D numerical models over a range of tidal displacements and Womersley numbers.

2. To study the effect of unsteady axial conduction at $Wo < 3$.

Designing appropriate experiments that can serve the desired purpose requires considerations of fluid leakage, heat losses, rig capability to oscillate, and the system cost. The size of the heat exchanger was chosen to be compatible with an available vibration exciter and to be suitable for numerical modeling. In previous experimental studies [4,5,7], oscillation was forced from one side only, while in other studies pistons were used to oscillate the cold and hot fluid in both reservoirs [8, 87] from both sides.

1. Bundle of Glass Tubes	2. Insulation (Fiberglass)	3. PVC Reservoir	4. Electrical Insulation
5. Resistance heating wire	6. Silicon Diaphragm	7. Hot Reservoir	8. Cold Reservoir
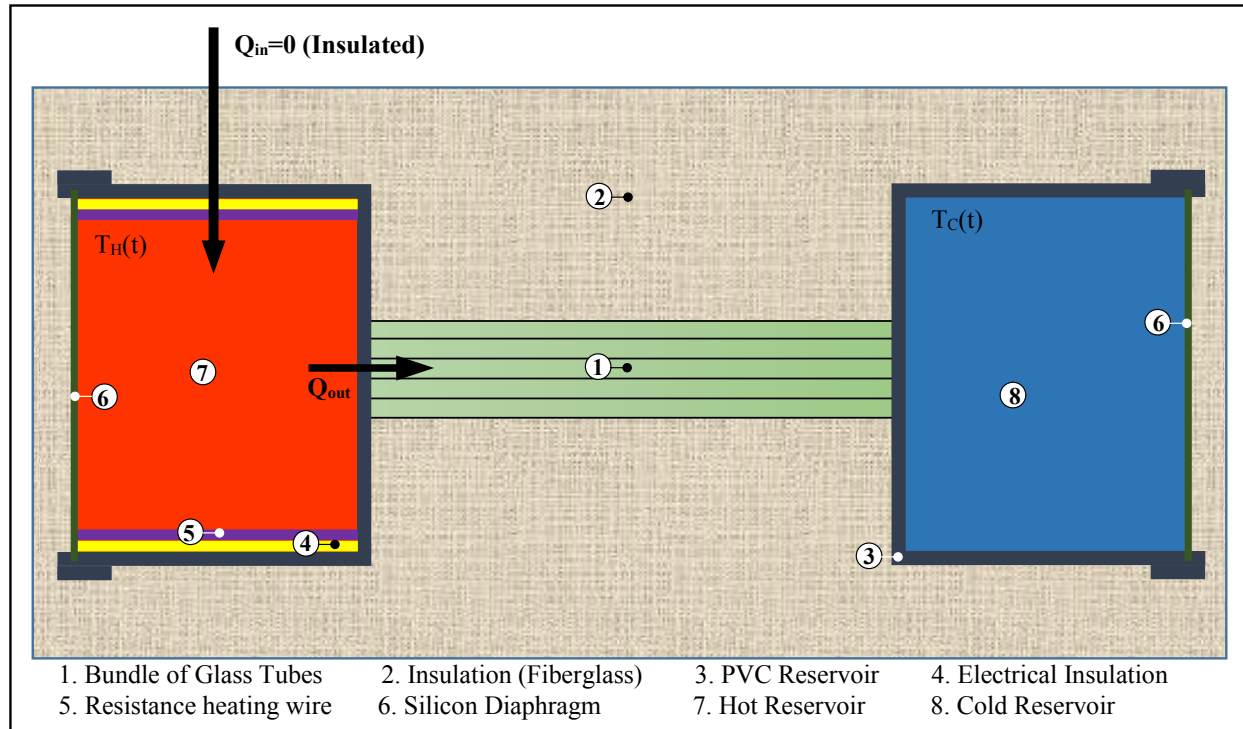
Figure 3.1: Schematic of the heat exchanger

3.3 Experimental Apparatus

The principal components are the vibration exciter, a data acquisition system, and two reservoirs. One reservoir was provided with a heater and was insulated completely. The tidal displacement was measured by flow visualization as the flow inside the tubes is visible. Air was used as the fluid to transfer heat axially along a bundle of tubes between the cold and hot reservoirs, by oscillating the reservoirs' diaphragms.

3.3.1 Heat Exchanger Design and Fabrication

The heat exchanger was designed to be of a size that minimizes heat losses, oscillates by driving hot and cold diaphragms simultaneously, and minimizes leakage. Figure 3.1 shows a drawing of the heat exchanger that was manufactured and used in experiments. It consists of a bundle of seven parallel tubes of $5mm$ inside diameter and $1.5mm$ thickness with length of $100mm$ and connects the hot and cold reservoirs. The hot reservoir was used as the heat source, while the cold reservoir

was the heat sink. The tube material is fused quartz whereas the two reservoirs are PVC (polyvinyl chloride). Fiberglass sheets were used to insulate the components. The physical properties of all materials and dimensions are specified in Table 2.6 and Figure 2.2. The 3D numerical model is identical to the experimental heat exchanger in all physical attributes.

Quartz and PVC provide simplicity in cutting, gluing, and assembling processes. In the early stage of testing the heat exchanger, it was disassembled several times as a result of leakage. The reservoirs have the same dimensions of $50mm$ length and $50mm$ diameter with $4mm$ wall thickness. The orientation of the hot reservoir above the cold reservoir in vertical direction is reproduced with the 3D model. This arrangement minimizes the gravitational effects such as natural convection. The seven glass tubes were attached to each other and were held together after insulation inside a cylindrical plastic tube. Each reservoir was fitted with a flexible silicon rubber sheet of $1/6$ inch thickness as a diaphragm which connects to the vibration exciter. Kanthal A-1 Ribbon resistance heating wire ($0.5mm \times 0.1mm$) was used to heat the hot reservoir space. The resistance wire was sewed through a series of holes in an insulation paper (DuPont Nomex paper Type 410), which offers high inherent dielectric strength, mechanical toughness,flexibility and resilience.

These components were combined together and insulated with fiberglass insulation around all sides to avoid heat losses during experiments as shown in Figure 3.2. The upper heat exchanger in this figure was used without insulation, so that flow visualization could be used in measuring the tidal displacement of the oscillatory flow. The valve at the end of the reservoir was used to fill both heat exchangers with water to check if there is leakage through the connections. This valve was removed from the insulated heat exchanger after checking but retained for liquid visualization purposes. The heating sheet was attached to the internal surface of the reservoir. The heat element was provided with the power by a Tenma 72-110 10A Variable Autotransformer, monitored by an LCD digital wattmeter.
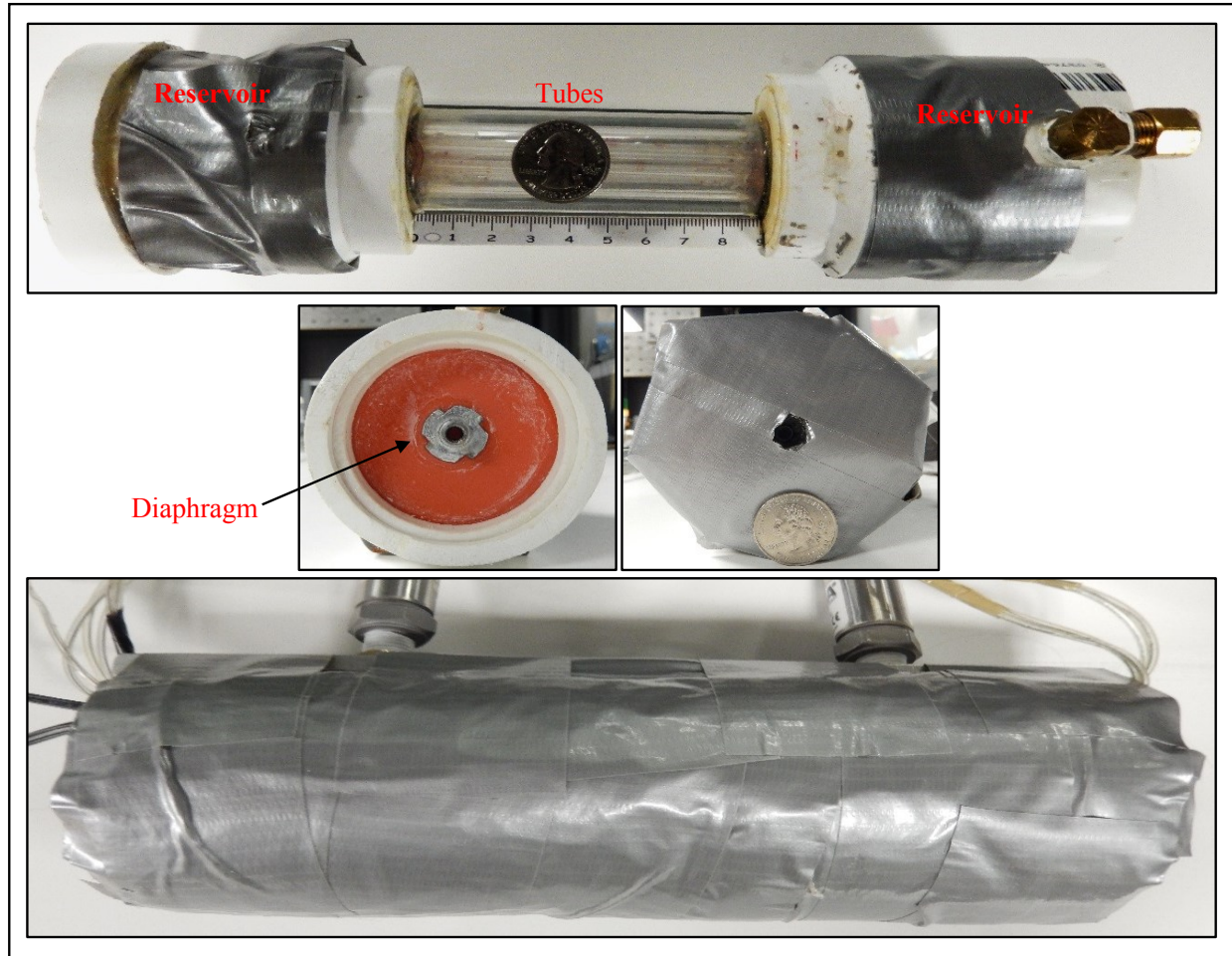
Figure 3.2: Assembled heat exchanger and reservoirs

3.3.2 Vibration Exciter and Its Components

A Bruel & Kjaer Permanent Magnetic Vibration Exciter Type 4808 was used to achieve the oscillatory motion of the fluid inside the heat exchanger. The heat exchanger was connected to the shaker by a frame. The two diaphragms were connected so as to oscillate simultaneously with the same amplitude. The exciter was controlled through the power supply by setting the frequency and driving voltage. A Bruel & Kjaer sine/noise generator type 1049 was used to select the required frequencies. To get a variable amplitude, a Bruel & Kjaer power amplifier type 2712 was used to drive the exciter with the appropriate amplitude at each frequencies. A digital dial gauge attached to the oscillated frame was used to measure the amplitude of the center of the diaphragm.

3.3.3   Data Acquisition

Tidal displacement, temperatures, and pressure are the three main quantities that were monitored and recorded in each experiment. One purpose of the experiment was also to validate the numerical models. The 3D numerical model was run for five seconds and the experiments run for about two minutes and compared over five seconds.
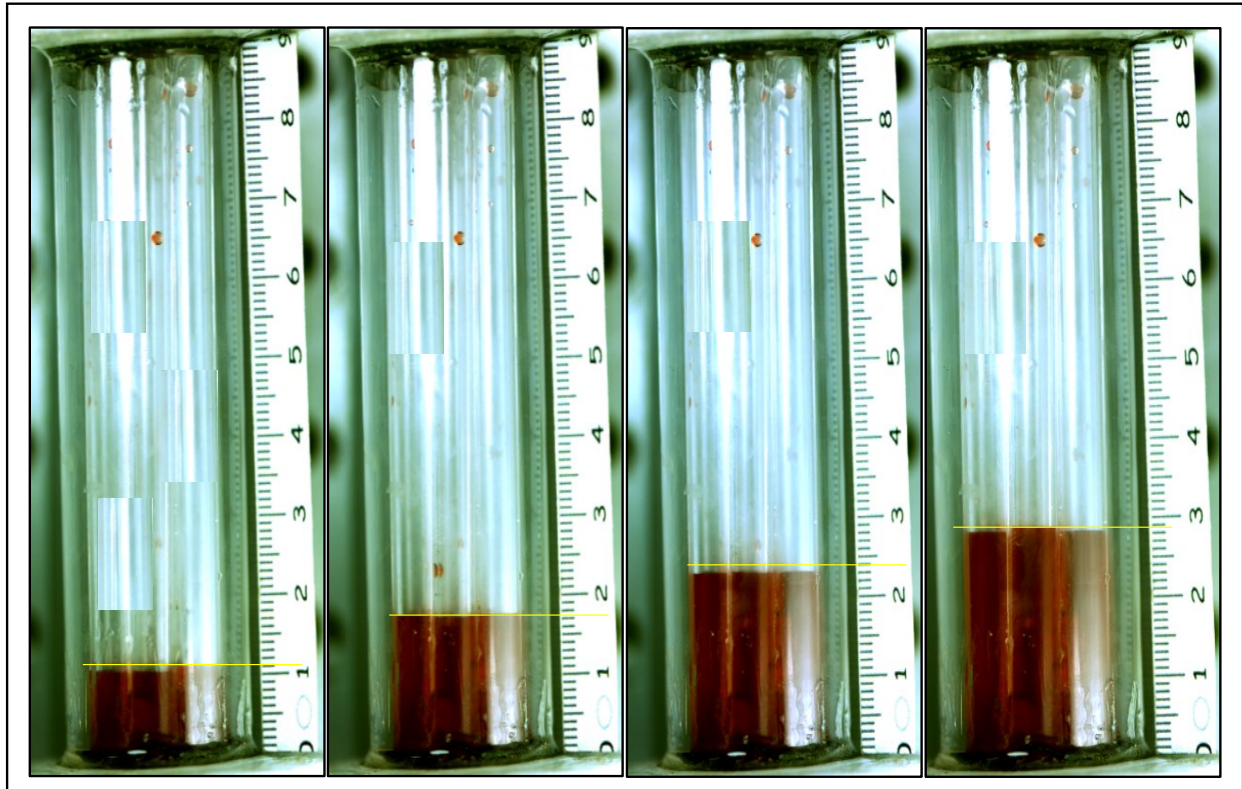
Figure 3.3: Flow displacement inside the tubes

3.3.3.1   Tidal Displacement

To measure experimentally the axial tidal displacement ΔZ, which represents the axial displacement in which the fluid moves every half period of the oscillatory cycle, inside the tubes for each diaphragm amplitude and frequency, the heat exchanger was positioned vertically and the lower reservoir filled with dyed water. A PHOTRON FASTCAM SA4 camera was used to observe the fluid displacement for different frequencies and amplitudes. PFV (Photron FASTCAM Viewer)

software was used to record the flow oscillatory motion. To find the peak to peak tidal displacement, a scale was attached to the side of the tubes as a reference to calculate the tidal displacements as shown in Figure 3.3.

3.3.3.2 Temperature and Pressure

The temperatures and pressures for the hot and cold reservoirs were acquired for each experiment with a 4-Slot, USB CompactDAQ Chassis (cDAQ 9174).A DAQ NI 9211 4-Channel, ±80mV C series was connected to the chassis to collect the temperature data of the thermocouples of the hot and cold probes. Each reservoir was fitted with two OMEGA thermocouples type T (COCO-015) of 0.38 mm diameter and 0.80 second response time with standard limits of error 0.75% to measure the temperature in each one. A DAQ NI 9205 $\pm 10V$, $250kS/s$, 16-Bit, 32-Channel C Series Voltage Input Module was used to collect pressure data in hot and cold reservoirs.

Omega PX309-015CGV pressure transducers were used to measure the amplitude of pressure oscillation with response time < 1 ms and error ± 0.25 of full scale. The pressure transducers were energized by an EXTECH 382203 analog display DC power supply. LabVIEW 2016 was used to create the code required for the current purposes. The sample rate of data was set at $1kHz$. The pressure gradient could be determined as the difference between reservoir pressures divided by the length of the connecting tubes, since the pressure gradient is uniform at any instant in time in a fully developed flow.

3.3.3.3 Other Experimental Details

Figures 3.4 and 3.5 show a schematic diagram and a photograph of the oscillatory flow experimental components. The pressure transducers were installed in middle of the reservoirs, where the T type thermocouples were installed at $(1/4)$ and $(3/4)$ of the reservoir's length locations to determine average value for the entire space. To minimize the effect of heat loss from the heat exchanger, each experiment ran for two minutes, but the data compared with numerical prediction for only first five seconds as the heat losses expected to be small. The hot and cold reservoirs

diaphragms were oscillated together simultaneously by a solid frame fabricated for this purpose. The frame was connected to the shaker where the heat exchanger clamped to a vertical stand to keep it fixed through the oscillatory motion.

Figure 3.4: Schematic of the experimental setup

3.4   Experimental Procedure

Transient experiments were run for four different diaphragm amplitudes, chosen to provide tidal displacement less than the tube length and $Wo = 1, 3, 5, 10$ for each tidal displacement. This range of measurements was considered to validate the numerical 3D model results.

The experiments began by providing the wave generator with the desired frequency and adjusting the amplifier to the appropriate amplitude. Then, we provide the hot reservoir with power
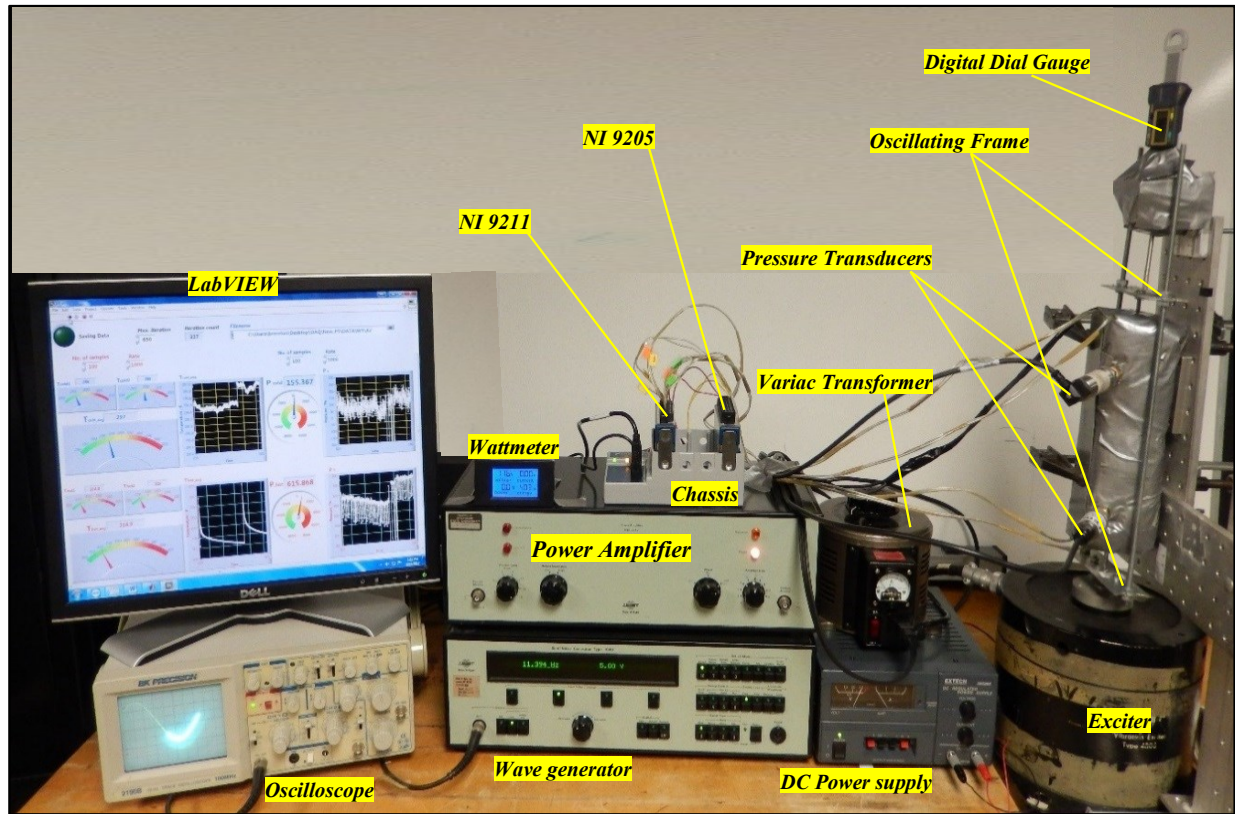
Figure 3.5: Photograph of the experimental components

through the heat element and monitor the average temperature of the hot reservoir without oscillation. The hot reservoir is heated to about 380K. We then turned off the heating element and turn on the shaker. The LabVIEW code was set to start acquiring data when the average temperature of the hot reservoir reached 350K and did so for two minutes. When the oscillation began at the desired amplitude and frequency, the transport of heat from the heat source to the sink through the tubes began. The temperature in the hot reservoir initially drops continuously with time as a result of the oscillatory motion. The gradient in temperature depends on the tidal displacement and Womersley number. The conductive walls were included in the numerical 3D model to allow an authentic comparison, with the only assumption made being the neglect of heat loss to surroundings. Including the conductive walls in the 3D model helps avoids making the assumption of no loss through the walls of the reservoirs and walls of the tubes but increases the simulations costs. In addition, the assumption of insulated walls may not be accurate with any amount of insulation. Therefore,

60

the effect of heat losses through the walls and insulation should be very similar in experiments and in the calculation for the 3D model numerical predictions.

In experiments, it is normal to incur errors. The physical properties of the fluid include thermal conductivity, the kinematic viscosity, and the density. All these properties are temperature dependent. Therefore, the 3D numerical model simulations were set to depend on temperature dependent properties to minimize these effects. Any deviation in dimensions between the experiments and the numerical model may cause errors. The numerical model has the precise dimensions specified in the design, but the experiments dimensions may be accurate only to measurement tolerances. The tube length is 100*mm* but through the cutting process, the length has about 0.5*mm* tolerance. The same issue arises with the tube radius, reservoirs length and diameters, and fitting parts.

Another error arose in the tidal displacement measurements with a high-speed camera in flow visualization. The experiments depended on diaphragm displacement, which was monitored by the digital dial gauge to specify the tidal displacements. The first experiments were intended to determine the tidal displacement, which is defined in sections 2.4.1 and 3.3.3.1, at different frequencies and diaphragm displacements. These data were obtained using the first heat exchanger, fabricated for this purpose to be able to observe the fluid inside the tube as shown in the upper image of Figure 3.2. In the insulated heat exchanger, which has all components attached, the diaphragm displacements were assumed to match the displacements used in flow visualization. We should mention here that the tidal displacement could vary with frequency for the same diaphragm amplitude because of different modes of vibration. Therefore, it may not be accurate to assume the displacement of the diaphragm or the piston leads to the same fluid tidal displacement for all frequencies. With a digital dial gauge, we tried to minimize the error by specifying the same amplitude. In the worst case, the error does not exceed 0.01mm according to our observation, which is about 1% for smallest displacement and 0.02% for the largest displacement (5*mm*) of the diaphragm. The temperature and pressure are measured simultaneously and recorded over time. This procedure was repeated for different cases. All data were analyzed and evaluated by MAT-LAB programmed software to calculate the oscillatory thermal conductivity and the amplitude of

pressure gradient. The amplitude of pressure gradient *P* was calculated by dividing the pressure difference between the hot and cold reservoir by the tube's length. The drop in temperature was fitted with an exponential fitting function to calculate the slope of temperature gradient at different time steps.
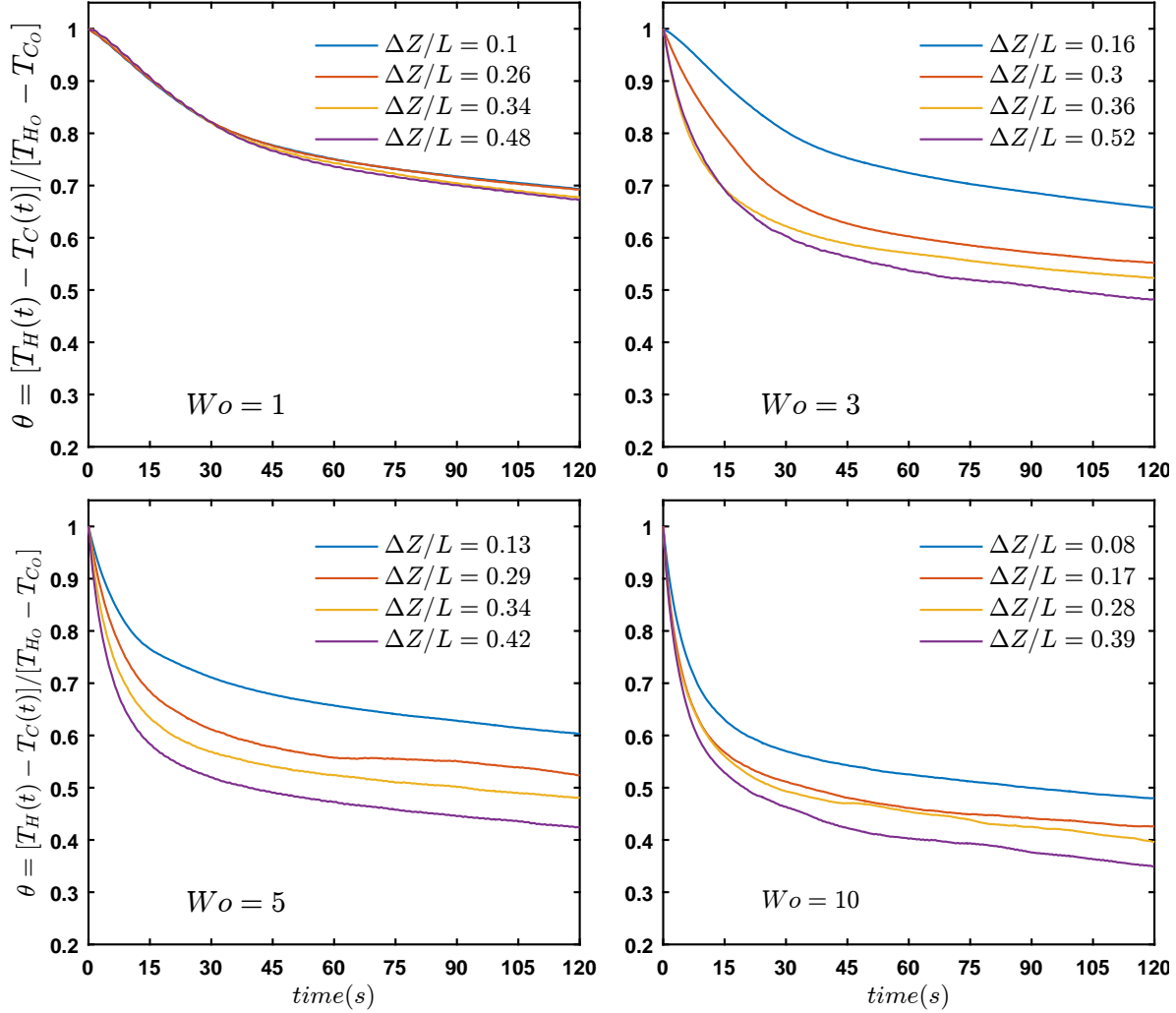
Figure 3.6: Experimental dimensionless temperatures gradient for different amplitudes and Womersley numbers

3.5 Temperature Drop Measurements

In these transient experiments, the temperatures for cold and hot reservoirs are acquired for different Womersley numbers and tidal displacements. When the oscillatory motion begins, the heat transport between the two reservoirs through the tubes is initiated. Figure 3.6 shows the normalized

temperature gradient at different fluid amplitudes and Womersley numbers. Each curve represents the dimensionless temperature θ values, which depend on the hot and cold reservoir temperatures variation over time $T_H(t)$ and $T_C(t)$ relative to the initial temperatures values $T_{H_o} = 300K$ and $T_{C_o} = 300K$. From the figure, it is clear that the drop in temperature depends on tidal displacement and Womersley number. Therefore, any oscillatory enhancement of axial heat transfer depends mainly on these two parameters. The results are presented in terms of axial flow displacement as the tidal displacements for Womersley number higher than 10 from flow visualization are untrustworthy. Also, the response time of the pressure transducers longer than the required time step for acquiring data.

Figure 3.6 illustrates the variation of measured dimensionless temperature gradient for the hot reservoir with four different axial diaphragms displacements and for four Womersley numbers. It is clear that the temperature gradient grows with an increase in the fluid displacement by different rates depending on Womersley number. At low Womersley numbers, the temperature drop with increasing the tidal displacement is not significant. At low Womersley numbers the cyclic advection/diffusion processes of the axial and radial heat transport is slow, which provides an enough time for the fluid to reach an instantaneous steady condition. Therefore, there is no significant effect for the tidal displacement in this developed flow conditions. An increase in Womersley number leads to an increase in the rate of temperature drop for each tidal displacement. To avoid the heat losses errors, the first five seconds of these results are used to validate the numerical predictions for the 2D and 3D models as the heat losses are small and are plotted in Figures 3.7 and 3.8 in sections 3.6.1 and 3.6.2.

3.6 Experimental Validation

The numerical results were validated against analytical solutions in chapter 2. The 2D and 3D models were identical in size to the experimental heat exchanger. The validation has been carried out by comparing the numerical results with available experimental results for the first five seconds to minimize the heat losses effects. Table 3.1 summaries all experimental cases that were

considered in the current study. The validation consists of two main parts: fluid flow validation and a heat transfer validation. From experiments, trustworthy data were obtained for four different Womersley numbers and four different tidal displacements at each *Wo*.

Table 3.1: Experimental tests

Experimental Cases																
Wo	1				3				5				10			
ΔZ/L	0.1	0.26	0.34	0.48	0.16	0.3	0.36	0.52	0.13	0.29	0.34	0.42	0.08	0.17	0.28	0.39

3.6.1 Fluid Mechanics Validation

The tidal displacement is an important parameter in oscillatory flow problem, which is determined by the momentum and continuity equations for a given pressure gradient. Therefore, it is considered as a validation reference. To validate the results, the measured dimensionless tidal displacements were plotted as a function of the flow Womersley number. The amplitude of axial displacement ΔZ of the fluid during the oscillatory motion was normalized by the amplitude of the pressure gradient P between the hot and cold reservoirs divided by the density times the square of the circular frequency [43, 78] as presented in section 2.5.1. Figure 3.7 shows the normalized tidal displacement variation with Womersley numbers for the numerical and experimental data and the analytical solution [43]. The figure includes the experimental results for four different tidal displacements at four different Womersley numbers. The numerical models used in this validation are the 2D and 3D models that are identical to the experimental design. The experimental and numerical data have the same trend of behavior in variation with Womersley numbers.

The difference between the experimental and the numerical data is about 8% on average for fluid mechanics results. This percentage difference is thought to result from experimental measurements' accuracy, especially in tidal displacement. Also, the difference in results between the numerical results itself is because each numerical model has a different mesh. The validation provides an indication that there is a good agreement between the experimental, numerical, and ana-
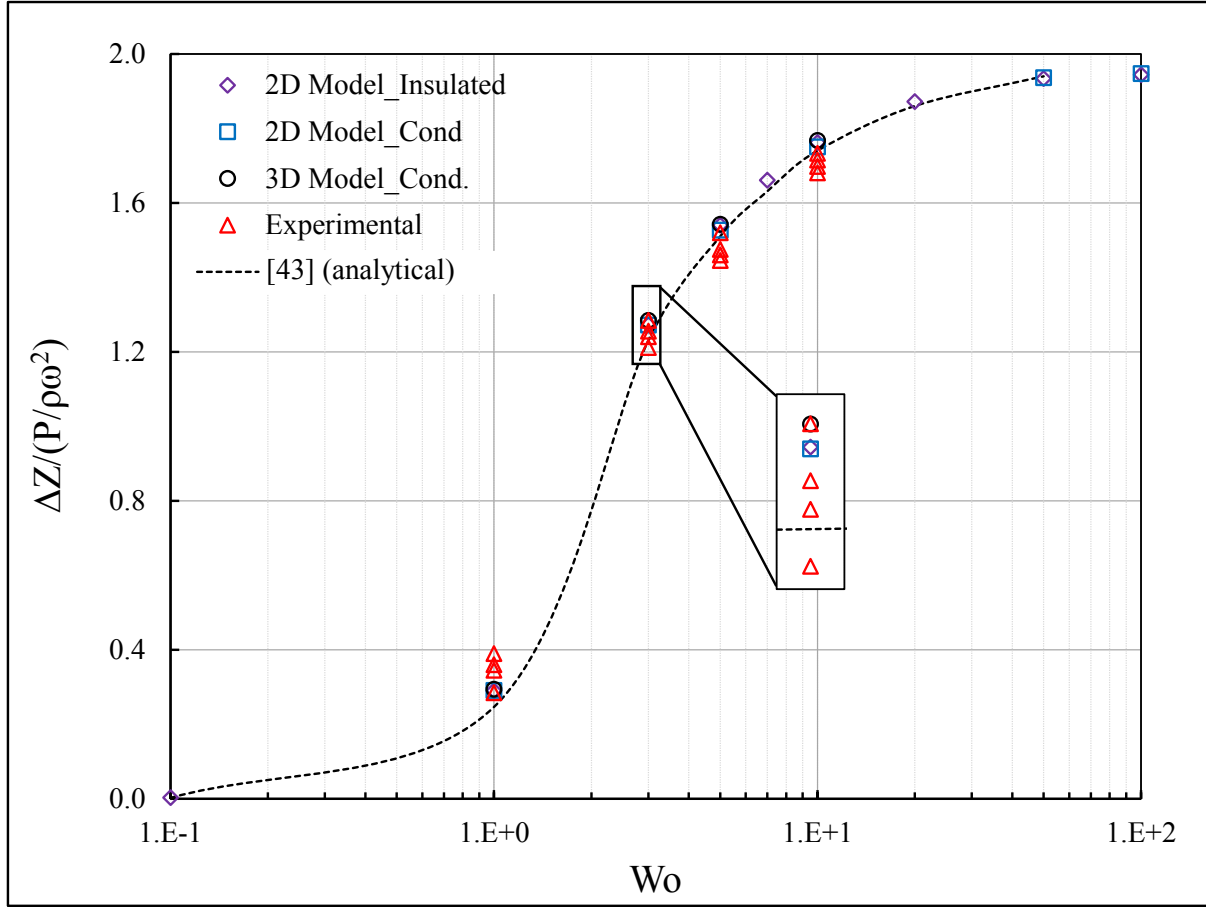
Figure 3.7: Experimental and numerical dimensionless tidal displacements

lytical [43] results. At low Womersley numbers, the experimental and numerical normalized tidal displacement values are close. As the Womersley number increases, the normalized experimental tidal displacement values start decreasing while tidal displacement values increase, especially at a Womersley number of ten. The axial flow displacement at high frequencies is difficult to determine by flow visualization (see 3.3.3),and so may produce this error.

3.6.2   Heat Transfer Validation

The other part of validation is the heat transfer aspect, which is discussed in section 2.5.2. There are several parameters that affect the accuracy of the experimental data. The heat losses have a significant effect on heat balance even though the numerical models are designed to be identical

Figure 3.8: Experimental and numerical normalized axial heat-transfer enhancement

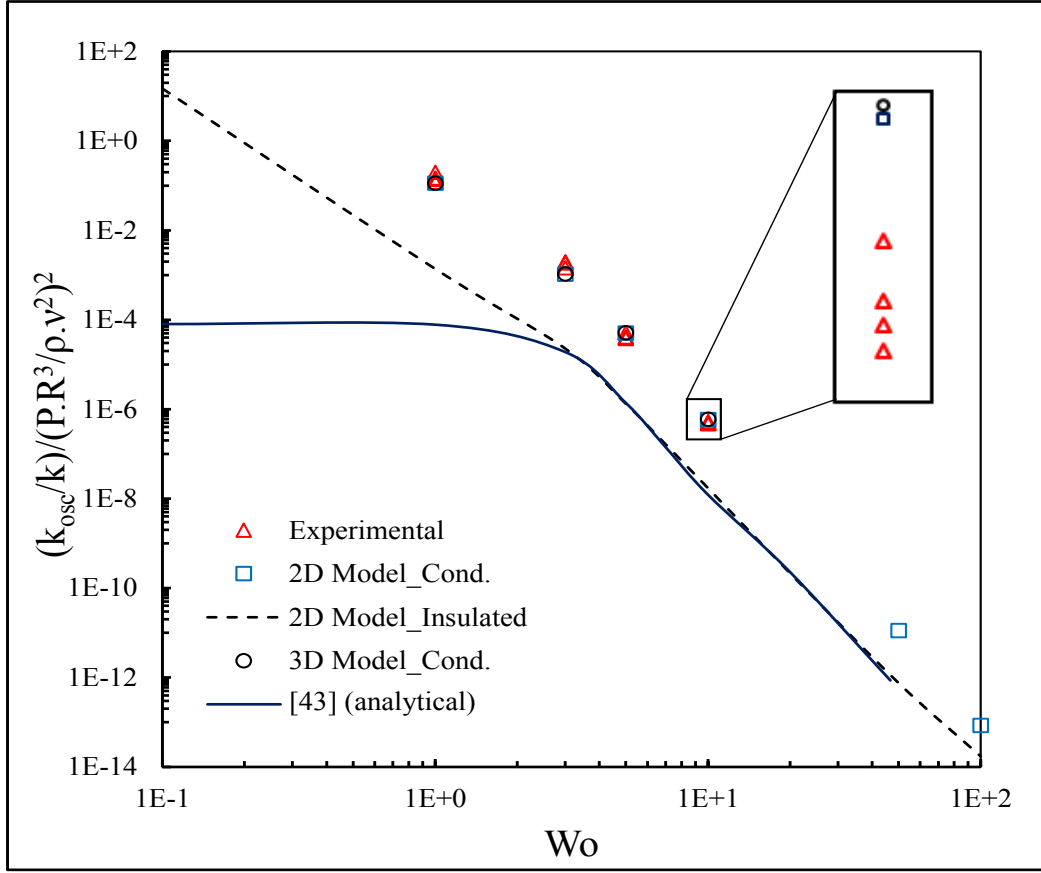to the experimental model, which helps in reducing any error. Figure 3.8 illustrates a comparison between the numerical results for conductive walls at $\Delta Z/L = 0.12$ and the experimental results at different tidal displacements. The figure shows the variation of normalized axial heat transfer enhancement as a function of Womersley number. The trend of the experimental and numerical results is quite similar. The heat losses are partly account for experimental errors at different tidal displacements. The experimental data on average is about 11% higher/less than the numerical results. The figure shows, in enlarged boxes, that as *Wo* increases the experimental results change from higher than the numerical results to lower than it. This discrepancy is related to the measurement accuracy and heat losses. One goal of the experiments, in addition to validate the numerical results, is to investigate the contribution of the unsteady differential axial conduction term ($\partial^2 T/\partial z^2$) in the energy equation for unsteady flow, as stated in equations 2.10 and 2.14,

66

which are not included in the previous studies analytical solutions [2, 21, 30, 31, 34, 43] described in the appendix . It is clear from the figure that the trend of normalized axial heat-transfer enhancement at $Wo < 3$ is very similar for numerical and experimental results. The role of the unsteady differential axial conduction term in unsteady flow is discussed in chapter four.

<center>CHAPTER 4</center>

<center>NUMERICAL RESULTS AND DISCUSSION</center>

4.1   Introduction

Time-dependent enhanced conductive heat transfer subjected to oscillatory motion is studied experimentally and numerically [78]. In this chapter, the numerical results for different cases are presented. The effects on axial heat transfer of tidal displacements, axial conduction, tube conductive wall thickness, bulk convective, and entrance/exit regions effects are discussed from numerical predictions in this chapter. The numerical results are for incompressible flow and neglect the viscous heat dissipation effect, which is considered in the next chapter.

4.2   Effect of Womersley Number on the Flow Field

Womersley number has an effect on the profile of the velocity as it changes from a quasi-parabolic profile at low values to approximately a slug flow at high Womersley numbers. Figure 4.1 shows the radial profiles of the time-dependent axial velocity at the middle of the tube for different phase angles over various Womersley numbers at tidal displacement of $\Delta Z/L = 0.24$. Each plot refers to the normalized axial velocity $\bar{u} = u/u_{max}$ and normalized radial location $\bar{r} = r/R$. The velocities are normalized by the maximum velocity for each Womersley number.

At high Womersley, the velocity profiles are divided into two parts;

1. Oscillatory near-wall Stokes flow.

2. Slug flow in the tube center.

The first part, which is the region close to the wall, is a thin Stokes boundary layer of thickness $\delta_{st} = \sqrt{2\nu/\omega}$. The second part is the core of the fluid where the flow is a uniform or slug flow. Figure 4.1 shows that at $Wo > 3$, the high frequency reduces the available time for the velocity profile to develop. As Womersley number increases, the flow at the core of the tube becomes nearly
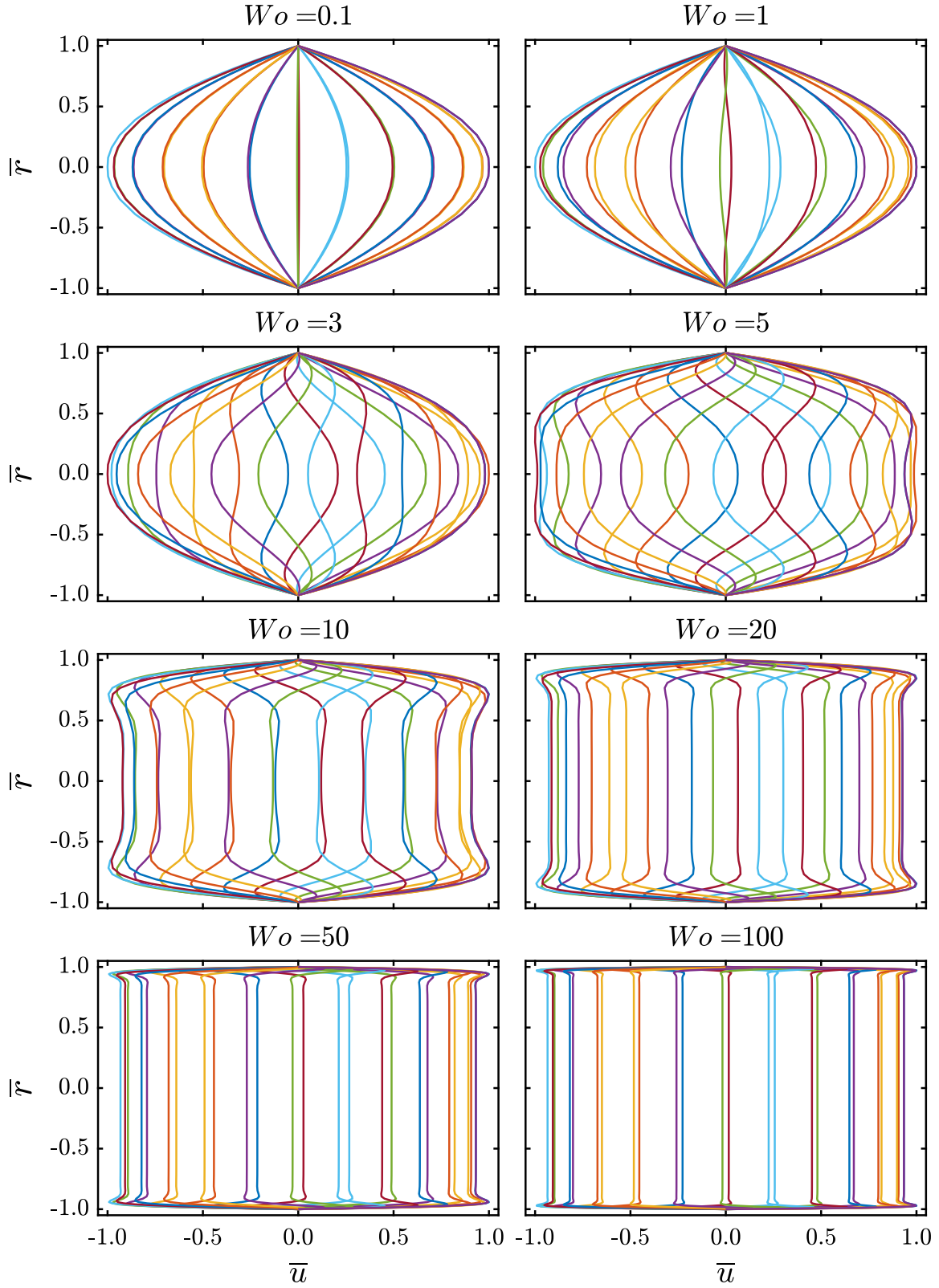
<center>68</center>

Figure 4.1: Instantaneous radial profile of normalized axial velocity at the middle of the tube for different Womersley numbers and a tidal displacement of $\Delta Z/L = 0.24$

uniform and the maximum velocity will be inside the Stokes layer (Richardson's annular effect). Therefore, the oscillatory flow at $Wo > 3$ is called ***undeveloped oscillatory flow*** and the flow is divided into two regions. Also, Womersley number affects the location of the maximum velocity. It is clear from Figure 4.1 that at low Womersley numbers the radial profile of axial velocity at different phase angles is similar to steady state Poiseuille flow with maximum velocity almost at the centerline and the velocity profile reaches a fully developed profile at these low frequencies. The oscillatory flow at these low frequencies $Wo < 3$ is called ***developed oscillatory flow*** [1].

4.3   Effect of Womersley Number on the Temperature Field

In section 4.2 the flow field was represented in two parts depending on Womersley number; developed and undeveloped oscillatory flow. In the first type of the flow, the radial temperature profile or variation $(\partial T/\partial r)$ for air $(Pr = 0.7)$ is similar to quasi-steady flow. Figure 4.2 shows the time variation of normalized radial temperature profiles at the middle of the tube for different Womersley numbers and a tidal displacement of $\Delta Z/L = 0.24$. With increasing the frequency, the oscillatory flow becomes "undeveloped". A uniform temperature region exists at the core of the tube. This uniform temperature core has an interface with a near wall boundary layer. The outward and inward diffusion processes that were presented in figure 1.2 will take place where temperature gradients exist below this interface. Also, it is clear that the temperature profile has a similar overshoot to the velocity profile (figure 4.1) at high Womersley number. This temperature overshoot is apparent near the interface between the core and the boundary layer.

One of the assumptions that has been considered in previous analytical solutions, given in appendix , is $\partial T/\partial z \ll \partial T/\partial r$. This assumption is used to simplify the problem by neglecting the differential axial conduction term in the thermal energy equation. However, figure 4.2 shows that $\partial T/\partial r$ is almost negligible at low Womersley number. On the other hand, $\partial T/\partial z$ may not be constant or negligible at low Womersley numbers, as discussed in section 4.5.

Figure 4.3 shows the near wall radial profiles of normalized axial velocity and temperature for different phase angles at the middle of the tube for $Wo = 20$ and $\Delta Z/L = 0.24$. It is clear that the
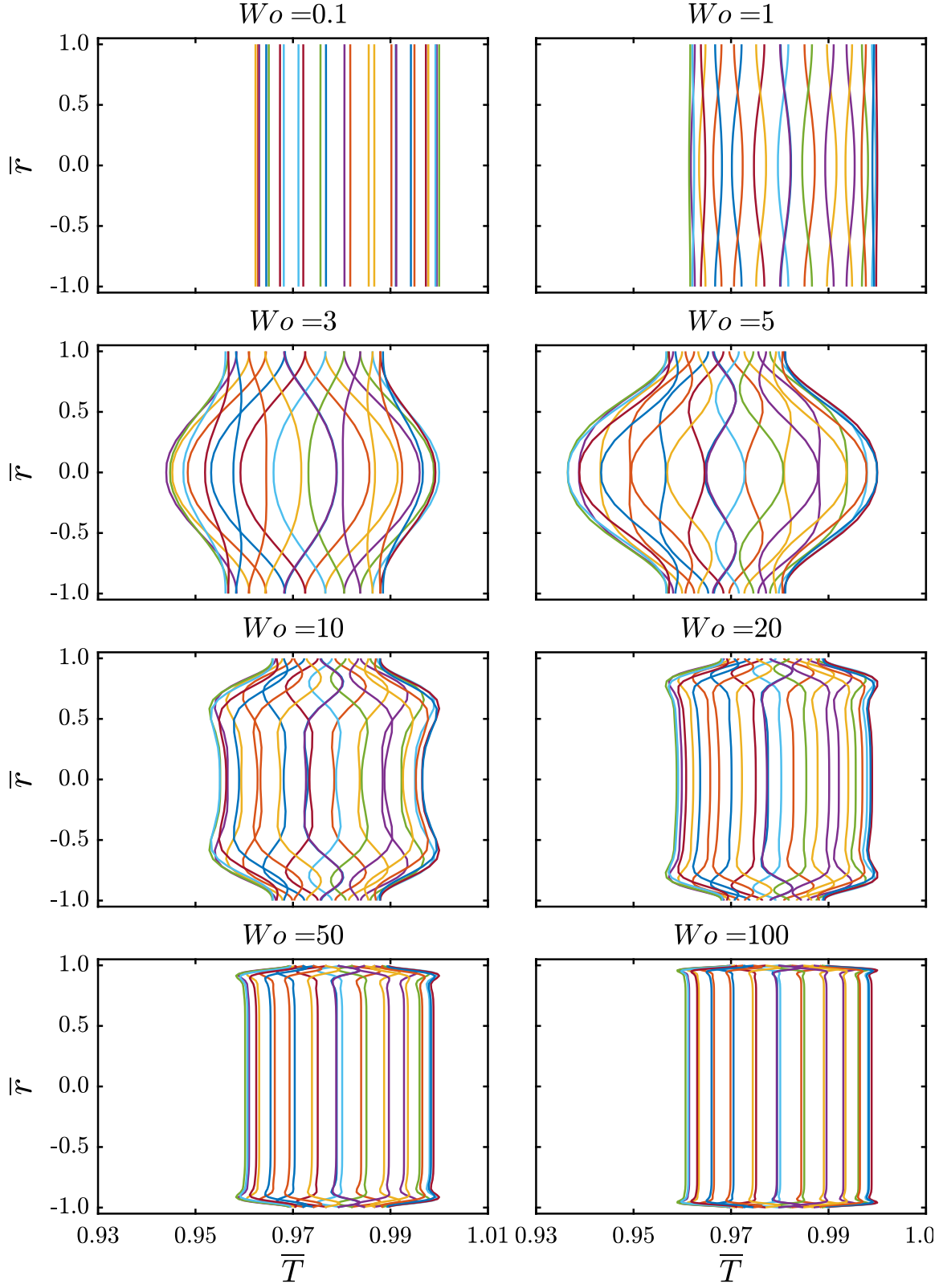
70

Figure 4.2: Instantaneous radial profiles of normalized temperature at the middle of the tube for different Womersley numbers and a tidal displacement of $\Delta Z/L = 0.24$

71

radial profile for the axial velocity and temperature are resolved near the wall.
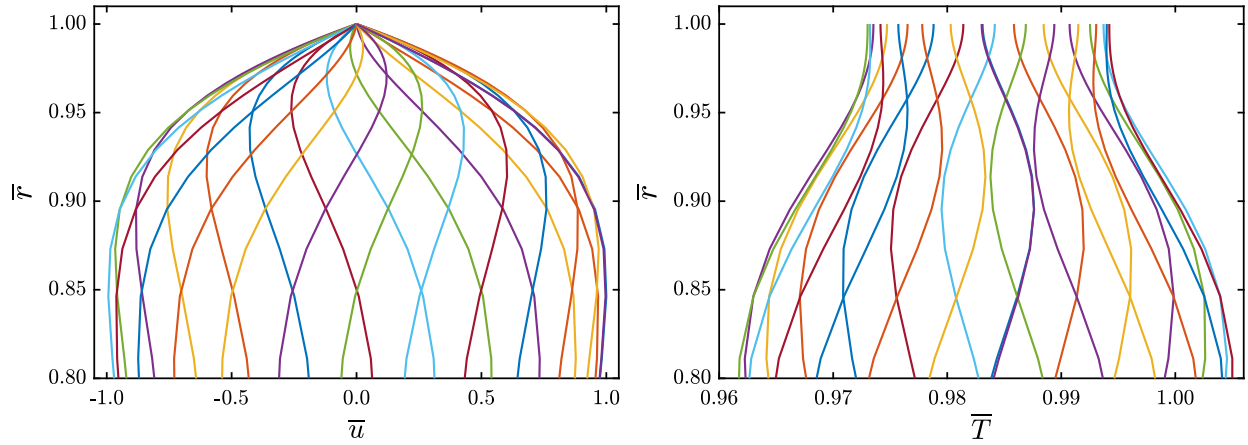

Figure 4.3: Near wall (outer 20 % of radius) instantaneous radial profiles of normalized axial velocity and temperature at the middle of the tube for $Wo = 20$ and $\Delta Z/L = 0.24$

4.4 Effect of Reservoirs in Temperature and Velocity Fields

As the current study considers components that exist in most practical applications including hot and cold reservoirs, it is relevant to discuss the effects of the hot and cold reservoirs on temperature and velocity fields. Figure 4.4 shows results for a tidal displacement of $\Delta Z/L = 0.24$ and $Wo = 5$ as a moderate tidal displacement and Womersley number. In Figure 4.4a radial profiles of normalized axial velocity are shown at different tube axial locations for all phase angles over one cycle of oscillation ($\phi = 0° \rightarrow \phi = 360°$). The similarity of the radial profile of axial velocity between $z/L_{tube} = 0.1$ and $z/L_{tube} = 0.9$ implies that entrance lengths are less than $0.1\ z/L_{tube}$. The velocity profiles become only slightly more uniform and symmetric far from the entrance/exit regions.

At the middle of the tube, the axial velocity profiles across the tube at each phase angles are plotted separately in Figure 4.4b. From these separate phase angle velocity profiles, the velocity has a stronger phase-dependent radial profile and there is phase shift between different radial locations of the axial velocity. This phase shift will cause the velocity in the core of the tube to lag that close to the tube wall.
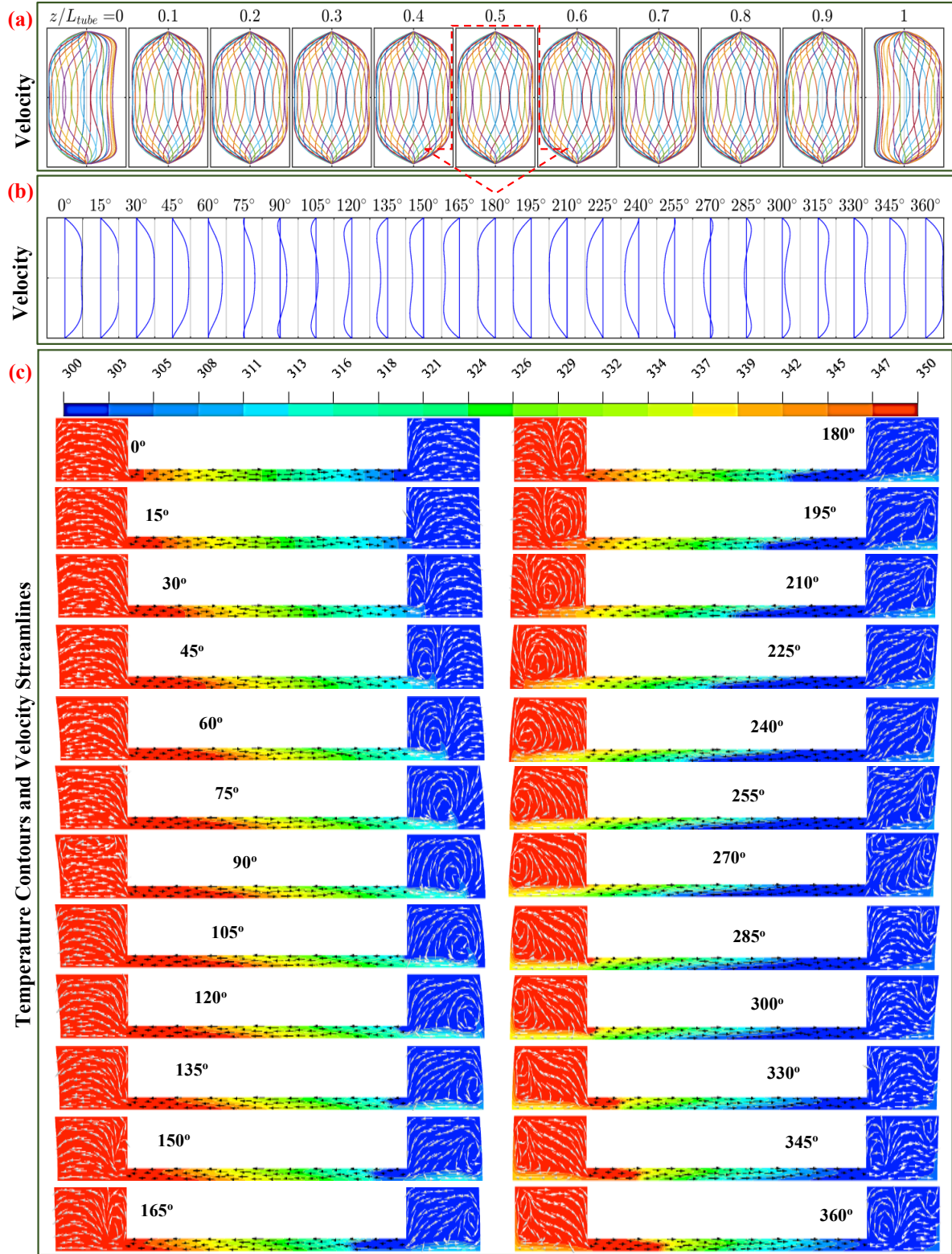
Figure 4.4: Results for Wo=5 and $\Delta Z/L = 0.24$ (a) velocity profiles at different phase along the tube (b) separate phase angle velocity profiles at the middle of the tube (c) time dependent temperature contours and velocity streamlines

For more clarification of the reservoirs' effect, snapshots of the temperature contours with stream lines are presented in Figure 4.4c. In this figure, the temperature contours and the streamlines are obtained at 24 different phase angles over an oscillatory cycle. The fluid starts to accelerate to the right from $\phi = 0°$, and the temperature field has a uniform axial temperature from the hot to the cold reservoirs, with a uniform flow pattern. At this instance, the hot fluid begins to move from the hot to cold reservoir through the tube. With the evolution of the time, the fluid will move along the tube by half of its tidal displacement ($\Delta Z/L = 0.24$), reaching $\phi = 90°$. The temperature contour at $\phi = 90°$ shows that the temperature field at the core of the tube is higher than that near the wall. During this quarter of the oscillatory cycle, the hot fluid moved to a colder region, which leads to a thermal diffusion from the hot region in the center of tube to the colder region near the wall. Also, in this preceding quarter of the oscillatory cycle, the flow starts to circulate in the cold reservoir. This circulation inside the reservoirs can yield extra enhancement in heat transfer rate compared to purely axial heat transfer inside the tube.

Subsequently, after the maximum tidal displacement, the fluid will move back from $\phi = 90°$ to $\phi = 270°$. In this period of the cycle, the cold fluid will move toward the hot reservoir. The reverse process then takes place. Moreover, recirculation takes place in the reservoir in this part of the cycle. The temperature contours show how the temperature in the hot reservoir decreases, especially in the central region. In the last quarter of the cycle ($\phi = 270° \rightarrow \phi = 360°$), the fluid moves forward again to complete the cycle. By comparing the temperature contour at $\phi = 0°$ with that at $\phi = 360°$, it is noticeable that the axial heat transfer enhanced. The reservoirs have a clear effect on the temperature contour and the flow pattern. This rate of thermal diffusion and the flow pattern will depend on the $Wo, \Delta Z/L$, and the pressure gradient $\frac{\partial p}{\partial z}$ and affects the oscillatory thermal conductivity k_{osc} as defined in equations 4.2 and 4.3 in section 4.6

4.4.1 Temperature Field with no Reservoirs Effects

In the case of low tidal displacements, where the flow oscillates inside the tube only, no cold fluid enters the hot reservoir nor does hot fluid enter the cold reservoir. The fluid moves back

and forth a short distance along the tube. These low tidal displacement motions are similar to the exact solutions of fully developed flow when there are no reservoirs' effects. In this case, including the reservoirs does not affect the axial heat transfer because the temperature field will not be affected by the flow circulations inside the reservoirs that are presented in section 4.4. The hot fluid circulates only inside the hot reservoir and the cold fluid circulates only insides the cold reservoir. Therefore, the rate of axial heat transfer enhancement, which is represented by the oscillatory thermal conductivity k_{osc}, may be less than its counterpart at high tidal displacement as discussed in section 4.6.

4.4.2   Effect of Entrance/Exit Region

The inclusion of hot and cold reservoirs in the current study produces a discontinuity in the cross-sectional area of the heat exchanger, at its entrance and exit. Entrance effects are a result of the velocity development to reach a fully developed profile depending on inertia effects and wall friction [23]. The oscillatory flow will be affected by the forward and backward steps at the edges of the tube. These effects are not accounted for within the exact solution of the problem or computations that ignored the reservoirs [57]. Also, the deviation of the centerline velocity from its fully developed magnitude in oscillatory flow depends on the phase angle. The combination of entrance fluid mechanics and heat transfer leads to thermal entrance/exit regions for the temperature field. For $Wo < 3$, the thermal entrance lengths are short. For high Wo, they did not exceed 10% of the tube length at this tidal displacement.

Figure 4.5 illustrates the spatial distribution of normalized centerline axial velocity for the corresponding 24 phase angles at different Womersley numbers, where $\bar{Z} = z/L$ is the normalized axial location along the tube. For quasi-steady flow $(Wo < 3)$, the velocity profile at the entrance/exit regions increases smoothly to its fully developed value with a behavior like a steady flow. Increasing the frequency of the enforced oscillatory motion caused an overshoot at the entrance/exit regions as an annular effect. Therefore, for various phase angles and Womersley numbers, it can be seen that the flow consists of three different regions: entrance, fully developed, and exit regions.
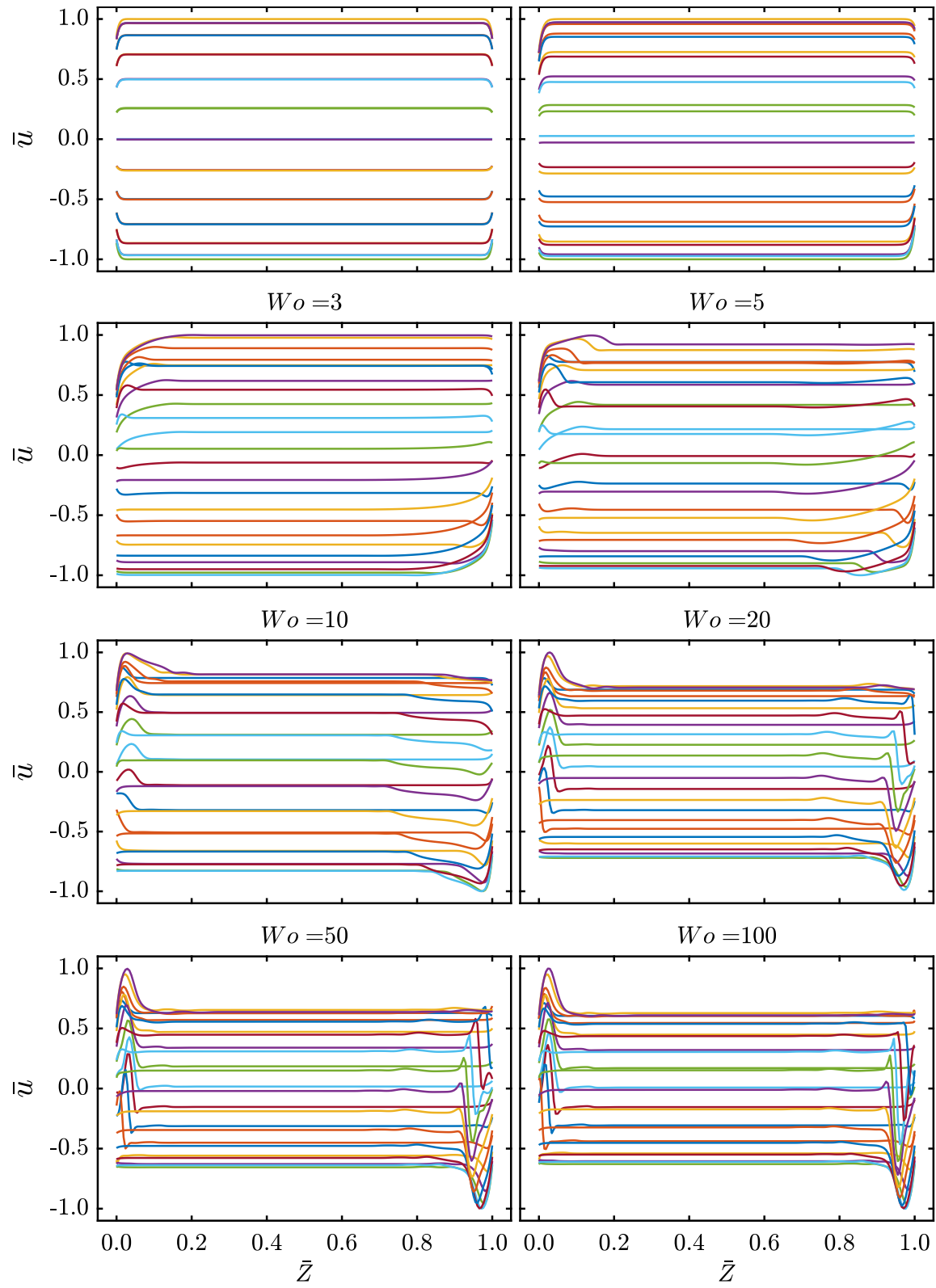
Figure 4.5: Effect of entrance/exit region on normalized instantaneous centerline axial velocity profile at different Womersley numbers and $\Delta Z/L = 0.24$
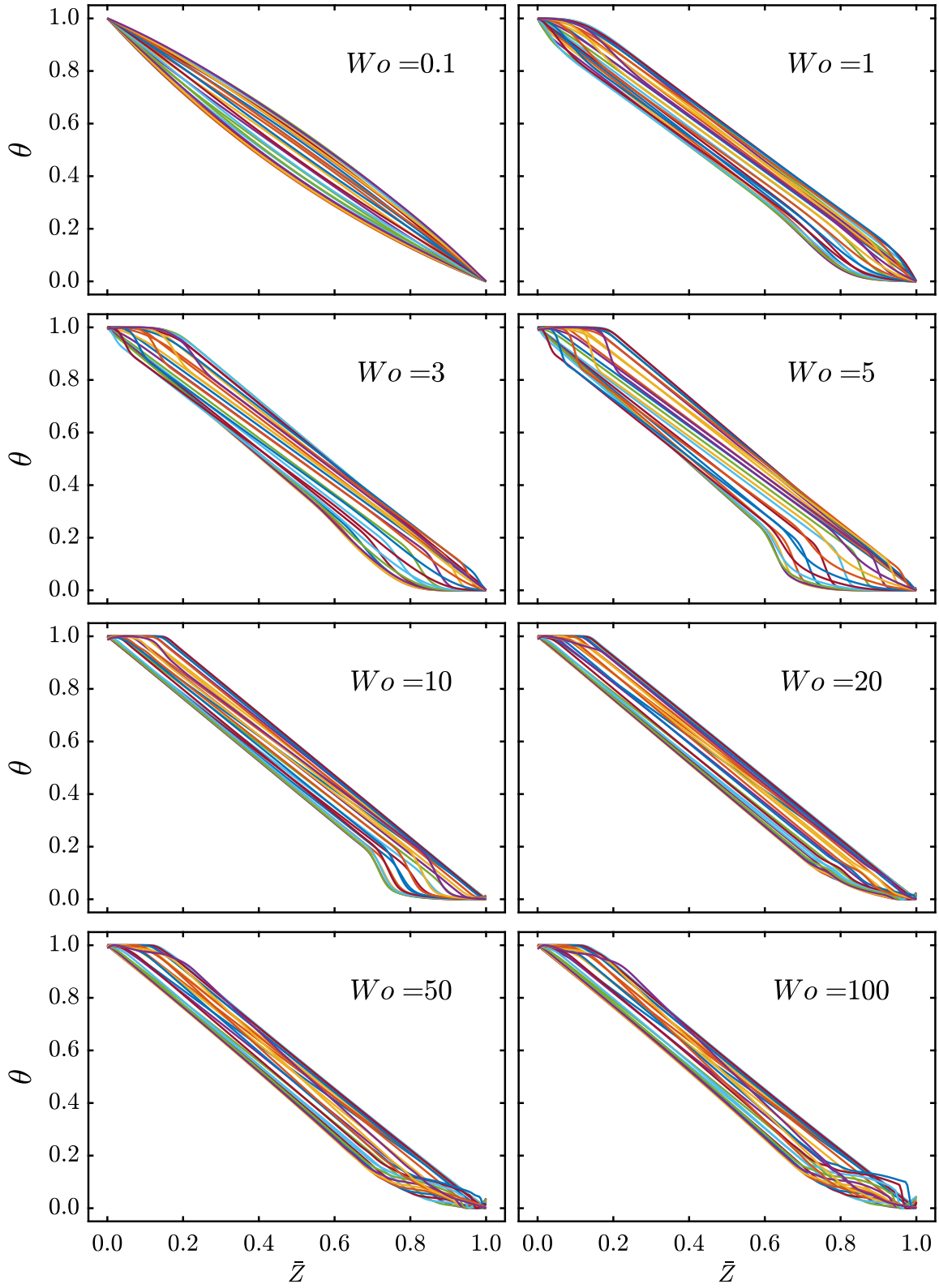
Figure 4.6: Effect of entrance/exit region on normalized instantaneous centerline temperature profile at different Womersley numbers and $\Delta Z/L = 0.24$

Figure 4.6 shows the distribution of normalized instantaneous centerline temperature along the tube ($\theta = (T - T_{min})/(T_{max} - T_{min})$), where T_{max} and T_{min} represent the hot and cold reservoirs' temperatures. It is clear that the temperature profiles are affected by the entrance/exit region especially at high Womersley numbers. The distribution of the centerline temperature shows an almost linear gradient along the tube, except at low frequencies. This linear temperature gradient is a necessary assumption of previous analytical studies [5, 21, 31, 43], which assume $\partial T/\partial z = constant$ and so $\partial^2 T/\partial z^2 = 0$. For quasi-steady flow or developed oscillatory flow at $Wo = 0.1$, it is clear that distribution of the centerline temperature is nonlinear in z. This nonlinearity in axial temperature distribution leads to $\partial^2 T/\partial z^2 \neq 0$.

4.5   Axial Conduction

According to the assumptions of previous studies given in the appendix , the unsteady differential axial conduction term $\partial^2 T/\partial z^2$ in the thermal energy equation (Eqs 2.10 and 2.14) was neglected by assuming that it is much less than the radial conduction term ($\partial T/\partial z \ll \partial T/\partial r$) and that a linear temperature gradient exists along the tube ($\partial T/\partial z = constant$). As one goal of this study, it is important to examine the limitations of this axial conduction assumption in unsteady flow. For a steady flow, Kays et al. [81] and Cole [88] have observed that the differential axial conduction is significant in the thermal energy equation if $Pe < 100$, especially for gases at low Reynolds numbers. For most liquids, they concluded axial conduction is seldom of significance.

In the case of unsteady flow, the effect of differential axial conduction depends on Wo. Figure 4.7 shows the normalized axial heat-transfer enhancement and Peclet numbers as a function of flow Womersley numbers for different tidal displacements. The predicted results are compared with the exact solutions and have a good agreement for $Wo > 3$ and tidal displacement less than the tube length. For $Wo > 3$ and tidal displacement larger than tube length ($\Delta Z/L = 1.2$), the results will start to diverge from the exact solution. This divergence in the results is because the flow will be dominated by the bulk heat exchange, high Re_s, and the effect of the entrance/exit region.

At $Wo < 3$, which represents the low oscillatory motion, the numerical results do not follow
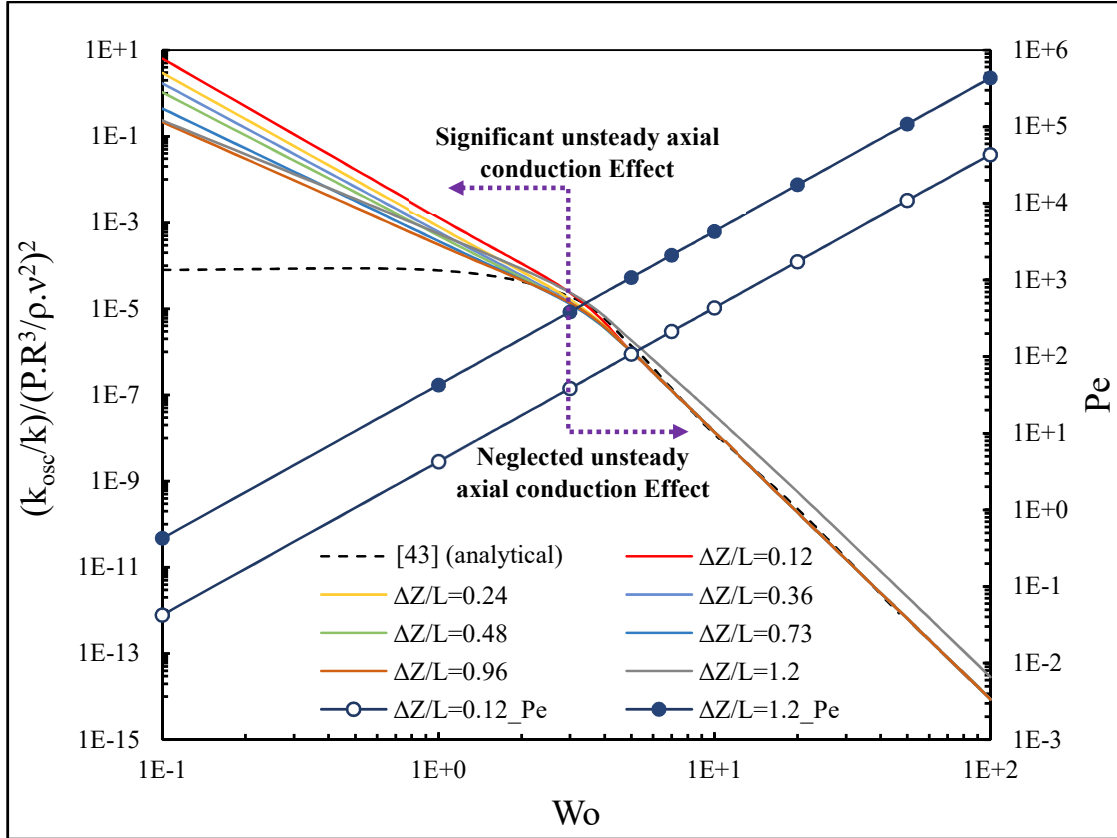
Figure 4.7: Normalized axial heat-transfer enhancement as a function of flow Womersley numbers for different tidal displacements and Peclet numbers

the exact solution as a result of the differential axial conduction contribution, which is neglected in the exact solution's energy equation. This behavior was observed in experimental results at low Wo as shown in Figure 3.8. Also, it is clear from Figure 4.6 that at $Wo = 0.1$ the temperature gradient along the wall is nonlinear in z. Therefore, the assumption $\partial T/\partial z = 0$ for quasi-steady flow is invalid at low Womersley numbers and $\partial^2 T/\partial z^2$ must be significant. This assumption will be more accurate with increasing Wo as shown in Figure 4.6 at high Womersley numbers.

According to the experimental results in Figure 3.8 at $Wo < 3$, the trend of normalized axial heat-transfer enhancement does not follow the analytical solution [43] behavior at low Wo, which is almost a horizontal line. The predicted results at $Wo < 3$ are closer to the exact solution when the tidal displacement increases, because the increases in Peclet number reduces the axial conduction effect for cases close to quasi-steady flow. The flow at $Wo < 3$ and low tidal displacement

$(\Delta Z/L = 0.12)$ is close to quasi-steady, therefore it will almost adhere to the criteria of steady flow as Pe < 100 [83].

When the flow becomes fully unsteady or developed oscillatory flow $(Wo > 3)$ the differential axial conduction does not have a significant effect. Therefore, at high tidal displacement $(\Delta Z/L = 1.2)$ and $Wo < 3$, although $Pe \simeq 390$, which is much higher than the limit specified for steady flow, the effect of differential axial conduction term is important. From this figure, the contribution of differential axial conduction in oscillatory flow could be defined in terms of Womersley number, not a Peclet number. Therefore, the effect of differential axial conduction vanishes for $Wo > 3$ in unsteady flow inside a tube with air as a working fluid. This criterion for unsteady axial conduction's significance is in contrast to previous studies' assumption of ignoring this term for all ranges of Womersley numbers, and underestimating rates of axial heat transfer enhancement at low Wo.
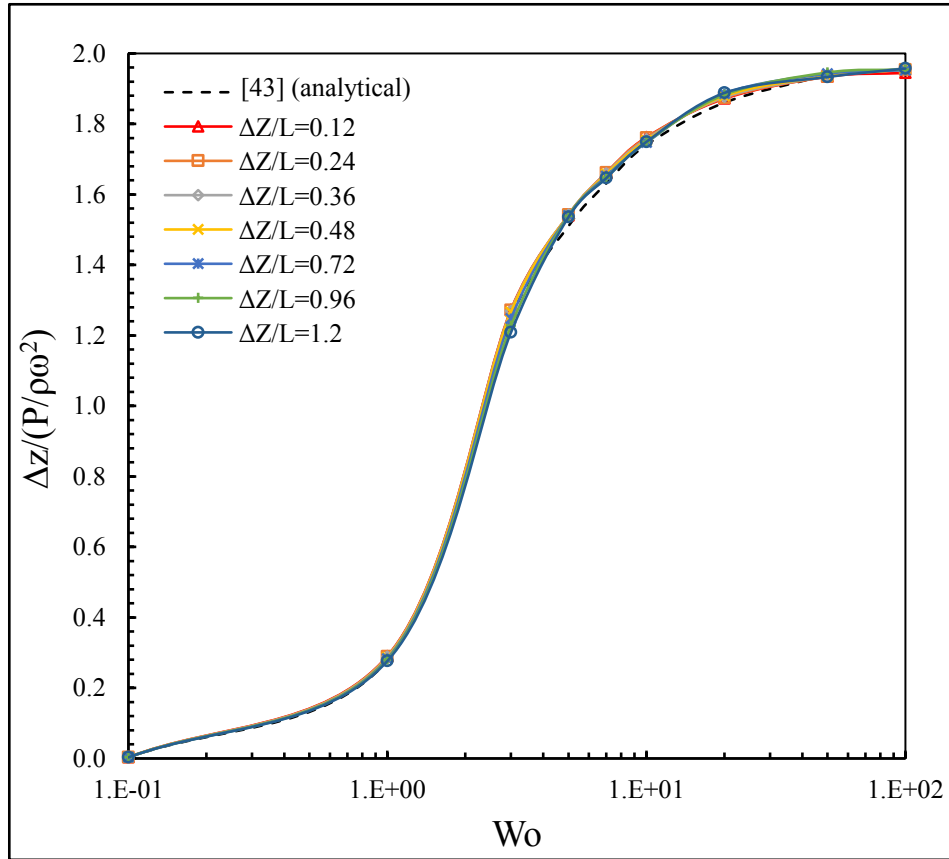

Figure 4.8: Variation of different normalized tidal displacements with Womersley numbers

4.6 Effect of Womersley Number and Tidal Displacement on the Rate of Heat Transfer Enhancement

As shown in Figure 4.8, the variation of dimensionless tidal displacement with Womersley numbers follows the same trend for different tidal displacements. This behavior indicates that the continuity and moment equations were converged perfectly, as the results almost matched the exact solution. This matching is expected because all significant terms in the continuity and momentum equations were considered in both numerical and analytical solutions. Also, as stated in equation A.7 (appendix), the normalized tidal displacement is a function of Womersley number only. It is clear that the dimensionless tidal displacement for different axial fluid displacements is varying approximately from zero to two depending on Womersley number value. The figure also indicates that as the flow goes from slower to faster oscillation, the pressure amplitude changes correctly with frequency. Once the flow reaches high Wo, the fluid follows at a constant $\Delta Z/(P/\rho\omega^2)$ as result of the capacitance of the fluid.

In previous studies, low tidal displacement oscillatory flows were considered and no computations were made at tidal displacement larger than half of the tube length. In the current study, large tidal displacements were studied. The fluid mechanics results do not change with increasing tidal displacement as shown in figure 4.8. Therefore, the results are useful to describe the effect of tidal displacement or the pressure gradient amplitude on effective axial conductivity.

Figure 4.9 shows the effect of the axial tidal displacement and Womersley number in enhancing the axial heat transfer rate. It is clear that with increasing Womersley from 0.1 to 100 and tidal displacement from 0.12 to 1.2, the oscillatory thermal conductivity is increased to about five order of magnitude compared with its molecular counterpart. This high rate of heat transfer enhancement is produced as a result of increasing the exchange heat surface area along the tube between the near wall fluid inside the Stokes layer and the core fluid with increasing the tidal displacement at same Womersley number. Also increasing Womersley numbers accelerates the rate of heat transport by increasing the number of back and forth motion per unit time. Therefore, the two parameters $\Delta Z/L$ and Wo play an essential role in enhancing the heat lateral diffusion and longitudinal advection.
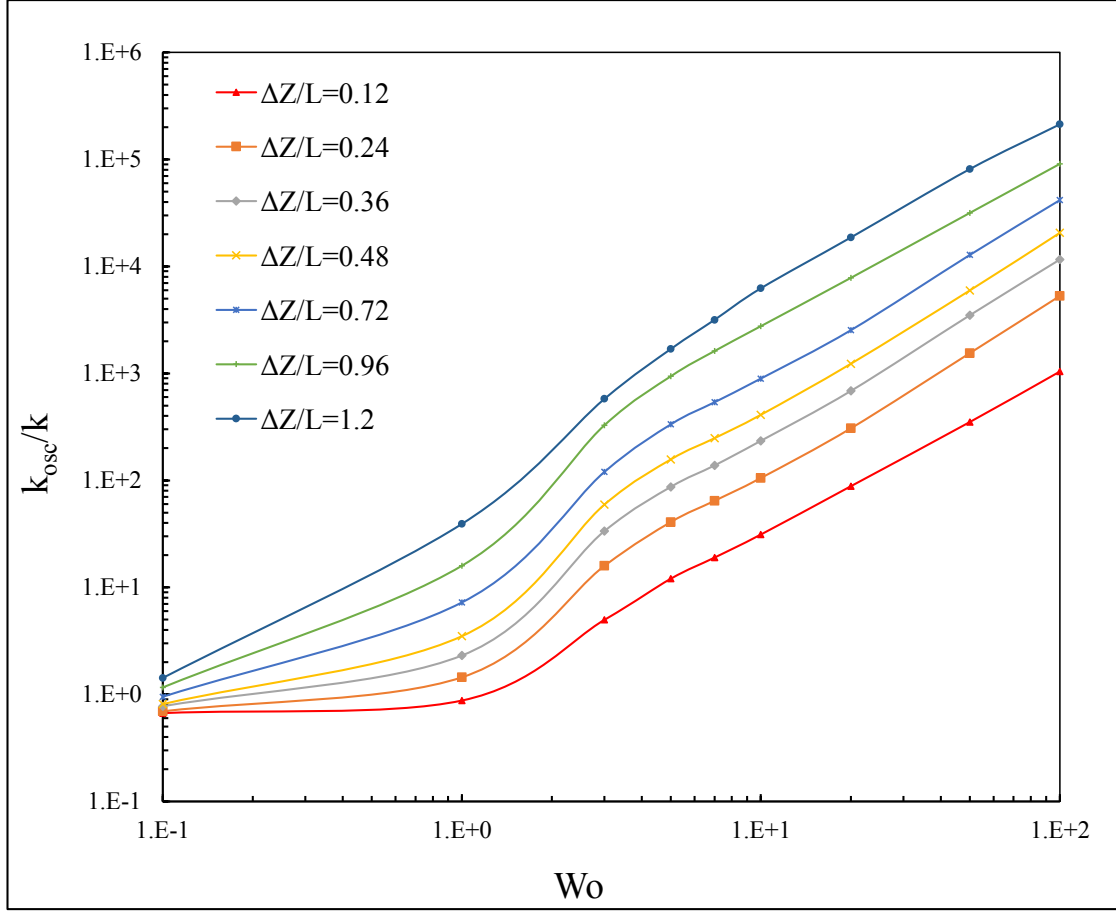
Figure 4.9: Effect of axial tidal displacement and Womersley number in heat-transfer enhancement

The rate of axial heat transfer enhancement for each tidal displacement can be defined as a function of Womersley number. Hence, data for $\Delta Z/L < 1$ presented in Figure 4.9 are normalized by $(\Delta Z/R)^2$, and two correlations are suggested to predict the rate of axial heat transfer enhancement in terms of Womersley number and tidal displacement. Figure 4.10 shows the axial heat-transfer enhancement for air for Womersley numbers from $0.1 - 100$ normalized by the square of tidal displacement, for different tidal displacements. This normalization leads to almost a collapse of all data for $Wo > 3$ to make all normalized data scale in proportion to $Wo^{1.62}$. These results are for incompressible flow, insulated walls, and ignore the viscous heat dissipation effect. According to these results, the axial diffusivity is enhanced by about $600,000$ times compared to its counterpart at low tidal displacements and Womersley numbers. Therefore, the oscillatory flow motion for

the current conditions has enhanced the oscillatory thermal conductivity by about five orders of magnitude. Increasing Womersley number helps in enhancing the rate of heat exchange by the back-and-forth motion of the fluid inside the tube and the circulation inside the reservoirs.
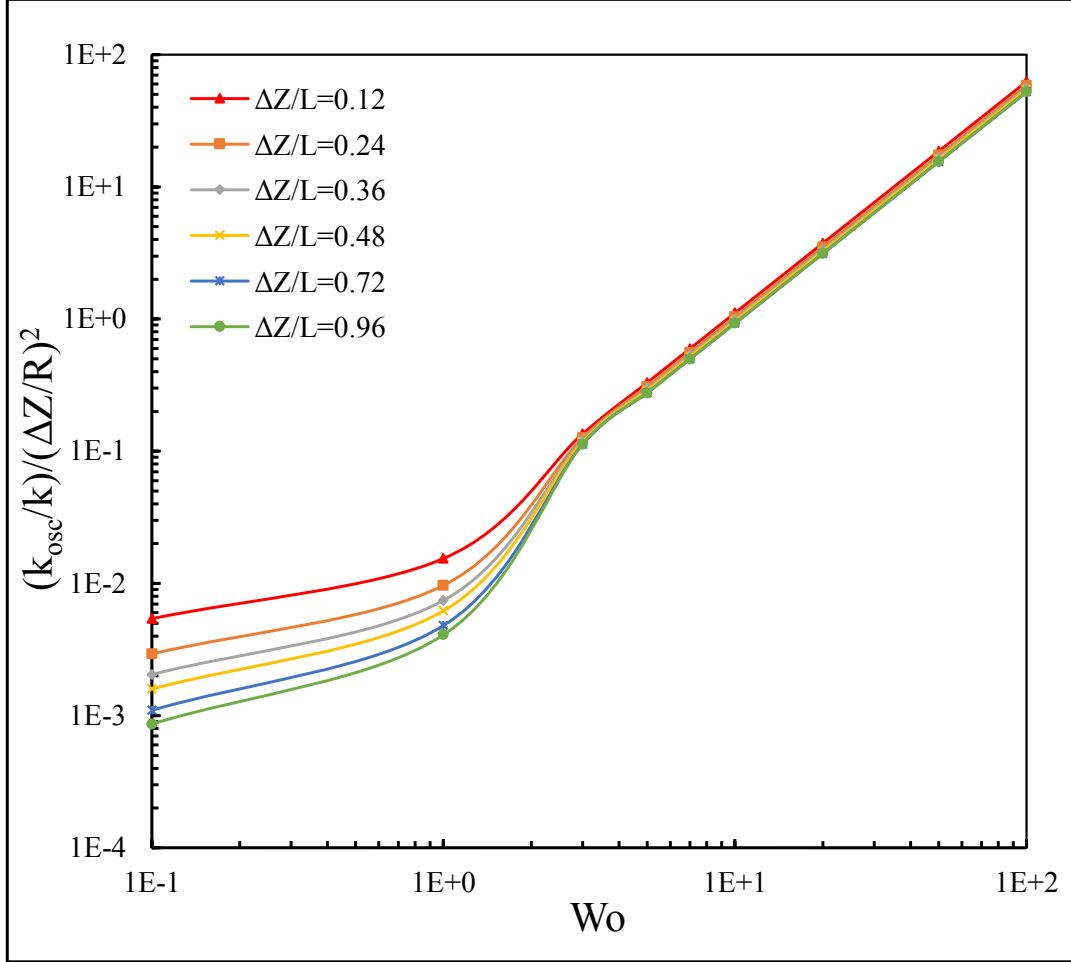
Figure 4.10: Effect of Womersley number and tidal displacements in enhancing oscillatory thermal conductivity

This normalized thermal conductivity, which represents the enhancement in the rate of axial heat transfer, is defined in a correlation as a function of Womersley number:

$$\frac{k_{osc}/k}{(\Delta Z/R)^2} = f\{Wo\} \tag{4.1}$$

The relation between oscillatory thermal conductivity and Womersley number was divided into two regions depending on the rate of enhancement and the unsteady differential axial conduction

effect. The first region covers results for Womersley numbers between 0.1 and less than 3 and describes the low rate of enhancement. In this region, the axial conduction has an effective contribution to the energy equation as described in section 4.5. Therefore, as shown in figure 4.10 the results do not merge at low Womersley numbers and converge to merge at Womersley numbers above three. The second region specifies the enhancement in oscillatory thermal conductivity for Womersley number ranges between 3 and 100. In this region, the results almost collapsed and showed a power-law behavior with increasing Womersley number for different tidal displacements.

From these results, correlations for axial heat transfer enhancement can be deduced. The correlations in equations 4.2 and 4.3 represent the exponential and power curve fitting for various Womersley numbers and tidal displacements. The minimum value of the coefficient for determination R^2 in all fittings was above 0.98. According to the predicted correlations, the axial heat transfer rate scaled in proportion to $Wo^{1.62}$ for high Womersley number ($Wo > 3$) and different tidal displacements, whereas, it behaves exponentially for low Wo with different scales depending on pressure gradient amplitude. These correlations define the enhancement of oscillatory thermal conductivity in terms of molecular thermal conductivity, tidal displacement, and Womersley number. The correlations can be used to predict the required enhancement in axial heat transfer depending on the appropriate tidal displacement and frequency. The limitations of the suggested correlations are its restriction to laminar flow, constant air properties, no viscous heat dissipation, and for tidal displacement less than the tube length.

$$\frac{k_{osc}/k}{(\Delta Z/R)^2} = \left(0.0021 \left(\frac{\Delta z}{R}\right)^{-0.81}\right).\exp\left(\left(1.44 \left(\frac{\Delta z}{R}\right)^{0.21}\right).Wo\right) \quad (0.1 \leq Wo < 3) \quad (4.2)$$

$$\frac{k_{osc}/k}{(\Delta Z/R)^2} = \left(0.025 \left(\frac{\Delta z}{R}\right)^{-0.11}\right).Wo^{1.62} \quad (3 \leq Wo \leq 100) \quad (4.3)$$

For the purposes of clarity the oscillatory flow inside the tube was classified into four different regions. These four regions describe the contribution of increasing the tidal displacement in

enhancing the axial heat transfer in the presence of the hot and cold reservoir mixing. The four categories can be classified depending on the mixing rate as:

1. **No mixing / Low tidal displacement ($\Delta Z/L \leq 0.12$)**

   In this region, the flow is fully-developed over most of the tube length, and it agrees with theoretical results at $Wo > 3$. The heat transport between the two reservoirs will be dominated by the oscillatory and molecular diffusion inside the tube without any mixing effect. The ratio of the oscillatory thermal conductivity k_{osc} to the molecular thermal conductivity k has increased from about $k_{osc}/k = 0.6$ at the lowest Womersley numbers ($Wo = 0.1$) to about $k_{osc}/k = 1040$ at the highest Womersley number ($Wo = 100$). This rate of axial heat transfer enhancement is used as a reference to obtain a factor for the enhancement in axial heat transfer rate when the reservoir mixing effect begins for various tidal displacement.

2. **Little mixing / Medium tidal displacement ($0.12 < \Delta Z/L \leq 0.5$)**

   The flow is fully-developed only over a part of the tube length with entrance/exit effects over a significant length of the tube but greater k_{osc}/k than the first region because of higher oscillatory diffusion effects. The average rate of axial heat transfer enhancement over various Womersley numbers is increased by a factor varying from 6.82 to 11.89 times compared with the previous low tidal displacement region, depending on the applied axial tidal displacement. The fluid in this region oscillates inside the tube with a little mixing with reservoirs' fluid.

3. **Much mixing / Large tidal displacement ($0.5 < \Delta Z/L < 1.0$)**

   This region will have much greater k_{osc}/k, with some convective exchange from one reservoir to the other, will exist in addition to large entrance/exit effects. Compared with the first region, k_{osc}/k has increased by a factor from about 24.83 times to 66.98 times as a result of mixing the fluid that departs from the tube inside the reservoirs.

4. **Fully mixing / Bulk convective / Convective exchange ($\Delta Z/L \geq 1.0$)**

In this fully mixing region, there is no connection with theory but even greater k_{osc}/k than in other regions. k_{osc}/k has increased to about 146 times the oscillatory thermal conductivity compared with no mixing or low tidal displacement region (first region). The high factor of axial heat transfer enhancement illustrates the significant contribution of the presence of the reservoirs in terms of fluid mixing. In this region the fluid will completely leave the tube and circulate inside the reservoirs. Figure 4.4c shows the flow pattern and the mixing process inside the reservoirs at different phase angles and how the circulations take place.

According to this proposed classification and proposed correlations for oscillatory air flow, the designer can specify the appropriate limitations and parameters to build an air heat exchanger with desired rate of heat removal. Each proposed region is appropriate for different practical applications. For instance, region one could be used for enhancing the diffusion of contaminants in gases or enhancing thermal diffusion, whereas, the last region will be appropriate for mixing systems.

4.7   Effect of Tube Wall Conduction on Oscillatory Heat Transfer

One parameter which has an important effect on the behavior of the oscillatory flow system and the design criteria is the conductive tube wall thickness. To study this effect, eight different tube thicknesses were studied at the same tidal displacement and different Womersley numbers. The physical properties of the tube wall (glass) are presented in Table 2.6. For conjugate heat transfer there is a coupling between the air and the tube wall. Equation 2.12 is used for the fluid region, and Equation 2.13 is used for the solid region.

Figure 4.11 shows the enhancement in oscillatory thermal conductivity as a result of wall thickness. In general, the conductive wall improves the axial heat transfer process as it adds extra capacity of heat storage at the fluid-solid interface. From this figure it can be seen that the axial heat transfer has been enhanced by about ten times compared with insulated tube walls. The results show that the contribution of wall thickness gradually decreases with increasing Womersley number. It is expected because of the thermal boundary layer varies inversely with the square root of

the oscillatory period as shown in Figure 4.2. As air (gas) is the working fluid, the thermal boundary layer will be thicker which will lead to larger thermal diffusivity. Therefore, the conductive tube wall will play an important role in the heat storage-release process.
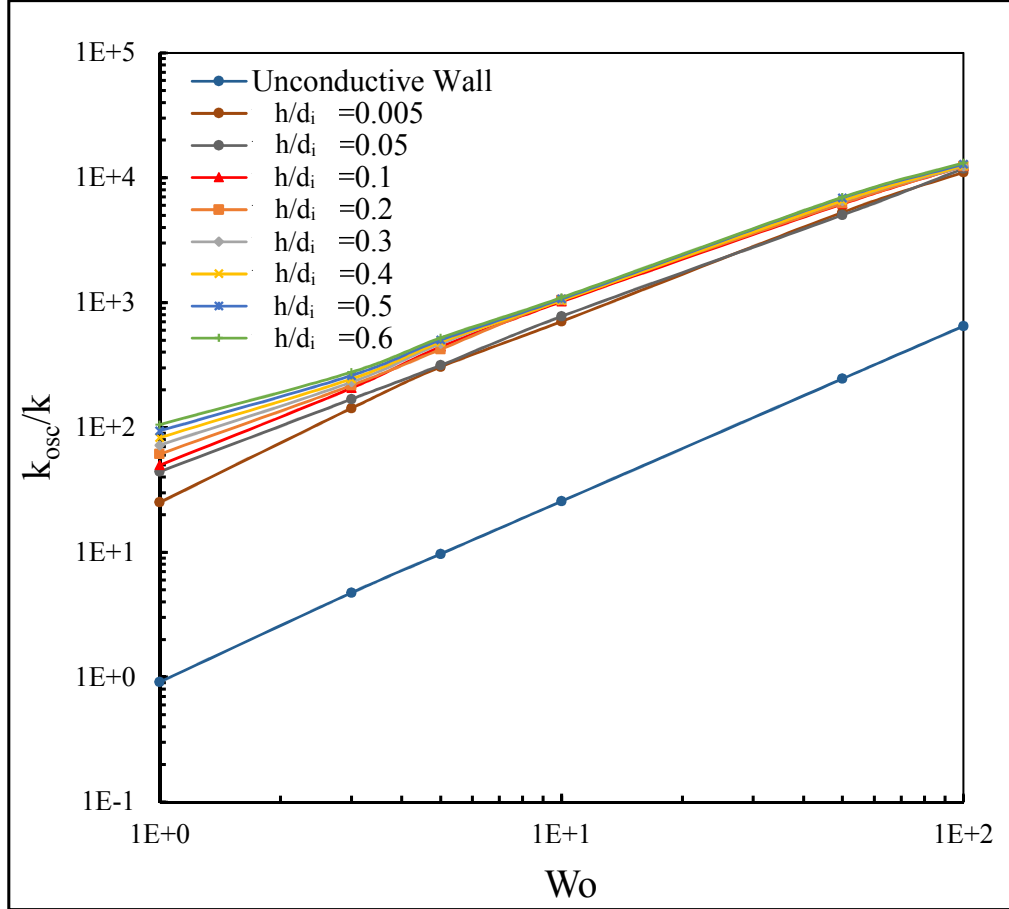
Figure 4.11: Effect of tube wall thickness h in enhancing the axial heat transfer rate
$(\Delta Z/L = 0.12)$

The effect of the tube wall thickness is more pronounced at low frequencies when the flow is close to quasi-steady. For the largest tube wall thickness the enhancement in oscillatory thermal conductivity decreases from about twenty times at $Wo = 1$ to about ten times at $Wo = 100$. Therefore, the tube wall thickness affects the storage-release process through the conductive penetration layer significantly, which leads to enhancing the heat transfer rate. This approximately ten times axial heat transfer rate enhancement could be achieved with a minimum tube wall thickness which is preferable in practical application to reduce the cost and weight of systems. This is clear from

Figure 4.11, in which the ratio of tube wall thickness h to the tube inner diameter d_i equal to 0.005, enhances the axial heat transfer rate by about ten times for different oscillation rates compared with insulated tube walls. Increasing this ratio to 0.6 enhances the oscillatory thermal conductivity by 100 to 10 times the molecular thermal conductivity. However, the effect of the thicker wall appears at low Wo and then decreases to close to that of the minimum tube wall thickness. Depending on the minimum tube wall thickness, we can multiply the suggested correlations in Equations 4.2 and 4.3 by up to 10 to get the total axial heat transfer enhancement rate.

CHAPTER 5

VISCOUS HEAT DISSIPATION

5.1 Introduction

Previous analytical studies have used the assumptions given in appendix to simplify the oscilla-
tory flow problem. One important parameter in oscillatory flow is Viscous Heat Dissipation(VHD).
This parameter has been neglected in most studies, and there is no clear criterion or limitation for
this factor in oscillatory flows' studies over any range of frequencies or displacements. Therefore,
there no known threshold for including or ignoring VHD in oscillatory flow. VHD becomes more
important in oscillatory flow as the oscillatory boundary layer near the wall becomes thinner with
an increase in the frequency, which increases the velocity gradient as shown in Figure 4.1. This
figure shows the variation in radial gradient of normalized axial velocity in the middle of the tube
with an increase in Wo for different phase angles. It is clear that $\partial u_z / \partial r$ is affected by increas-
ing the frequency, which reduces the thickness of the oscillatory boundary layer. This oscillating
boundary layer is the Stokes layer where $(\delta_s = \sqrt{2\nu/\omega})$.

In this chapter, oscillatory flow is studied to account for VHD's effect [89]. The objective of
the analysis in this chapter is to determine a threshold for when VHD should be accounted for in
studies of oscillatory flow. The threshold will indicate when the assumption of ignoring VHD is
significant in the thermal energy equation. In addition, the rate of increasing the fluid temperature
by VHD in the tube, reservoirs, and the tube-reservoirs' systems is discussed. Because of the low
Prandtl number for air, VHD in air is more important than in liquids. Viscous heat dissipation
represents the heat transformed from work done by the fluid due to the effect of shear forces on
adjacent layers. VHD has a substantial contribution in many practical applications of steady and
unsteady flows. This effect appears as an increase in the system's temperature with time.

In oscillatory flow, the fluid shear over a solid surface penetrates into the fluid by a Stokes layer
thicknessδ_s. The radial gradient in velocity inside Stokes layer is the primary factor in developing

the rate of viscous heat dissipation. Since the dissipation rate $\Phi = \mu(\partial u_z/\partial r)^2$ in fully developed pipe flow, VHD will take place inside this penetrated layer, especially at high frequencies when the radial gradient of velocity will be sharp. By considering 2D-axisymmetric numerical simulations for incompressible oscillatory flow with adiabatic non-conductive walls, the limitations of VHD will be specified in terms of axial tidal displacement by fluid per tube length $\Delta Z/L$ and the Womersley number Wo.
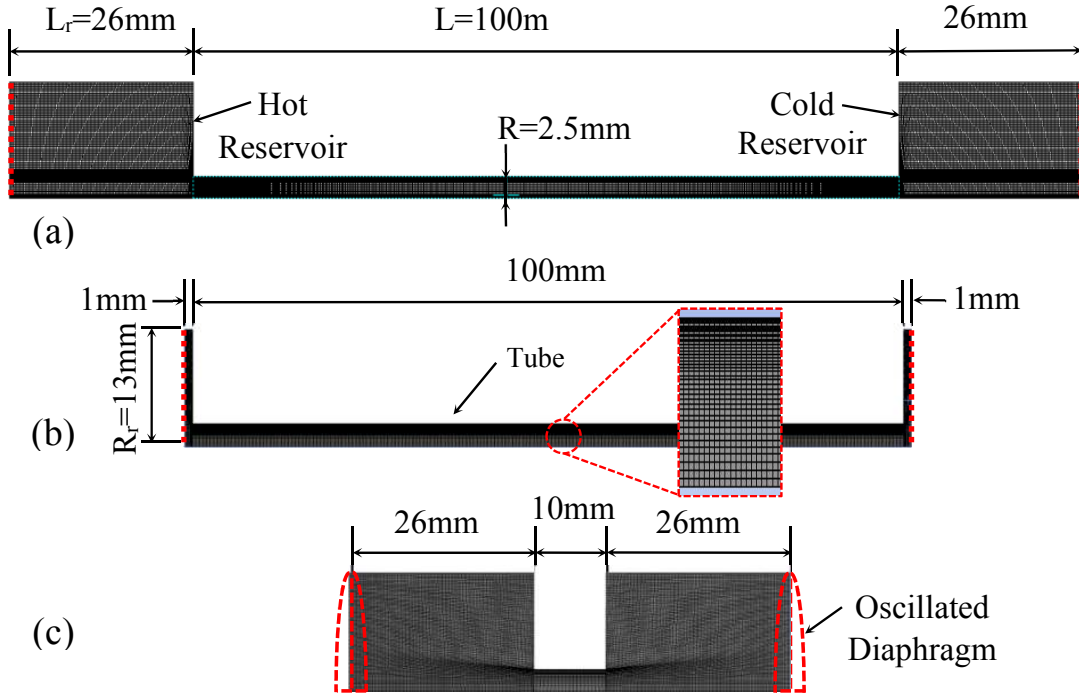
Figure 5.1: The schematic, dimensions, and meshes of the computational domains,(a) tube-reservoirs system, (b) tube, (c) reservoirs

Three computational domains are considered in this VHD study. These three domains are presented in Figure 5.1. The model in Figure 5.1b was used to validate the predicted results based on computations by comparing them with the analytical solution of oscillatory flow in a tube only, which is given by Brereton and Jalil [43]. Also, the two reduced models (Figures 5.1b and 5.1c) are used to study VHD when either the tube or reservoirs dominates the system. Figure 5.1a represents the main model that is considered at various frequencies and axial tidal displacements. As shown in Figure 5.1a, the model consist of three main parts: the cold reservoir, hot reservoir, and the tube,

which connects the reservoirs. The reservoirs radius R_r is 13mm with length 26mm, and the tube radius(R) is 2.5mm with length 100mm.

5.2 Governing Equations

The governing equations for two-dimensional axisymmetric incompressible viscous oscillatory flow are shown below [79, 80].

- Continuity equation

$$\frac{\partial u_z}{\partial z} + \frac{\partial u_r}{\partial r} + \frac{u_r}{r} = 0 \tag{5.1}$$

- Momentum equations

$$\frac{\partial u_z}{\partial t} + \frac{1}{r}\frac{\partial r u_z u_z}{\partial z} + \frac{1}{r}\frac{\partial r u_r u_z}{\partial r} = -\frac{1}{\rho}\frac{\partial p}{\partial z}$$
$$+ \frac{1}{r}\frac{\partial}{\partial z}\left[2r\nu\frac{\partial u_z}{\partial z}\right] + \frac{1}{r}\frac{\partial}{\partial r}\left[r\nu\left(\frac{\partial u_z}{\partial r} + \frac{\partial u_r}{\partial z}\right)\right] \tag{5.2a}$$

$$\frac{\partial u_r}{\partial t} + \frac{1}{r}\frac{\partial r u_z u_r}{\partial z} + \frac{1}{r}\frac{\partial r u_r u_r}{\partial r} = -\frac{1}{\rho}\frac{\partial p}{\partial r}$$
$$+ \frac{1}{r}\frac{\partial}{\partial r}\left[2r\nu\frac{\partial u_r}{\partial r}\right] + \frac{1}{r}\frac{\partial}{\partial z}\left[r\nu\left(\frac{\partial u_r}{\partial z} + \frac{\partial u_z}{\partial r}\right)\right] - \frac{2\nu u_r}{r^2} \tag{5.2b}$$

- Energy equation

$$\rho c_p\left(\frac{\partial T}{\partial t} + u_r\frac{\partial T}{\partial r} + u_z\frac{\partial T}{\partial z}\right) = \frac{1}{r}\frac{\partial}{\partial r}\left(kr\frac{\partial T}{\partial r}\right) + \frac{\partial}{\partial z}\left(k\frac{\partial T}{\partial z}\right) + \Phi \tag{5.3a}$$

where Φ is the viscous heat dissipation heating term. Specifically

$$\Phi = 2\mu\left[\left(\frac{\partial u_r}{\partial r}\right)^2 + \left(\frac{u_r}{r}\right)^2 + \left(\frac{\partial u_z}{\partial z}\right)^2\right] + \mu\left(\frac{\partial u_z}{\partial r} + \frac{\partial u_r}{\partial z}\right)^2 \tag{5.3b}$$

91

by assuming that the flow is a fully developed flow, $\partial/\partial z = 0$ and taking an integral for the both sides of the continuity equation with ($u_r = 0 \ at \ r = R$), which leads to ($u_r = 0$), Equation 5.3b is simplified to

$$\Phi \approx \mu \left(\frac{\partial u_z}{\partial r} \right)^2 \tag{5.3c}$$

5.3 Scaling of the Thermal Energy Equation

The shear and fluid's viscosity play central roles in transferring fluid's kinetic energy into internal energy. This irreversible process leads to the fluid's temperature rising with time. In oscillatory flow, the rate of increasing the fluid's temperature depends on Wo and ΔZ of the fluid as they represent the oscillatory motions. Without accounting for the effect of VHD, other studies may underestimate fluid temperature rise.

Dissipation of mechanical work into heat affects the heat transfer characteristics. Since the dissipation rate term in the thermal energy equation depends on the radial velocity gradient squared $(\partial u/\partial r)^2$, it's effect on the oscillatory temperature field can not be determined from linear harmonic analyses of the thermal energy equation. Thus the analytical solution for any oscillatory temperature field ignores the effect of viscous dissipation. It is expected that over some ranges, it can be valid to ignore the temporal viscous heat dissipation, especially at low Womersley numbers. However, these ranges have not been specified. Therefore, this lack of understanding motivated this study of characterizing the effect of VHD in oscillatory flows.

The dissipation rate can be found from the numerical solution of the full thermal energy equation, which includes the VHD term. In particular, the commercial CFD code (FLUENT) provides the ability to activate or deactivate the VHD term in the energy equation. Therefore, the effect of VHD on numerical computations of temperature fields can be easily seen. By activating the VHD term, the thermal energy equation for the 2D-axisymmetric incompressible flow is as given in Equation 5.3a [79]. From Equation 5.3a, the thermal energy that is generated by VHD will be a source of heat. When the temperatures of hot and cold reservoirs reach an equilibrium temperature

$T_C = T_H$, the effect of VHD will be noticeable as the fluid temperature will be increased with different rates depending on the oscillatory motion. Therefore, in a closed system, the rate of VHD will balance the rate of field temperature $\partial T/\partial t$ rises. If $\Phi = 0$, then $\partial T/\partial t$ should be equal to zero at $T_C = T_H$. But when the VHD term is included in the energy equation $\Phi \neq 0$, the unsteady temperature rate will not be zero. After this equilibrium state, the fluid temperature continues to rise with time. Hence, the rate of viscous dissipative heat per unit volume $\dot{q}'''_{diss} = \frac{1}{V} \int \Phi dV$ will approximately balance the amount of heat that causes the rise in the temperature of the fluid as below

$$\dot{q}'''_{diss} \approx \rho c_p \frac{\partial T}{\partial t} \tag{5.4}$$

Also, for a unit volume of fluid, the rate of viscous dissipative heat $\dot{q}'''_{diss}$ balances the rate of viscous work done $\dot{W}$ per unit volume (which can be determined as a time average from analytical solutions)

$$\dot{q}'''_{diss} = \frac{\dot{W}}{L} \cdot \frac{1}{\pi R^2} \tag{5.5}$$

as the physical properties (ρ, c_p) of the fluid (air) and the geometry dimensions are constant, equating Equation 5.4 and Equation 5.5 will yield Equation 5.6

$$\rho c_p \frac{\partial T}{\partial t} = \frac{\dot{W}}{L} \cdot \frac{1}{\pi R^2} \implies \frac{\partial T}{\partial t} = \frac{\dot{W}}{L} \cdot \frac{1}{\pi R^2 \rho c_p} \implies \frac{\partial T}{\partial t} = C \frac{\dot{W}}{L}$$

$$\frac{\partial T}{\partial t} \propto \frac{\dot{W}}{L} \tag{5.6}$$

where C is a constant.

5.4 Viscous Heat Dissipation

5.4.1 VHD in Tubes

To validate the effect of viscous heat dissipation, the analytical solution [43] will be compared with low tidal displacement ΔZ numerical results at low and high Womersley numbers Wo in this study. To study the effect of the tube only, the lengths of the hot and cold reservoirs were reduced from $26mm$ to $1mm$ as shown in Figure 5.1b. In this case, VHD in the tube will be the dominant effect. Therefore, the computations should be consistent with the exact solution of flow in tubes only [43].

5.4.1.1 Low Womersley Number Analysis

From numerical results for an adiabatic system, the rate of increasing the fluid temperature is calculated as a function of Wo and ΔZ. The following scales with reference values denoted by the subscription $\circ$ are used to normalize the left-hand side of Equation 5.6:

- Time scale: $\qquad t_{scale} = \frac{1}{\omega} \qquad \implies \quad t^* = \omega t$

- Womersley number: $\qquad Wo = R\sqrt{\frac{\omega}{\nu}} \quad \implies \quad \omega \approx Wo^2$

- Temperature scale: $\qquad T_{scale} = T_{H_\circ} - T_{C_\circ} = \Delta T_\circ \quad \implies \quad T^* = \frac{T - T_{C_\circ}}{T_{H_\circ} - T_{C_\circ}}$

Using the above scaling, Equation 5.6 can be written as

$$\frac{\partial T^*}{\partial t^*} \propto \frac{\dot{W}}{L}\frac{1}{Wo^2} \tag{5.7}$$

The right-hand side of Equation 5.7 will be normalized at low and high Womersley numbers with a constant of approximation. This equation will be used to validate the numerical results with the analytical solution of the problem for a tube only, which only provides the rate of work done [43] or average dissipation, and not the time-dependent dissipation and its effect on the oscillatory temperature field. Therefore, by converting the relationship between the rate of work done and ΔZ

into a correlation between Wo and ΔZ, the numerical results will be validated at low ΔZ for the VHD inside the tube only.

The results of the analytical solution in Figure 2.11 for fully developed oscillatory flow in a tube (Appendix) at low Womersley numbers $(0.1 \leq Wo \leq 1)$ and low tidal displacement ΔZ showed that

$$\frac{\Delta Z}{P/\omega^2} \sim Wo^2 \qquad and \qquad \frac{\dot{W}}{L} \sim P^2$$

with an appropriate constant for each approximation. By substituting the above approximations of the exact solution in Equation 5.7

$$\frac{\partial T^*}{\partial t^*} \sim \left[\left(\frac{\Delta Z}{L} \right)^2 Wo^2 \right]^{1.0} \tag{5.8}$$

where P is the pressure gradient amplitude along the tube. The approximation, which is denoted by $\sim$, refers to the exact solution scaling [43] between the left and right sides of Equation 5.8. A constant of approximation will be defined for different Wo and ΔZ.

$$\partial T^*/\partial t^* = 1 \times 10^{-6}[(\Delta Z/L)^2 Wo^2]^{0.986}$$
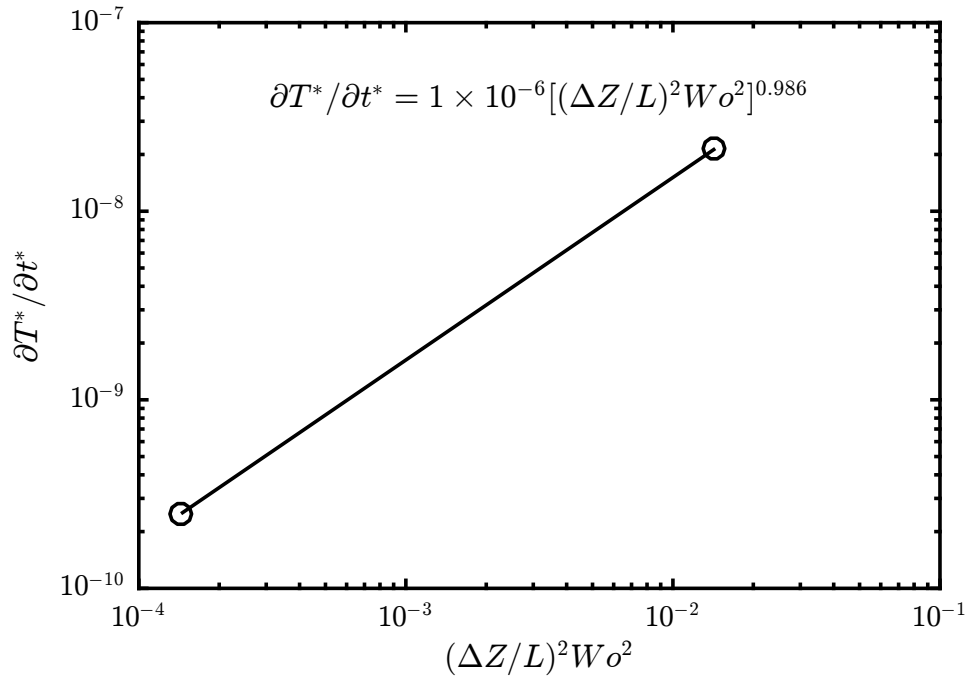
Figure 5.2: Estimate of $\partial T^*/\partial t^*$ for the range $0.1 \leq Wo \leq 1, \Delta Z/L = 0.12$ in the tube

95

Equation 5.8 shows that the normalized unsteady temperature has a quadratic scaling on the ΔZ and Wo. The numerical results are plotted together with the defined correlation in Equation 5.8 as shown in Figure 5.2. The figure illustrates the rate of increasing the normalized unsteady temperature $\partial T^*/\partial t^*$ with an increase in Wo from 0.1 to 1.0 and $\Delta Z/L = 0.12$. According to Equation 5.8, the normalized unsteady temperature $\partial T^*/\partial t^*$ should be proportional to the power one of $(\Delta Z/L)^2 Wo^2$ with an appropriate constant. By a power-law fitting for the numerical results, it is clear that the power of $(\Delta Z/L)^2 Wo^2$ is almost equal to 1. Thus, it proves that at low Wo and low ΔZ, the numerical results for VHD in the tube are consistent with the exact solution. This means that the time-averaged applied kinetic energy, which is represented by the work done, correctly balances the generated internal energy.

5.4.1.2   High Womersley Number Analysis

The same analysis was considered for high Womersley numbers ($50 \leq Wo \leq 100$) and low ΔZ. From Figure 2.11, the analytical solution of the oscillatory flow in the tube (Appendix) indicated that

$$\Delta Z \sim \frac{P}{\omega^2} \qquad and \qquad \frac{\dot{W}}{L} \sim P^2 Wo^{-3}$$

by substituting the above approximations into Equation 5.7

$$\frac{\partial T^*}{\partial t^*} \sim \left[\left(\frac{\Delta Z}{L} \right)^2 Wo^3 \right]^{1.0} \tag{5.9}$$

Equation 5.9 indicates that the normalized unsteady temperature $\partial T^*/\partial t^*$ has a quadratic scaling on ΔZ, but it has a cubic scaling on Wo. Figure 5.3 displays the numerical results according to Equation 5.9. Figure 5.3 specifically presents the rate of increasing the normalized unsteady temperature with increasing Wo from 50 to 100. From Equation 5.9, the normalized unsteady temperature is proportional to $(\Delta Z/L)^2 Wo^3$ to the power of one with an appropriate constant. Also, by applying a power fitting for the numerical results, the fitting equation shows that the power of
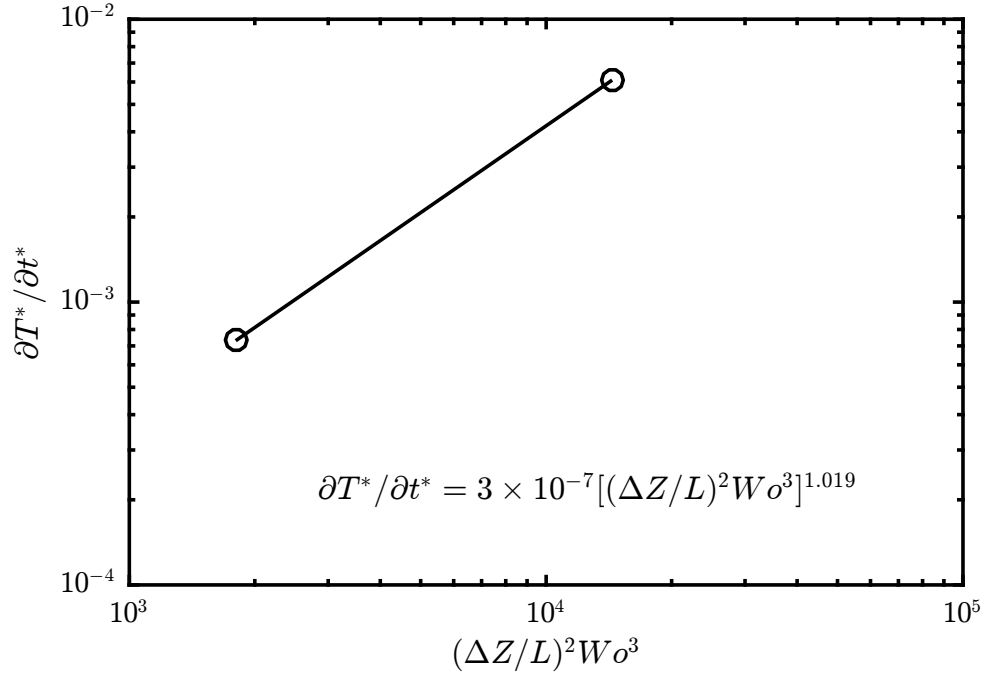
96

Figure 5.3: Estimate of $\partial T^*/\partial t^*$ for the range $50 \leq Wo \leq 100$, $\Delta Z/L = 0.12$ in the tube

$(\Delta Z/L)^2 Wo^3$ is almost equal to 1. This indicates that at high Wo and low ΔZ the numerical results for VHD in the tube are also consistent with the exact solution.

It can be concluded from the numerical results for the viscous heat dissipation in a tube that the normalized rate of temperature rise is proportional to the second power of ΔZ for both low and high Wo oscillation. Its proportionality varies from the second power to the third power of Wo with increasing the frequency of oscillation from $Wo = 0.1$ to $Wo = 100$. The low and high Wo regions were used in validations because the intermediate region in the exact solution [43] has a nonlinear profile between ΔZ and Wo in Figure 2.11 and Figure 4.9. Figure 5.4 shows how the temperature rate rises with time from low to high Womersley numbers and the scaling of the dissipation rate converts from Wo^2 at low Womersley numbers to Wo^3 at high Womersley numbers.

5.4.2 VHD in Reservoirs

In the previous section, the numerical results were consistent with the correlations defined and proposed from the exact solution [43]. These correlations are valid for work done in tubes only.

Figure 5.4: Variation of normalized unsteady temperature rate for the complete range in the tube $0.1 \leq Wo \leq 100$, $\Delta Z/L = 0.12$ in the tube

$$\partial T^*/\partial t^* = 4 \times 10^{-8}[(\Delta Z/L)^2 Wo^2]^{1.262}$$

Figure 5.5: Estimate of $\partial T^*/\partial t^*$ for the range $0.1 \leq Wo \leq 1$, $\Delta Z/L = 0.12$ in the reservoirs

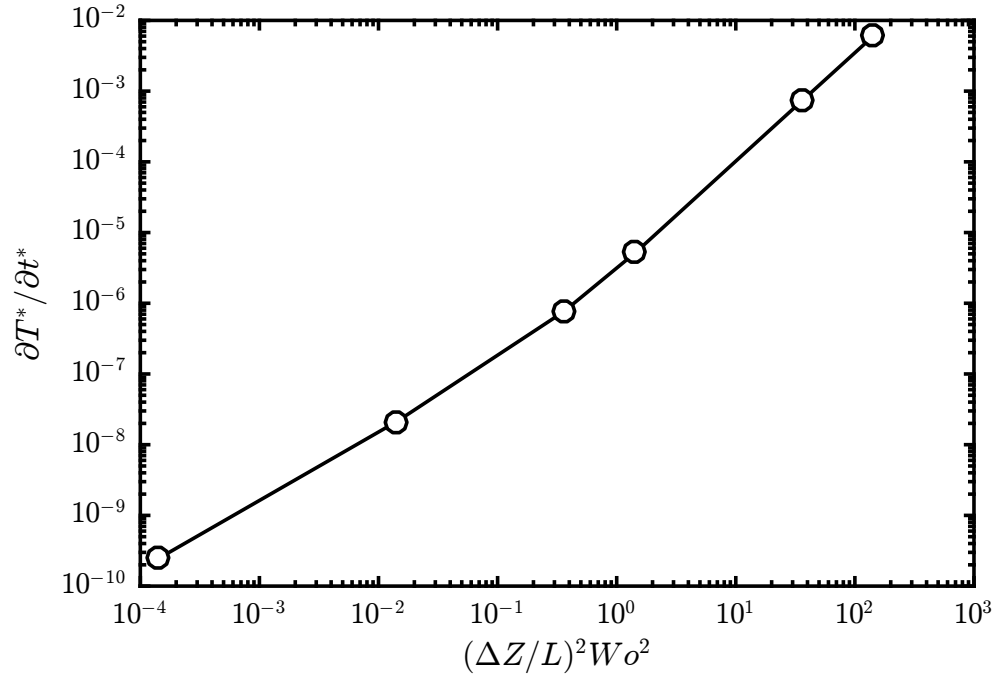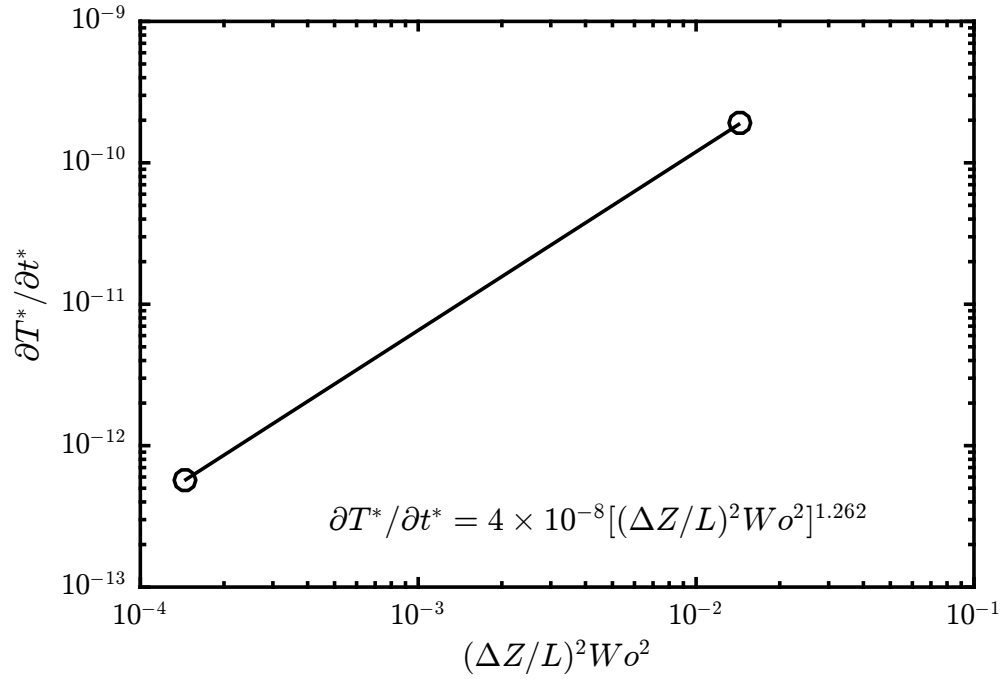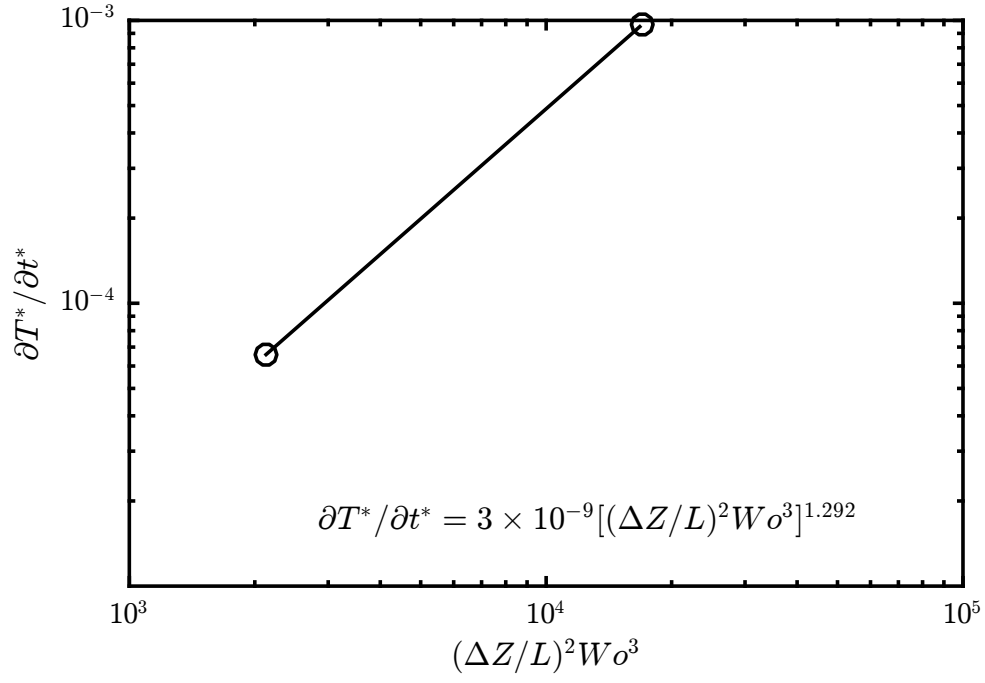Figure 5.6: Estimate of $\partial T^*/\partial t^*$ for the range $50 \leq Wo \leq 100$, $\Delta Z/L = 0.12$ in the reservoirs
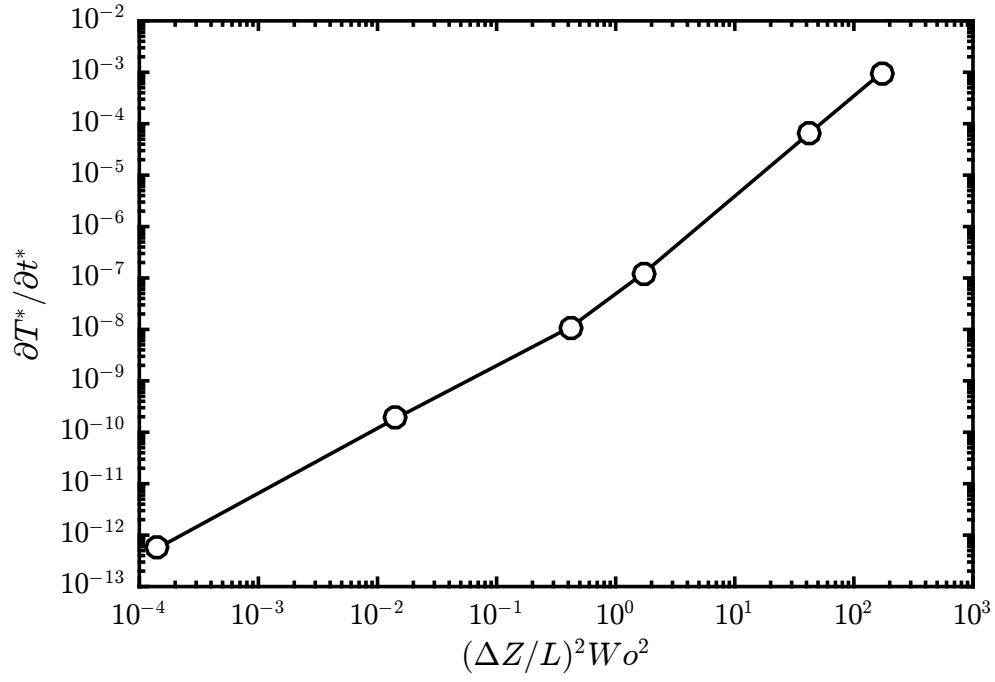

Figure 5.7: Variation of normalized unsteady temperature rate for the complete range $0.1 \leq Wo \leq 100$, $\Delta Z/L = 0.12$ in the reservoirs

Therefore, they will not be valid in the case of reservoirs. To study the effect of the reservoirs, the length of the tube was reduced to 10% of its 100*mm* original length as shown in Figure 5.1c. The results are plotted at low and high *Wo* for the same low axial tidal displacement ($\Delta Z/L = 0.12$). Figures 5.5 and 5.6 shows the rate of increasing the normalized unsteady temperature at low and high *Wo*. It is clear from the fitting equations that the dimensionless unsteady temperature does not scale proportionally to the power one of $[(\Delta Z/L)^2 Wo^2]$ or $[(\Delta Z/L)^2 Wo^3]$ at low and high *Wo*. These results are expected because of the domination of the reservoirs in dissipatory flow. Also, the amount of the temperature rise in the case of flow in a tube only is higher than its counterpart in the reservoirs because of the sharper velocity gradient in the tube compared with the reservoirs. In addition, the proposed correlation, which is defined from the exact solution, depends on a linear pressure gradient along the tube and ignores the entrance/exit region effect. The change in the rate of temperature rise in the reservoirs with *Wo* and ΔZ is plotted in Fig. 5.7.
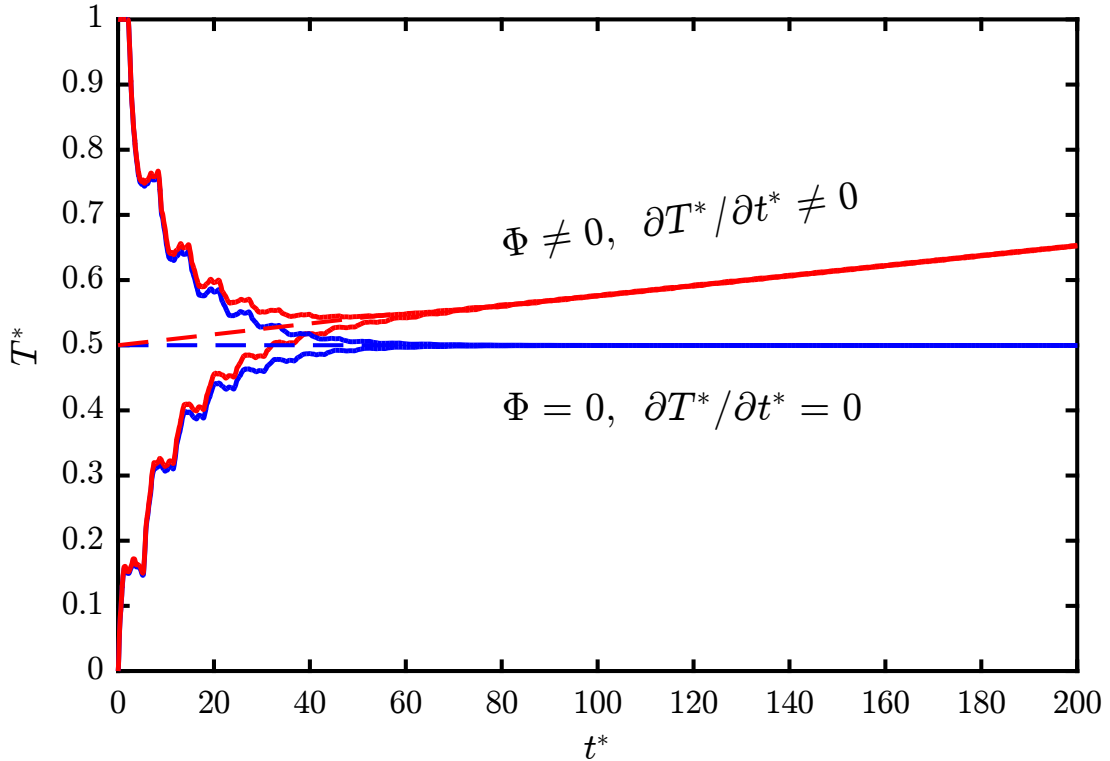

Figure 5.8: Effect of viscous heat dissipation in raising the fluid temperature

5.4.3 VHD in Tube-Reservoir's System

The tubes and reservoirs are the main parts of most practical oscillatory flow applications. To consider a real working case, the effect of these two parts are included in the simulations. The hot and cold reservoirs are initialized at $350K$ and $300K$ respectively. The hot and cold reservoirs have the same size, so both reservoirs will reach the thermal equilibrium at their mid temperature 325K without further increase in the field temperature with time if there is no VHD effect ($\Phi = 0$). Without including the VHD term in simulations, the hot reservoir is continuously cooled and the cold reservoir is continuously heated until reaching the thermal equilibrium state. As there is no external source of heating and the model was simulated with adiabatic boundary conditions, the hot and cold reservoirs were maintained at their average temperature without any rise in temperature with time as shown in Figure 5.8. By including the VHD term in the thermal energy equation($\Phi \neq 0$), the temperature in the system will start rising with time after reaching an equilibrium state. To reduce the cost of simulation, an equilibrium or average temperature was chosen to initialize all cases with the VHD term in the thermal energy equation. This average temperature is equal to $325K$. Also, the dashed lines in Figure 5.8 show that the normalized temperature gradient lines for both cases have intersected at this average temperature of the hot and cold reservoirs. The VHD will be more effective as ΔZ and Wo increase, especially for air as it is a low Prandtl number fluid.

The rate of raising the fluid temperature depends on Wo and the axial displacement of the fluid. Therefore, the effect of VHD will be negligible at the lower limits of these two parameters and then will be significant. Figure 5.9 shows the increase in the temperature of the fluid with time for different Wo and ΔZ. It is clear from the figure that at low Wo there is no noticeable rise in the system temperature. As the frequency of oscillation increases, the Stokes layer becomes thinner, which increases the radial gradient of axial velocity near the wall. This increase in the radial gradient of axial velocity will lead to a rise in air temperature because there is more viscous heat dissipated in the system. The same procedures, which were dependent on the validation of VHD for the tube or reservoirs, are considered in order to find the effect of dissipation in the tube-reservoir system.
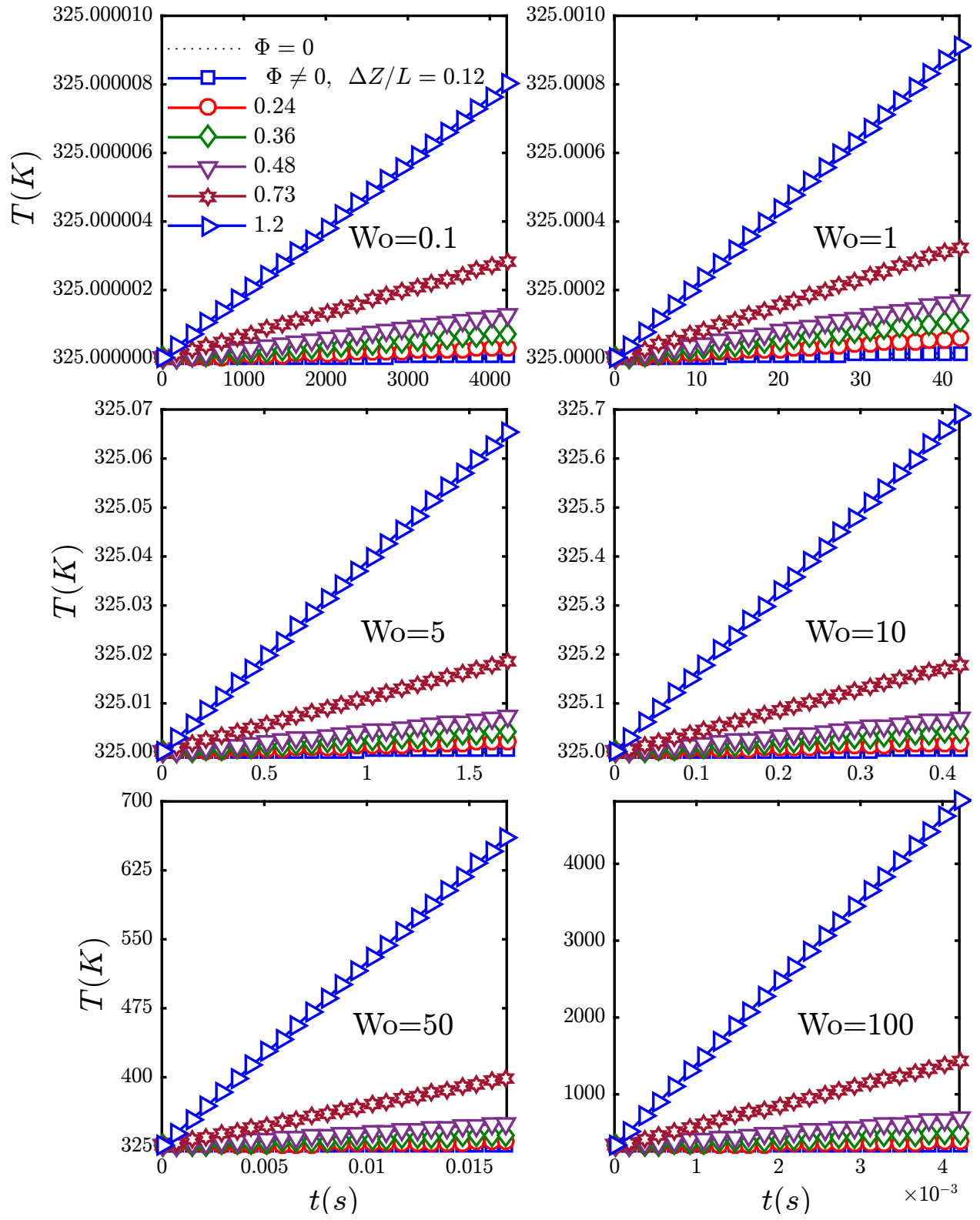
Figure 5.9: Effect of viscous heat dissipation in heating the air at different Womersley numbers and axial tidal displacements
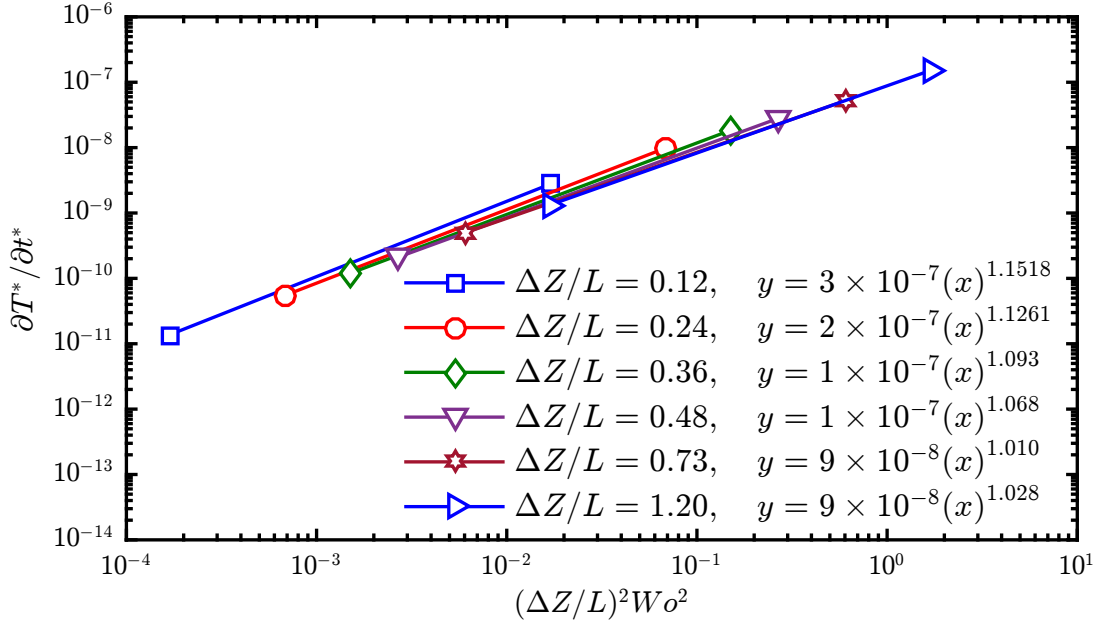
Figure 5.10: Variation of unsteady temperature rate for $0.1 \leq Wo \leq 1$ and different ΔZ for the tube-reservoir's system

The effect of the VHD is presented in term of $(\Delta Z/L)^2 Wo^2$ as the normalized parameter for the oscillatory flow system. From the numerical results and for low Womersley ($Wo \leq 1$) and various ΔZ, the results have different behaviors as shown in Figure 5.10. At low ΔZ, the power of the proportionality is about 1.15, which is between the power of dissipation dominated by the tube and the dissipation dominated by the reservoirs. The rate of rise in the normalized temperature is proportional to $(\Delta Z/L)^2 Wo^2$ to a power varying from 1.15 at low ΔZ to about 1.02 at high ΔZ. This variation in proportionality occurs because as ΔZ increases the dissipation in the tube becomes more important. Therefore, from the fitting equations, the power of variable x, which represents $(\Delta Z/L)^2 Wo^2$, reduces with an increase in ΔZ to be almost equal to 1 at the highest axial displacement.

Figure 5.11 shows the numerical results for high Womersley numbers ($Wo \geq 50$) and for different axial tidal displacements. The dimensionless unsteady temperature was plotted against $(\Delta Z/L)^2 Wo^3$. The results show that the rate of increasing the system temperature does not scale to Wo^3 as for VHD in tubes. The power of proportionality increased from unity for the tube's

Figure 5.11: Variation of unsteady normalized temperature rate with $(\Delta Z/L)^2 Wo^3$ for $50 \leq Wo \leq 100$ and different axial tidal displacement for the tube-reservoir's system

dissipation to about 1.3 on average for the tube-reservoirs dissipation as indicated in the fitting equations. Therefore, these results show the effect of the reservoirs on the scaling between the rate of temperature rise and Wo.
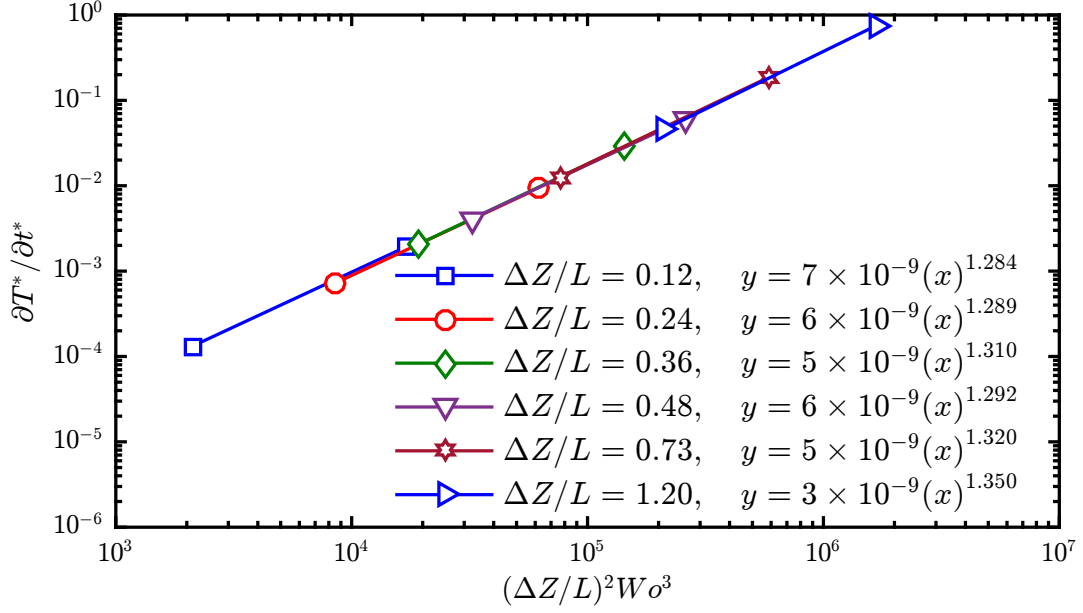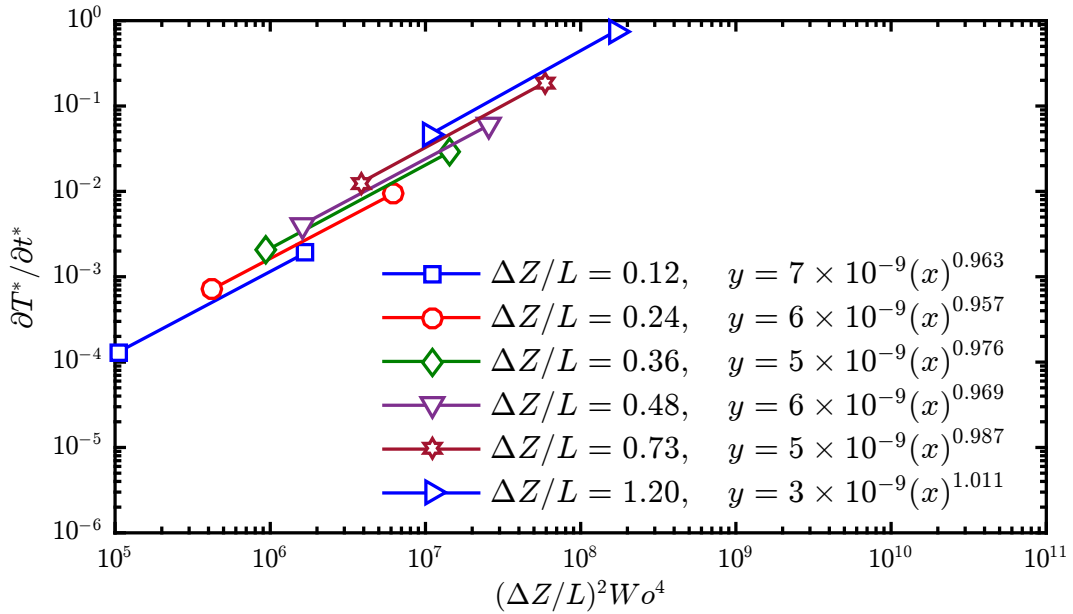

Figure 5.12: Variation of unsteady normalized temperature rate with $(\Delta Z/L)^2 \text{Wo}^4$ for $50 \leq Wo \leq 100$ and different axial tidal displacements for the tube-reservoir's system

104

To get an approximate scaling for the tube-reservoir's system dissipation rate, the results are presented in Figure 5.12 by plotting the rate of temperature change against $(\Delta Z/L)^2 \mathrm{Wo}^4$. The power fitting for all axial tidal displacements show that the normalized unsteady temperature is proportional to $(\Delta Z/L)^2 \mathrm{Wo}^4$ to the power approximately equal to 1. Therefore, it is important to include the reservoir effect in solving such a problem, especially at high Wo for low or large axial fluid displacements. From the above results, it is clear that the VHD scales quadratically with Wo and ΔZ for dissipation in tubes only at low Wo and ΔZ. In the tube-reservoir's system the VHD scaling from about 15% extra of the quadratic Wo and ΔZ at low ΔZ to a quadratic Wo at high ΔZ. At high Wo, the rate of VHD in a tube only scales to cubic Wo and to the quartic Wo in the tube-reservoir's system.

Figure 5.13 shows the change in normalized unsteady temperature at the same low axial tidal displacement $(\Delta Z/L = 0.12)$ for the three studied cases: tube, reservoirs, and tube-reservoir's system. The figure indicates that the highest rate of dissipation is generated inside the tube as expected because of the high radial gradient of the axial velocity near the tube wall and the large amount of fluid inside the reservoirs compared with tube. In addition, the amount of heat dissipation as a result of the velocity gradient will be dissipated with a specific rate in each region. Therefore, the temperature field will be increased depending on the specific heat capacity of the fluid. Hence, for the same amount of dissipated heat, the fluid inside the tube will heated up more than the fluid inside the reservoir as a results of the sufficient fluid mass inside the reservoir. This mass of fluid will balance the addition of heat from the viscous heat dissipation. The results of the tube-reservoir system are in between of the tube's and reservoirs' results in its rate of increasing the normalized unsteady temperature with Wo.

5.5 Significance of Viscous Heat Dissipation

5.5.1 Nondimensionalization of the Thermal Energy Equation

To define a threshold for VHD effects, it is preferable to write the thermal energy equation (Eq. 5.3a) in its nondimensional form. In addition to the characteristic quantities that were defined in
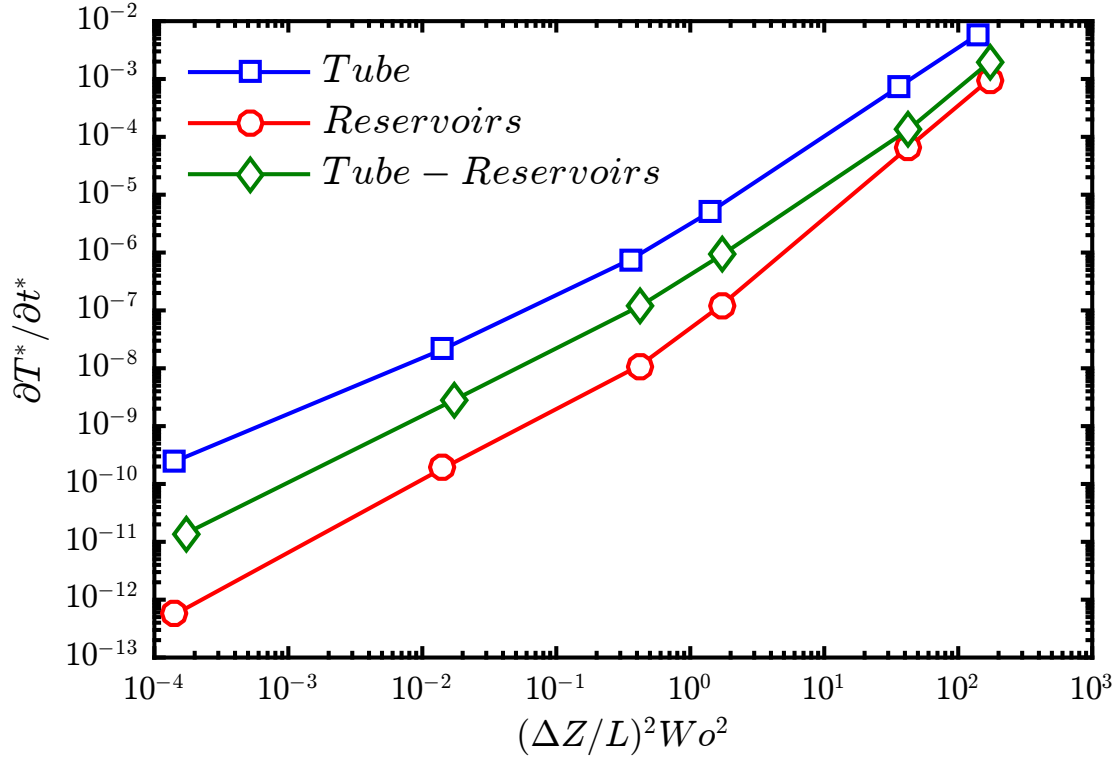
Figure 5.13: Variation of unsteady temperature rate for tube, reservoirs, and tube-reservoir's system at $\Delta Z/L = 0.12$

section (5.3), the tube radius R and the averaged cross-sectional-area velocity amplitude $|u_{avg}|$ are considered as a characteristics length and velocity. From these characteristic quantities, the following dimensionless parameters are defined: ₒ

$$t^* = \omega t \ , \qquad r^* = \frac{r}{R} \ , \qquad z^* = \frac{z}{R} \ , \qquad u_r^* = \frac{u_r}{|u_{avg}|} \ , \qquad u_z^* = \frac{u_z}{|u_{avg}|} \ ,$$

$$\mu^* = \frac{\mu}{\mu_\circ} \ , \qquad c_p^* = \frac{c_p}{c_{p_\circ}} \ , \qquad \rho^* = \frac{\rho}{\rho_\circ} , \qquad k^* = \frac{k}{k_\circ} , \qquad \alpha^* = \frac{k^*}{\rho^* c_p^*} \ ,$$

$$\Delta T_\circ = T_{H_\circ} - T_{C_\circ} \ , \qquad T^* = \frac{T - T_{C_\circ}}{\Delta T_\circ} \ , \qquad \Phi^* = \frac{\Phi}{\Phi_\circ} = \frac{\mu \left(\frac{\partial u_z}{\partial r} \right)^2}{\mu_\circ \left(\frac{|u_{avg}|}{R} \right)^2} = \left(\frac{R^2}{\mu_\circ |u_{avg}|^2} \right) \Phi$$

$$Pr = \frac{c_{p_\circ} \mu_\circ}{k_\circ} \ , \qquad Ec = \frac{|u_{avg}|^2}{c_{p_\circ} \Delta T_\circ} \ , \qquad Br = Pr.Ec \ , \qquad Pe = Pr.Re$$

where Pr is the Prandtl number, Pe is the Peclet number, Ec is the Eckert number, and Br is the Brinkman number. By substituting these dimensionless parameters in Equation 5.3a, the thermal energy equation can be written as

106

$$PrWo^2\left(\frac{\partial T^*}{\partial t^*}\right) + PrRe\left(u_r^*\frac{\partial T^*}{\partial r^*} + u_z^*\frac{\partial T^*}{\partial z^*}\right) =$$

$$\left(\frac{\alpha^*}{r^*}\frac{\partial}{\partial r^*}\left(r^*\frac{\partial T^*}{\partial r^*}\right) + \alpha^*\frac{\partial}{\partial z^*}\left(\frac{\partial T^*}{\partial z^*}\right)\right) + PrEc\left(\frac{\Phi^*}{\rho^*c_p^*}\right) \quad (5.10a)$$

The first and second terms on the right-hand side of Equation 5.10a represent the conductive heat transfer and viscous dissipation terms. For the purpose of comparison between these two terms, the maximum value for each dimensionless quantity in Equation 5.10a is assumed to be about 1. Therefore, Equation 5.10a can be simplified and written as in Equation 5.10b

$$Pr.Wo^2 + Pr.Re = 1.0 + Pr.Ec$$

$$Pr.Wo^2 + Pe = 1.0 + Br$$

$$\text{(5.10b)}$$

Since conduction is always considered to be important, the question is when the viscous heat dissipation will be more important than the conduction. The scaling in Equation 5.10b indicates that when $Pr.Ec \geq 1$ then it is expected that the VHD is more important than conduction. The Eckert number Ec, which represents the ratio of advective mass transfer or kinetic energy of the flow to the enthalpy or heat dissipation potential, is used to define the limitation of the effect of the fluid self-heating as a consequence of VHD. As the current study considers an oscillatory flow, it is useful to present the Eckert number in terms of the Womersley number Wo and the tidal displacement ΔZ. If the averaged cross-sectional-area velocity amplitude $|u_{avg}|$ is defined as $|u_{avg}| = \Delta Z\omega$, then the Eckert number can be written as

$$Ec = \frac{(\Delta Z\omega)^2}{c_{p_\circ}\Delta T_\circ} \quad (5.11a)$$

$$PrEc = \frac{Pr\Delta Z^2}{c_{p_\circ}\Delta T_\circ}\left[\frac{\nu Wo^2}{R^2}\right]^2 \quad (5.11b)$$

When $Pr.Ec \ll 1$, the effect of energy dissipation can be ignored relative to fluid heat conduction. With increasing $Pr.Ec$ the dissipated energy in the fluid becomes a more significant parameter

in the heat transfer process. When $Pr.Ec \geq 1$, VHD will play an important role in the overall heat transfer. Therefore, the effect of VHD can be classified into three categories; negligible, significant, and important.

5.5.2 Temperature Distribution and Dissipation in the Analogous Constant-Reservoir Temperature Problem

The time-area averaged temperature distribution along the tube will be affected by the viscous heat dissipation. This temperature distribution will be changed from a linear profile for $\Phi = 0$ to a convex profile for $\Phi > 0$ as shown below. The thermal energy equation can be written as

$$\frac{\partial T}{\partial t} + u_r \frac{\partial T}{\partial r} + u_z \frac{\partial T}{\partial z} = \frac{\alpha}{r} \frac{\partial}{\partial r} \left(r \frac{\partial T}{\partial r} \right) + \alpha \frac{\partial^2 T}{\partial z^2} + \Phi \tag{5.12a}$$

by averaging Equation 5.12a over the tube cross-section area, $\partial T_{avg}/\partial r$ will be zero and Equation 5.12a can be written as

$$\frac{\partial T_{avg}}{\partial t} + \left(u_r \frac{\partial T}{\partial r} \right)_{avg} + \left(u_z \frac{\partial T}{\partial z} \right)_{avg} = \alpha \frac{\partial^2 T_{avg}}{\partial z^2} + \Phi_{avg} \tag{5.12b}$$

and by integrating Equation 5.12b over time for reciprocating flow, which is fully reversing as the flow changes its direction cyclically with zero mean velocity, as shown in Figure 1.1b, Equation 5.12b can be written as

$$\frac{d^2 \overline{T}_{avg}}{dz^2} = C.\overline{\Phi}_{avg} \tag{5.12c}$$

where C is a constant and Φ does not depend on z (except in case of entrance effects)

By applying the boundary conditions $(\overline{T}_{avg}(z) = T_{Ho}$ at $z = 0)$ and $(\overline{T}_{avg}(z) = T_{Co}$ at $z = L)$, there will be two solutions for Equation 5.12c. Therefore, the temperature gradient along the tube can be stated as

$$\text{If } \Phi \begin{cases} = 0 & \begin{cases} \dfrac{d\overline{T}_{avg}}{dz} = const. \\[2mm] \overline{T}_{avg} = \overline{T}_H + (\overline{T}_C - \overline{T}_H)\dfrac{z}{L} \quad \text{(Linear temperature profile)} \end{cases} \\[10mm] > 0 & \begin{cases} \dfrac{d\overline{T}_{avg}}{dz} = C.\overline{\Phi}_{avg}.z + const. \\[2mm] \overline{T}_{avg} = \overline{T}_H + (\overline{T}_C - \overline{T}_H)\dfrac{z}{L} - C.\overline{\Phi}_{avg}\dfrac{L^2}{2}\dfrac{z}{L} + C.\overline{\Phi}_{avg}\dfrac{z^2}{2} \end{cases} \end{cases}$$

Figure 5.14 shows the effects of VHD ($\Phi \neq 0$) on time-averaged centerline temperature variation along the tube for different *PrEc* values compared with $\Phi = 0$. It is clear that at *PrEc* values ($\Phi > 0$) the temperature profile almost matches the linear temperature profile for $\Phi = 0$. At this rate of dissipation, the viscous heat dissipation will be almost negligible, which is of order $O(10^{-2})$. With increasing Womersley number the VHD will be more significant. In this range of dissipation the air temperature increases inside the tube with different rates depending on Womersley number but does not exceed the hot reservoir temperature. When the air temperature exceeds that of the hot reservoir temperature, the VHD will be important, which is of order $O(10^0)$. It is clear how the dissipation effect is increased significantly at this region compared with dissipation at *PrEc* of order $O(10^{-1})$. This significant increment in the dissipation rate because of Womersley number increased from 50 to 100 , which represents an increase in frequency from about 900 Hz to 3700 Hz that causes a high velocity gradient near the wall with high dissipation rate.

If it is assumed that the contribution of VHD compared to conductive heat transfer in each of these three categories (negligible, significant, important) is of order $O(10^{-2}), O(10^{-1}), O(10^0)$ respectively, then Equation 5.10b can be stated as below for any oscillatory flow

$$\text{If } \left[\frac{Pr\Delta Z^2}{c_{p_\circ}\Delta T_\circ} \left(\frac{vWo^2}{R^2} \right)^2 \right] \begin{cases} \leq O(10^{-2}) \;\; OR \;\; \ll 1, & \Phi \approx 0 \quad \text{(VHD Negligible)} \\[2mm] O(10^{-2}) < [...] < O(10^0), & \Phi > 0 \quad \text{(VHD Significant)} \\[2mm] \geq O(10^0) \;\; OR \;\; \geq 1, & \Phi \gg 0 \quad \text{(VHD Important)} \end{cases}$$

The above statement or criterion can be use for oscillatory flows with different Prandtl numbers as it is derived from the full thermal energy equation.
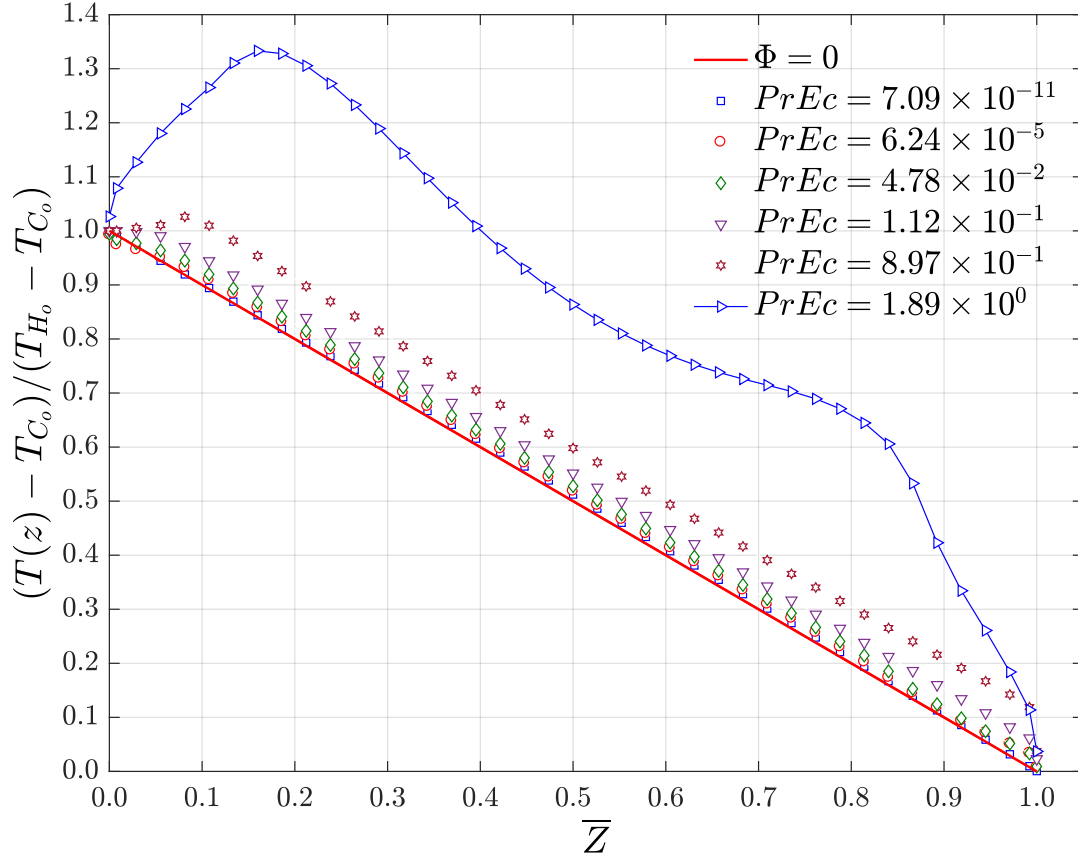
Figure 5.14: Effects of VHD on time-averaged centerline temperature distribution along the tube

5.5.3 Proposed Criterion and Correlation for the Current Study

From Equation 5.10b, after substituting the physical properties for air, a threshold can be defined in terms of Womersley number Wo and the normalized axial tidal displacement $\Delta Z/L$ as shown in Figure 5.15. This is the criterion for including or ignoring the effect of VHD of air in oscillatory flow. Therefore, for $Pr.Ec \geq 1$ when the dissipation effects are significant, the following limitations are proposed for the current oscillatory air flow study and initial temperature differences

$$
\text{If } \left[\left(\frac{\Delta Z}{L}\right)^2 Wo^4\right]
\begin{cases}
\leq O(10^4), & \Phi \approx 0 \quad \text{(VHD Negligible)} \\
O(10^4) < \left(\frac{\Delta Z}{L}\right)^2 Wo^4 < O(10^6), & \Phi \neq 0 \quad \text{(VHD Significant)} \\
\geq O(10^6), & \Phi \neq 0 \quad \text{(VHD Important)}
\end{cases}
$$
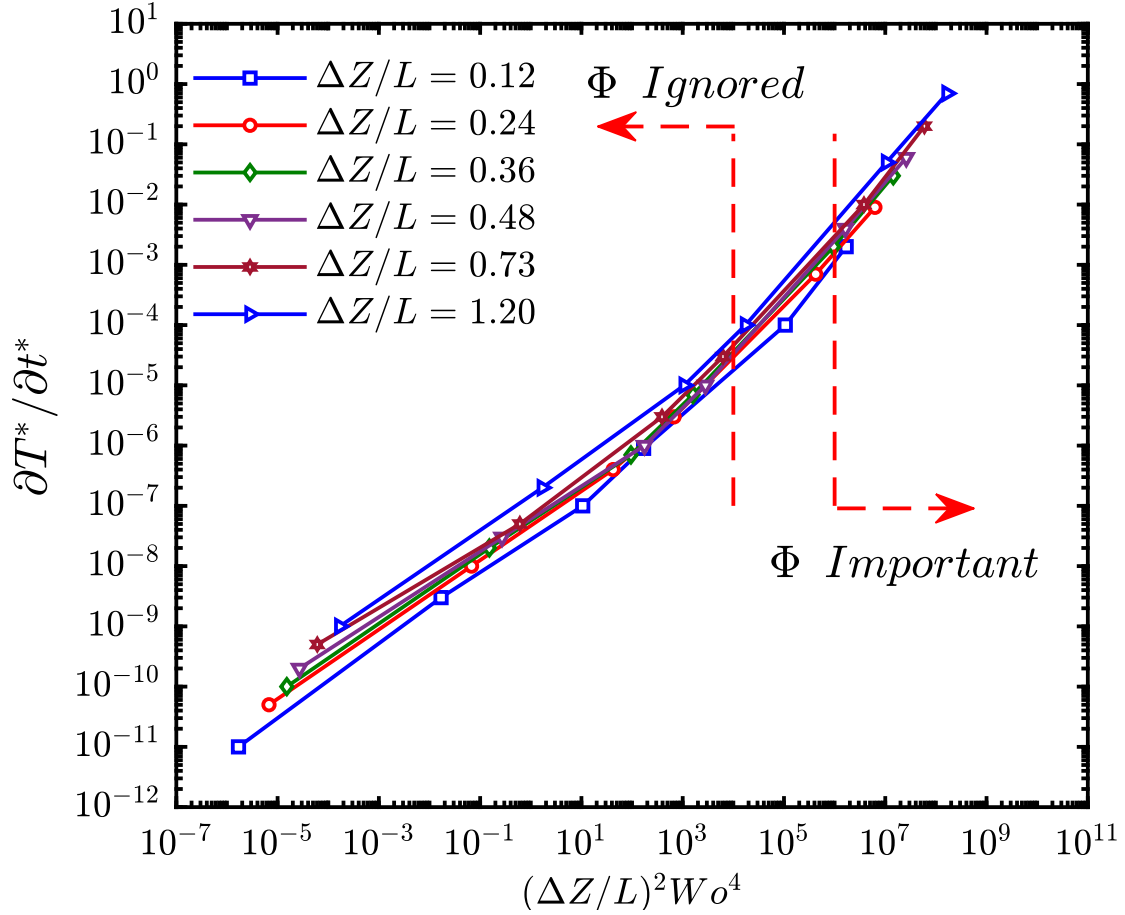
Figure 5.15: Variation of normalized unsteady temperature rate for $0.1 \leq Wo \leq 100$ and different axial tidal displacements

From the numerical results presented in Figure 5.9 for different Wo and ΔZ, the VHD effect appears at different values of $(\Delta Z/L)^2 Wo^4$; it is not effective at low $PrEc$. The effect of the VHD becomes noticeable at $PrEc > O(10^{-2})$ for various axial tidal displacements according to the predicted data. Figure 5.15 illustrates the rate of increase in normalized temperature for different axial tidal displacements under the effect of oscillatory motion in the tube-reservoir system.

Based on the computations in Figure 5.9, the onset of the rise in the rate of the field temperature takes place at $(\Delta Z/L)^2 Wo^4 \approx O(10^4)$ for various axial tidal displacements. In this region, the rate of viscous work is small, and does not impose sufficient kinetic energy to convert into internal energy to heat the fluid. By increasing Wo and ΔZ, the VHD rate will be affected more by the oscillatory motion as a result of the high gradient of velocity near the wall, which in-

111

creases the rate of viscous work. The rate of the rise in the fluid temperature will be important at $(\Delta Z/L)^2 Wo^4 \geq O(10^6)$. The rate of raise in the temperature field could be calculated from any of the predicted correlations in Figures 5.10, 5.11, or 5.12, especially for high Womersley numbers. This criterion takes a simple form because it depends on only two parameters (Wo and ΔZ). These two parameters contain all essential flow and geometry aspects (R, L, P, u, ω, ν) for air.

$$\frac{\partial T^*}{\partial t^*} = 6 \times 10^{-9} \left[\left(\frac{\Delta Z}{L} \right)^2 Wo^3 \right]^{1.3} \tag{5.13}$$

It is clear from Figure 5.11 that the temperature rise is similar for different axial tidal displacements at high frequencies. Increasing the frequency will lead to a thinner Stokes layer and a higher velocity gradient, which causes this similarity in results. Therefore, the frequency will be the dominated factor in raising the field temperature. To simplify the findings of the current study, a general correlation is suggested to calculate the variation in the rate of normalized temperature in term of Wo and ΔZ. A power-law fit is applied to the collapsed results in Figure 5.11 to get a correlation to describe the effective region of VHD as in Equation 5.13. This equation can be used to predict the field temperature over time and estimate the amount of heat that will be generated by the viscous dissipation. This suggested correlation is valid for air with tidal displacement ΔZ up to the tube length and $Wo > 10$.

CHAPTER 6

CONCLUSIONS AND FUTURE RESEARCH

6.1   Conclusions

The current study investigated the oscillatory axial heat transfer enhancement between hot and cold reservoirs connected by a bundle of cylindrical tubes under constant air properties, both excluding and including the viscous heat dissipation effect. Womersley number, pressure gradient amplitude, and axial tidal displacement are the main parameters considered in the calculations. A 3D numerical model was designed to be identical to the experimental setup and to match practical heat exchangers. Four different Womersley numbers were considered in the experiments with four different tidal displacements for each Wo, which were used to validate the numerical models. The numerical results have been validated experimentally and analytically. The validation consists of two parts: fluid mechanics validation and heat transfer validation. Both validations showed a good agreement with the experimental and analytical results. The results at low tidal displacement, where the flow fully-developed over most of the tube length, were validated by comparing with previous analytical studies.

To achieve one of the study goals, two correlations of enhanced thermal conductivity normalized by the square of the tidal displacement were suggested as a function of Womersley number and tidal displacement. According to the suggested correlations, the axial heat transfer rate scale in proportion to $Wo^{1.62}$ for different tidal displacements at $Wo \geq 3$, as it collapses above this Womersley number under normalization. For $Wo < 3$ the results will vary exponentially depending on the tidal displacement. This enhancement has improved the rate of axial heat transfer by about five orders of magnitude for different oscillating conditions. The correlations were suggested under working conditions close to practical applications. The two correlations in Equations 4.2 and 4.3 are important for applications working with fixed axial stroke displacement and variable oscillatory speed. These correlations have a wide range of applicability for researchers after validating

113

their results according to normalized results in Figures 4.7 and 4.8.

To simplify the oscillatory flow system for the designer, the oscillatory flow was classified into four different regions depending on the axial fluid displacement inside the tube: low tidal displacement which defines the fully-developed flow, medium tidal displacement, large tidal displacement which represents the oscillatory flow with little mixing, and the large tidal displacement where the flow becomes a bulk exchange between the reservoirs and the flow will be dominated by the bulk convective heat transfer. The experimental and numerical results indicated that for unsteady state flow the unsteady axial conduction term in the energy equation will be significant at $Wo < 3$ which is close to quasi-steady. This term has been ignored in previous analytical studies by assuming its value is much less than the unsteady radial conduction and there is a linear temperature gradient along the tube, which is not valid for $Wo < 3$. The other important parameter which is studied is the tube wall thickness. By adding a non-zero thermal conductivity wall thickness to the tube, the rate of heat transfer can be enhanced by more than ten times. The results showed that the effect of the conductive wall does not increase beyond a specific tube wall thickness and Womersley number.

The current study uses a new oscillatory method to match the practical applications by oscillating the fluid from both sides of the heat exchanger and with specified axial displacements, by flexible diaphragms. Also, it includes the effects of reservoirs which contribute to entrance/exit effects with flow circulation. Moreover, the study discussed the contribution of the unsteady axial conduction term in the thermal energy equation which is ignored in previous unsteady flow studies. The study results are presented in term of tidal displacement, Womersley number, and the pressure gradient amplitude for various tidal displacement and frequencies, for ease of comparison with different system geometries.

Viscous heat dissipation has been ignored in most previous unsteady flow studies. Ignoring such an important factor in unsteady flow studies may underestimate the fluid's temperature, especially, at high frequencies with high-velocity gradients $(\partial u/\partial r)^2$. The current study is one of the first to explore this limitation in oscillatory air flow solutions.

In this study, it is found from computations that the effect of the VHD is present at low oscillatory motion but without a significant effect on the temperature field. Therefore, a threshold is defined in terms of *Wo* and ΔZ as a criterion for when to include or neglect the VHD in the thermal energy equation. The criterion indicates that it is acceptable to neglect the contribution of the VHD term in the thermal energy equation only if the quantity $(\Delta Z/L)^2 Wo^4$ is approximately less than 1×10^4 in oscillatory air flows. These new results help in describing and predicting the contribution of the VHD in unsteady air flow for different frequencies and axial tidal displacements. In addition, a general correlation is suggested as a function of *Wo* and ΔZ to calculate the rate of an increase in a normalized field temperature and the contribution of the dissipative bulk heating.

6.2 Recommendations for Future Research

This section presents recommended directions for future research.

1. Studying the effect of the axial tidal displacement and Womersley number for temperature and pressure dependent flow properties.

2. Characterize the effects of viscous heat dissipation at different *Wo* and ΔZ for temperature and pressure dependent flow properties.

3. Studying the effect of using nanofluids in enhancing the rate of heat transfer by oscillatory flow for various oscillatory motion ranges.

4. Studying the axial heat transfer enhancement for transitional and turbulent oscillatory flow conditions.

5. Accelerate the thermal diffusion inside the Stokes boundary layer for example, adding an appropriate vortex generator.

APPENDIX

APPENDIX

ANALYTICAL SOLUTIONS FOR VELOCITY AND TEMPERATURE FIELDS IN FULLY DEVELOPED OSCILLATORY FLOW

This appendix provides an introduction to the analytical solutions for flow and axial heat transfer in fully developed oscillatory tube flow that have been presented in previous studies [2, 15, 30–40, 42, 43]. These solutions are for flow inside tubes only without including the effects of reservoirs. The exact solution of the fully developed oscillatory flow is used to validate fluid mechanics and heat transfer results at low tidal displacements in the current study.

To simplify the governing equations for the exact solution, several assumptions have been made in previous analytical studies for oscillatory flow inside pipes: constant properties, fully developed flow, incompressible flow, and neglect of axial heat diffusion and viscous heat dissipation.

According to these assumptions, the two-dimensional linear momentum and thermal energy equations for flow in a pipe are written as [43]

- Linear momentum equation

$$\frac{\partial u_z}{\partial t} = -\frac{1}{\rho}\frac{\partial p}{\partial z} + \frac{v}{r}\frac{\partial}{\partial r}\left(r\frac{\partial u_z}{\partial r}\right) \tag{A.1}$$

- Energy equation

$$\frac{\partial T}{\partial t} + u_z\frac{\partial T}{\partial z} = \frac{\alpha}{r}\frac{\partial}{\partial r}\left(r\frac{\partial T}{\partial r}\right) \tag{A.2}$$

where α is the thermal diffusivity.

A.1 Velocity Field Profile

These analytical studies assume that the fluid is driven by an oscillatory axial pressure gradient $\partial p/\partial z$, which is equal to $(-P.cos(\omega t))$, where P is the pressure gradient amplitude. Also, the

instantaneous radial variation in axial velocity $u_z(r,t)$ is represented by the real part of $\upsilon(r)e^{i\omega t}$. By substituting these two quantities in equation A.1, the linear momentum equation is written as

$$i\omega\upsilon = -\frac{P}{\rho} + \frac{\nu}{r}\frac{d}{dr}\left(r\frac{d\upsilon}{dr}\right) \tag{A.3}$$

The boundary conditions of $\upsilon = 0$ at the wall of the tube $(r = R)$ and symmetry about the tube centerline $(r = 0)$ are applied to equation A.3. Hence, equation A.3 is written in terms of the Bessel function of the first kind (J_o) of zeroth order as in equation A.4

$$\upsilon = \frac{iP}{\omega\rho}\left[\frac{J_o(ir^+)}{J_o(iR^+)} - 1\right] \tag{A.4}$$

where $r^+ = r\sqrt{i\omega/\nu}$ and $R^+ = R\sqrt{i\omega/\nu}$. The amplitude of cross-sectional area averaged axial velocity $|\bar{u}|$ is deduced by integrating the solution in equation A.4 radially as written in equation A.5

$$|\bar{u}| = \frac{P}{\omega\rho}\left|\frac{2J_1(ir^+)}{R\sqrt{\omega/\nu}J_o(iR^+)} - 1\right| \tag{A.5}$$

The axial tidal displacement of the fluid along a tube in oscillatory flow is defined in previous analytical studies [34, 43] as peak-to-peak axial displacement of the fluid over a half oscillatory cycle. This axial displacement is calculated from the cross-sectional-area averaged volume of the oscillated fluid as defined in equation A.6 by Zhang and Kurzweg [21] and Kaviany [34]:

$$\Delta Z = 2\left|\int_{-\pi/2}^{\pi/2}\int_0^R u_z(r,t)\ r\ dr\ dt\right| \tag{A.6}$$

From the previous solution for the linear momentum equation, a normalized tidal displacement is introduced by Zhang and Kurzweg [21] and Brereton and Jalil [43] as a function of Womersley number Wo only, as in equation A.7. This normalized tidal displacement is used to validate the current study fluid mechanics results at various tidal displacements, as shown in Figures 2.11,3.7, and 4.8.

$$\frac{\Delta Z}{P/\rho\omega^2} = f\{Wo\} \tag{A.7}$$

The analytical solution results [43] of fully developed oscillatory flow in a tube showed that for

• **Womersley numbers $(0.1 \leq Wo \leq 1)$**

$$\frac{\Delta Z}{P/\omega^2} \sim Wo^2$$
$$\frac{\dot{W}}{L} \sim P^2 \tag{A.8}$$

• **Womersley numbers $(50 \leq Wo \leq 100)$**

$$\Delta Z \sim \frac{P}{\omega^2}$$
$$\frac{\dot{W}}{L} \sim P^2 Wo^{-3} \tag{A.9}$$

These two equations(A.8 and A.9) are used in chapter five to validate the numerical results with including the viscous heat dissipation effect.

A.2   Temperature Field Profile

The temperature field in oscillatory flow is found analytically from equation A.2 by assuming a linear temperature gradient $(dT/dz = constant)$ along the tube [31]. By considering the linear gradient assumption of the axial temperature, the temperature drop along the tube from $(z = z_o)$ at the tube inlet is presented in equation A.10 [43].

$$T(r,t) - T_o = \frac{dT}{dz}\left[(z_o - z) + Re\left(\theta(r)e^{i\omega t}\right)\right] \tag{A.10}$$

By substituting equation A.10 in equation A.2, the thermal energy equation is written as

$$i\omega\theta - \upsilon = \frac{\alpha}{r}\frac{d}{dr}\left(r\frac{d\theta}{dr}\right) \tag{A.11}$$

where θ is a complex length-scale that is used to obtain the momentary temperature at various radial locations.

Assuming the tube wall is insulated and the temperature is symmetric about the tube centerline, the local momentary temperature gradient $(d\theta/dr)$ at $r = R$ and $r = 0$ will be zero. Applying these two boundary conditions yields an exact solution for equation A.11. EquationA.12 represents the solution of θ for $Pr \neq 1$.

$$\theta = \frac{P}{\omega^2 \rho} \left[\frac{Pr}{Pr-1} \left(\frac{J_o(ir^+)}{J_o(iR^+)} - \frac{1}{\sqrt{Pr}} \frac{J_1(iR^+)}{J_o(iR^+)} \frac{J_o(ir^+\sqrt{Pr})}{J_1(iR^+\sqrt{Pr})} \right) - 1 \right] \qquad \text{(A.12)}$$

To calculate the rate of heat transfer enhancement by the oscillatory flow, the ratio of oscillatory thermal conductivity k_{osc} to the molecular thermal conductivity$k$ is introduced in terms of υ and θ as written in equation A.13 [43].

$$\frac{k_{osc}}{k} = \frac{1}{4\alpha A} \int_A \left(\upsilon \overline{\theta} + \overline{\upsilon} \theta \right) dA \qquad \text{(A.13)}$$

$$\frac{k_{osc}/k}{(PR^3/\rho\nu^2)^2} = f\{Wo, Pr\} \qquad \text{(A.14)}$$

Most previous studies have presented their thermal results in dimensional forms, which make it unhelpful in comparison and validation because there are no identical working conditions for all studies. Therefore, a new normalized relationships introduced by Brereton and Jalil [43] is represented by the normalized oscillatory thermal conductivity as written in equation A.14. This equation is used to validate the numerical results.

120

BIBLIOGRAPHY

BIBLIOGRAPHY

[1] J. D. Patil and B. S. Gawali, "Experimental study of heat transfer characteristics in oscillating fluid flow in tube," *Experimental Heat Transfer*, vol. 30, no. 4, pp. 328–340, 2017.

[2] E. J. Watson, "Diffusion in oscillatory pipe flow," *Journal of Fluid Mechanics*, vol. 133, pp. 233–244, 1983.

[3] J. R. Womersley, "Method for the calculation of velocity, rate of flow and viscous drag in arteries when the pressure gradient is known.," *The Journal of physiology*, vol. 127, pp. 553–563, 1955.

[4] C. H. Joshi, R. D. Kamm, J. M. Drazen, and A. S. Slutsky, "An experimental study of gas exchange in laminar oscillatory flow," *J. Fluid Mech. flui*, vol. 133, no. 1983, pp. 245–254, 1983.

[5] U. H. Kurzweg and L. de Zhao, "Heat transfer by high-frequency oscillations: A new hydro-dynamic technique for achieving large effective thermal conductivities," *Physics of Fluids*, vol. 27, no. 11, pp. 2624–2627, 1984.

[6] U. H. Kurzweg, G. Howell, and M. J. Jaeger, "Enhanced dispersion in oscillatory flows," *Physics of Fluids*, vol. 27, no. 5, p. 1046, 1984.

[7] U. H. Kurzweg and M. J. Jaeger, "Diffusional separation of gases by sinusoidal oscillations," *Physics of Fluids*, vol. 30, no. 4, pp. 1023–1025, 1987.

[8] M. Kaviany and M. Reckker, "Performance of a Heat Exchanger Based on Enhanced Heat Diffusion in Fluids by Oscillation: Experiment," *Journal of Heat Transfer*, vol. 112, no. 1, pp. 56–63, 1990.

[9] T. S. Zhao and P. Cheng, "Oscillatory Heat Transfer in a Pipe Subjected to a Laminar Recip-rocating Flow," *Journal of Heat Transfer*, vol. 118, no. 3, p. 592, 1996.

[10] M. A. Habib, A. M. Attya, A. I. Eid, and A. Z. Aly, "Convective heat transfer characteristics of laminar pulsating pipe air flow," *Heat and Mass Transfer/Waerme- und Stoffuebertragung*, vol. 38, no. 3, pp. 221–232, 2002.

[11] U. Akdag, M. Ozdemir, and A. F. Ozguc, "Heat removal from oscillating flow in a vertical annular channel," *Heat and Mass Transfer/Waerme- und Stoffuebertragung*, vol. 44, no. 4, pp. 393–400, 2008.

[12] R. Pendyala, S. Jayanti, and A. R. Balakrishnan, "Convective heat transfer in single-phase flow in a vertical tube subjected to axial low frequency oscillations," *Heat and Mass Transfer*, vol. 44, no. 7, pp. 857–864, 2007.

[13] U. Akdag and A. F. Ozguc, "Experimental investigation of heat transfer in oscillating annular flow," *International Journal of Heat and Mass Transfer*, vol. 52, no. 11-12, pp. 2667–2672, 2009.

[14] U. Kurzweg, "Enhanced heat conduction in osillating viscous flows within parallel-plate channels," *Journal of Fluid Mechanics*, vol. 156, pp. 291–300, 1985.

[15] S. Nishio, X.-H. Shi, and W.-M. Zhang, "Oscillation-induced heat transport : heat transport characteristics along liquid-columns of osciillation-controlled heat transport tubes," *International Journal of Heat and Mass Transfer*, vol. 38, no. 13, pp. 2457–2470, 1995.

[16] B. Mehta and S. Khandekar, "International Journal of Thermal Sciences Local experimental heat transfer of single-phase pulsating laminar fl ow in a square mini-channel," *International Journal of Thermal Sciences*, vol. 91, pp. 157–166, 2015.

[17] W. Kamsanam, X. Mao, and A. J. Jaworski, "Development of experimental techniques for measurement of heat transfer rates in heat exchangers in oscillatory flows," *Experimental Thermal and Fluid Science*, vol. 62, pp. 202–215, 2015.

[18] W. Kamsanam, X. Mao, and A. J. Jaworski, "Thermal performance of finned-tube thermoacoustic heat exchangers in oscillatory flow conditions," *International Journal of Thermal Sciences*, vol. 101, pp. 169–180, 2016.

[19] C. Wantha, "Effect and heat transfer correlations of finned tube heat exchanger under unsteady pulsating flows," *International Journal of Heat and Mass Transfer*, vol. 99, pp. 141–148, 2016.

[20] K. Tang, J. Yu, T. Jin, Y. P. Wang, W. T. Tang, and Z. H. Gan, "Heat transfer of laminar oscillating flow in finned heat exchanger of pulse tube refrigerator," *International Journal of Heat and Mass Transfer*, vol. 70, pp. 811–818, 2014.

[21] J. G. Zhang and U. H. Kurzweg, "Numerical simulation of time-dependent heat transfer in oscillating pipe flow," *Journal of Thermophysics and Heat Transfer*, vol. 5, pp. 401–406, jul 1991.

[22] T. Zhao and P. Cheng, "A numerical solution of laminar forced convection in a heated pipe subjected to a reciprocating flow," *International Journal of Heat and Mass Transfer*, vol. 38, no. 16, pp. 3011–3022, 1995.

[23] T. Zhao and P. Cheng, "A Numerical Study of Laminar Reciprocating Flow in a Pipe of Finite Length," *Applied Scientific Research*, vol. 59, no. 1, pp. 11–25, 1997.

[24] P. Li and K. T. Yang, "Mechanisms for the heat transfer enhancement in zero-mean oscillatory flows in short channels," *International Journal of Heat and Mass Transfer*, vol. 43, no. 19, pp. 3551–3566, 2000.

[25] C. Sert and A. Beskok, "Numerical Simulation of Reciprocating Flow Forced Convection in Two-Dimensional Channels," *Journal of Heat Transfer*, vol. 125, no. June 2003, pp. 403–412, 2003.

[26] M. K. Aktas and T. Ozgumus, "Nonzero Mean Oscillatory Flow in Symmetrically-Heated Shallow Enclosures: An Analysis of Acoustic Streaming," *Numerical Heat Transfer, Part A: Applications*, vol. 57, no. 11, pp. 869–891, 2010.

[27] J.-Y. Yu, W. Lin, and X.-T. Zheng, "Effect on the flow and heat transfer characteristics for sinusoidal pulsating laminar flow in a heated square cylinder," *Heat and Mass Transfer*, vol. 50, no. 6, pp. 849–864, 2014.

[28] Q. Dai, Y. Chen, and L. Yang, "CFD investigation on characteristics of oscillating flow and heat transfer in 3D pulse tube," *International Journal of Heat and Mass Transfer*, vol. 84, pp. 401–408, 2015.

[29] J. Liu, G. Xie, and B. Sundén, "Flow pattern and heat transfer past two tandem arranged cylinders with oscillating inlet velocity," *Applied Thermal Engineering*, vol. 120, pp. 614–625, 2017.

[30] G. Taylor, "Dispersion of Soluble Matter in Solvent Flowing Slowly through a Tube," *Proceedings of the Royal Society A: Mathematical, Physical and Engineering Sciences*, vol. 219, no. 1137, pp. 186–203, 1953.

[31] P. C. Chatwin, "On the longitudinal dispersion of passive contaminant in oscillatory flows in tubes," *Journal of Fluid Mechanics*, vol. 71, no. 03, pp. 513–527, 1975.

[32] U. H. Kurzweg, "Enhanced Heat Conduction in Fluids Subjected to Sinusoidal Oscillations," *Journal of Heat Transfer*, vol. 107, no. 2, p. 459, 1985.

[33] U. H. Kurzweg, "Enhanced Diffusional Separation in Liquids by Sinusoidal Oscillations," *Separation Science and Technology*, vol. 23, no. 1-3, pp. 105–117, 1988.

[34] M. Kaviany, "Performance of a Heat Exchanger Based on Enhanced Heat Diffusion in Fluids by Oscillation: Analysis," *Journal of Heat Transfer*, vol. 112, no. 1, pp. 49–51, 1990.

[35] J. G. Zhang, W. C. Zegel, and U. H. Kurzweg, "Enhanced Axial Dispersion in Oscillating Pipe Flow With Different Solute Concentrations at Its Ends," *Journal of Fluid Engineering*, vol. 118, no. March 1996, pp. 160–165, 1996.

[36] T. Moschandreou and M. Zamir, "Heat transfer in a tube with pulsating flow and constant heat flux," *International Journal of Heat and Mass Transfer*, vol. 40, no. 10, pp. 2461–2466, 1997.

[37] C. Walther, H. Kuhl, T. Pfeffer, and S. Schulz, "Influence of developing flow on the heat transfer in laminar oscillating pipe flow," *Forsch Ingenieurwes*, vol. 64, pp. 55–63, 1998.

[38] A. Lambert, S. Cuevas, and J. del Río, "Enhanced heat transfer using oscillatory flows in solar collectors," *Solar Energy*, vol. 80, no. 10, pp. 1296–1302, 2006.

[39] H. Chattopadhyay, F. Durst, and S. Ray, "Analysis of heat transfer in simultaneously developing pulsating laminar flow in a pipe with constant wall temperature," *International Communications in Heat and Mass Transfer*, vol. 33, no. 4, pp. 475–481, 2006.

[40] D. Yin and H. B. Ma, "Analytical solution of oscillating flow in a capillary tube," *International Journal of Heat and Mass Transfer*, vol. 66, pp. 699–705, 2013.

[41] H. Yuan, S. Tan, J. Wen, and N. Zhuang, "International Journal of Thermal Sciences Heat transfer of pulsating laminar fl ow in pipes with wall thermal inertia," *International Journal of Thermal Sciences*, vol. 99, pp. 152–160, 2016.

[42] D. Yin and H. B. Ma, "Analytical solution of heat transfer of oscillating flow at a triangular pressure waveform," *International Journal of Heat and Mass Transfer*, vol. 70, pp. 46–53, 2014.

[43] G. J. Brereton and S. M. Jalil, "Diffusive heat and mass transfer in oscillatory pipe flow," *Physics of Fluids*, vol. 29, no. 7, p. 073601, 2017.

[44] D. Chen, Æ. C. Chen, P. Stansby, and Æ. M. Li, "Boundary layer structure of oscillatory open-channel shallow flows over smooth and rough beds," *Experiments in Fluids*, vol. 42, no. 5, pp. 719–736, 2007.

[45] R. Blythman, T. Persoons, N. Jeffer, D. B. Murray, N. Jeffers, and D. B. Murray, "Effect of oscillation frequency on wall shear stress and pressure drop in a rectangular channel for heat transfer applications," in *Journal of Physics: Conference Series*, vol. 745, 2016.

[46] B. H. Yan, L. Yu, and Y. H. Yang, "Heat transfer with laminar pulsating fl ow in a channel or tube in rolling motion," *International Journal of Thermal Sciences*, vol. 49, no. 6, pp. 1003–1009, 2010.

[47] F. Xu, *Self-excited oscillations of flexible-channel flow with fixed upstream flux*. PhD thesis, University of Nottingham, 2014.

[48] A. Beskok, M. Raisee, B. Celik, B. Yagiz, and M. Cheraghi, "Heat transfer enhancement in a straight channel via a rotationally oscillating adiabatic cylinder," *International Journal of Thermal Sciences*, vol. 58, pp. 61–69, 2012.

[49] A. Fan, D. Fulmer, and J. Hartenstine, "Experimental study of oscillating flow heat transfer," in *ASME. International Conference on Micro/Nanoscale Heat Transfer, ASME 2008 First International Conference on Micro/Nanoscale Heat Transfer,*, pp. 347–354, 2008.

[50] U. H. Kurzweg, "Flows Within Parallel-Plate Channels," *Journal of Fluid Mechanics*, vol. 156, pp. 291–300, 1985.

[51] T. Nishimura, N. Oka, Y. Yoshinaka, and K. Kunitsugu, "Influence of imposed oscillatory frequency on mass transfer enhancement of grooved channels for pulsatile flow," *International Journal of Heat and Mass Transfer*, vol. 43, no. 13, pp. 2365–2374, 2000.

[52] K. S. Kim and M. S. Chun, "Pulsatile poiseuille flows in microfluidic channels with back-and-forth mode," *Korea Australia Rheology Journal*, vol. 24, no. 2, pp. 89–95, 2012.

[53] S. Li, V. Chatoorgoon, and S. J. Ormiston, "Numerical study of oscillatory flow instability in upward flow of supercritical water in two heated parallel channels," *International Journal of Heat and Mass Transfer*, vol. 116, pp. 16–29, 2018.

[54] X. J. R. Avula, *Unsteady flow in the entrance region of a circular tube*. PhD dissertation, Iowa State University of Science and Technology, 1968.

[55] P. N. Tandon, L. M. Srivastavaa, and K. Kushwahab, "Developing blood flow in the entrance region of an artery," *International Journal of Bio-Medical Computing*, vol. 36, pp. 257–265, 1994.

[56] R. L. Batra, "Entrance region flow of blood," *International Journal of Engineering Science*, vol. 28, no. 5, pp. 407–419, 1990.

[57] A. J. Jaworski, X. Mao, X. Mao, and Z. Yu, "Entrance effects in the channels of the parallel plate stack in oscillatory flow conditions," *Experimental Thermal and Fluid Science*, vol. 33, no. 3, pp. 495–502, 2009.

[58] M. Sumida, "Pulsatile entrance flow in curved pipes: Effect of various parameters," *Experiments in Fluids*, vol. 43, no. 6, pp. 949–958, 2007.

[59] K. H. Ahn and M. B. Ibrahim, "Laminar / turbulent oscillating flow in circular pipes," *Performance Evaluation*, vol. 13, no. 4, pp. 340–346, 1992.

[60] Z. X. Mao and T. J. Hanratty, "Studies of the wall shear stress in a turbulent pulsating pipe flow," *Journal of Fluid Mechanics*, vol. 170, pp. 545–564, 1986.

[61] Y. G. Lai and R. M. C. So, "On near-wall turbulent flow modelling," *J. Fluid Mech*, vol. 221, pp. 641–673, 1990.

[62] C. R. Lodahl, B. M. Sumer, and J. Fredson, "Turbulent combined oscillatory flow and current in a pipe," *J. Fluid Mech*, vol. 373, pp. 313–348, 1998.

[63] G. J. Brereton and J. L. Hwang, "The spacing of streaks in unsteady turbulent wall-bounded flow," *Physics of Fluids*, vol. 6, no. 7, pp. 2446–2454, 1994.

[64] G. Binder, S. Tardu, R. F. Blackwelder, and J. L. Kueny, "Large amplitude periodic oscillations in the wall region of a turbulent channel," in *In5th Symposium on Turbulent Shear Flows 1985, Cornell Univ.*, pp. 16.1–16.6, 1985.

[65] Z. Gete and R. L. Evans, "A computational investigation of unsteady turbulent wake-boundary-layer interaction," *Journal of Fluids and Structures*, vol. 17, no. 8, pp. 1145–1159, 2003.

[66] H. Gül, "Experimental Investigation on the Heat Transfer of Turbulent Flow in a Pipe Oscillating At Low Frequencies," *Experimental Heat Transfer*, vol. 21, no. 1, pp. 24–37, 2008.

[67] G. Xie, X. Liu, H. Yan, and J. Qin, "Turbulent flow characteristics and heat transfer enhancement in a square channel with various crescent ribs on one wall," *International Journal of Heat and Mass Transfer*, vol. 115, pp. 283–295, 2017.

[68] R. R. Mankbadi and A. Mobark, "Quasi-steady turbulence modeling of unsteady flows," *International Journal of Heat and Fluid Flow*, vol. 12, no. 2, pp. 122–129, 1991.

[69] Z. Mao and T. J. Hanratty, "Influence of large Aamplitude oscillations on turbulent drag," *AIChE Journal*, vol. 40, no. 10, pp. 1601–1610, 1994.

[70] Y. Kita, Y. Adachi, and K. Hirose, "Periodically Osillating Turbulent Flow," *Bulletin of JSME*, vol. 23, no. 179, pp. 654—-664, 1980.

[71] L. Shemer and E. Kit, "An experimental investigation of the quasisteady turbulent pulsating flow in a pipe," *Physics of Fluids*, vol. 27, no. 1, pp. 72–76, 1984.

[72] A. Scotti and U. Piomelli, "Numerical simulation of pulsating turbulent channel flow," *Physics of Fluids*, vol. 13, no. 5, pp. 1367–1384, 2001.

[73] P. J. Lefebvre and F. M. White, "Experiments on transition to turbulence in an oscillatory pipe flow," *Journal of Fluids Engineering*, vol. 111, p. 428, 1989.

[74] M. Popovac and K. Hanjalic, "Compound wall treatment for RANS computation of complex turbulent flows and heat transfer," *Flow, Turbulence and Combustion*, vol. 78, no. 2, pp. 177–202, 2007.

[75] B. Jensen, B. Sumer, and J. Fredsøe, "Turbulent oscillatory boundary layers at high Reynolds numbers," *J . Fluid Mech*, vol. 206, pp. 265–297, 1989.

[76] H. Saberinejad and A. Keshavarz, "Reciprocating turbulent flow heat transfer enhancement within a porous medium embedded in a circular tube," *Applied Thermal Engineering*, vol. 102, no. 15, pp. 1355–1365, 2016.

[77] P. R. Spalart, "Direct simulation of a turbulent boundary layer up to $R\theta = 1410$," *J . Fluid Mech*, vol. 187, pp. 61–98, 1988.

[78] S. M. Jalil, "Experimental and numerical investigation of axial heat transfer enhancement by oscillatory flows," *International Journal of Thermal Sciences*, vol. 137, no. March 2019, pp. 352–364, 2019.

[79] ANSYS, "ANSYS Fluent Theory Guide, Release 17.1," Tech. Rep. April, ANSYS, 2016.

[80] G. K. Batchelor, *An Introduction to Fluid Dyanmics*. Cambridge, England: Cambridge Univ.Press, 1967.

[81] W. M. Kays and M. E. Crawford, *Convective Heat and Mass Transfer*. New York: McGraw-Hill, 3rd ed., 1993.

[82] R. Akhavan, R. D. Kamm, and a. H. Shapiro, "An investigation of transition to turbulence in bounded oscillatory Stokes flows Part 2. Numerical simulations," *Journal of Fluid Mechanics*, vol. 225, no. -1, p. 423, 1991.

[83] B. M. Hino, M. Hino, M. Sawamoto, and S. Takasu, "Experiments on transition to turbulence in an oscillatory pipe flow," *Journal of Fluids Engineering*, vol. 75, no. 2, pp. 193–207, 1976.

[84] D. M. Eckmann and J. B. Grotberg, "Experiments on transition to turbulence in oscillatory pipe flow," *Journal of Fluid Mechanics*, vol. 222, pp. 329–350, 1991.

[85] D. A. Van Der A, P. Scandura, and T. O'Donoghue, "Turbulence statistics in smooth wall oscillatory boundary layer flow," *J . Fluid Mech*, vol. 849, pp. 192–230, 2018.

[86] J. Yuan and O. S. Madsen, "Experimental study of turbulent oscillatory boundary layers in an oscillating water tunnel," *Coastal Engineering*, vol. 89, pp. 63–84, 2014.

[87] J. D. Patil and B. Gawali, "Experimental investigation of heat transfer enhancement factors in the oscillating flow heat exchanger using Kurzweg's and Nishio's correlations," *Experimental Thermal and Fluid Science*, vol. 83, pp. 37–46, 2016.

[88] K. D. Cole and B. Çetin, "The effect of axial conduction on heat transfer in a liquid microchannel flow," *International Journal of Heat and Mass Transfer*, vol. 54, no. 11-12, pp. 2542–2549, 2011.

[89] S. M. Jalil, "Numerical Characterization of Viscous Heat Dissipation Rate in Oscillatory Air Flow," *Journal of Heat Transfer*, vol. 142, no. 1, 2020.